New Concepts for Transverse Beam Stability in High-Current Heavy-Ion Synchrotrons

Vom Fachbereich für Elektrotechnik und Informationstechnik
der Technischen Universität Darmstadt
zur Erlangung
der Würde eines Doktor-Ingenieurs (Dr.-Ing.)
genehmigte

Dissertation

von

Dipl.-Ing.
Roman Rojko
Geboren am 11. September 1971
in Trenčín

durchgeführt bei der
Gesellschaft für Schwerionenforschung mbH, Darmstadt

Darmstadt 2002
(D17)

Rojko, Roman:
New Concepts for Transverse Beam Stability in High-Current Heavy-Ion Synchrotrons / Roman Rojko. – Als Ms. gedr.. – Berlin : dissertation.de – Verlag im Internet GmbH, 2003
Zugl.: Darmstadt, Techn. Univ., Diss., 2003
ISBN 3-89825-732-0

Vom Fachbereich für Elektrotechnik und Informationstechnik der Technischen Universität Darmstadt als Dissertation angenommen.

Referent:	Prof. Dr. Eng. Dr.h.c.mult. H. L. Hartnagel; F.-IEEE; CPhys; FInstP (TU-Darmstadt)
Korreferent:	Dr. N. Angert (GSI)
Tag der Einreichung:	Dezember 2002
Tag der mündlichen Prüfung:	10.Juli 2003

Bibliografische Information Der Deutschen Bibliothek

Die Deutsche Bibliothek verzeichnet diese Publikation in der Deutschen Nationalbibliografie; detaillierte bibliografische Daten sind im Internet über <http://dnb.ddb.de> abrufbar.

dissertation.de - Verlag im Internet GmbH
Pestalozzistraße 9
10 625 Berlin

URL: http://www.dissertation.de

Abstract

Development of modern circular accelerators is nowadays focused on increasing energy and intensity of the beam. For high current operation, the electromagnetic fields self-generated by the beam can become sufficiently strong to cause beam instabilities.
In this thesis, new concepts for the damping of coherent transverse instabilities in the heavy ion synchrotron SIS of the GSI at high intensities, e.g. with $2 \cdot 10^{11}$ Ne^{10+} ions and $4 \cdot 10^{10}$ U^{73+} are investigated. In particular, a new wide band transverse feedback system (TFS) has been designed, installed and tested.
The new concept, based on digital-signal processing, which allows to integrate all required functions on a single chip, is presented. To implement a high-speed digital-signal processing system with variable parameters at a peak data processing rate of 800 MBytes/s, novel methods for data processing in real time are investigated.
To cover all working modes, e.g. coasting beam during injection, bunched beam during acceleration and extraction, a programmable variable delay up to 10 μs is designed which includes novel methods for a delay step resolution of 1 ns.
Thus, a theoretical description of a transverse feedback system taking into account the influence of its transfer function on a beam, as well as the design and installation of a 12 bits/100 MHz automatic digital feedback system are presented.

Kurzfassung

Bei der Entwicklung von modernen Kreisbeschleunigern ist die Erhöhung der Strahlenergie und -intensität von entscheidender Bedeutung. Bei hoher Intensität können die vom Strahl selbst generierten elektromagnetischen Felder genügend stark sein um Strahlinstabilitäten hervorzurufen.
In der vorliegenden Dissertation wird ein neues Konzept zur Dämpfung von kohärenten transversalen Instabilitäten im Schwerionensynchrotron SIS der GSI fur hohe Strahlintensitäten, z.B. mit $2 \cdot 10^{11}$ Ne^{10+} Ionen und $4 \cdot 10^{10}$ U^{73+}, untersucht, realisiert und getestet.
Durch ein transversales Feedbacksystem, wie es in dieser Arbeit entworfen und aufgebaut wurde, können diese kohärenten Instabilitäten gezielt gedämpft werden. Die Strahlstabilisierung während der Injektions-, Beschleunigungs-, und Extraktionsphase erfordern eine programmierbare variable Verzögerung mit hoher Auflösung. Besonderes Augenmerk wird auf eine kombinierte Methode von analogem und digitalem Verfahren gelegt.
Dieses neuartige Konzept zwingt nach neuen Wegen und Methoden zu suchen, um die Zeitverzögerung und die vektorielle Summation durch digital Signalverarbeitung zu realisieren. Um die Datenübertragungsgeschwindigkeit bis zu 800 MBytes/s in Echtzeit bearbeiten zu können, wurden neuartige Methoden fur die digitale Signalverarbeitung untersucht und entwickelt.
Das komplette Design und der Aufbau des neuartigen 12 bits/100 MHz automatischen digitalen Feedbacksystems wird in dieser Arbeit umfassend beschrieben.

List of Abbreviations and Acronyms

AA	Antiproton Accumulator at FNAL, USA
ACT	Acoustic Charge Transport
ADC	Analogue to Digital Converter
ALS	Advanced Light Source at Lawrence Berkeley National Laboratory, USA
ALTERA	Trade mark of supplier of programmable logic devices (PLDs)
BAW	Bulk Acoustic Wave
BOSS	Beam Offset Signal Suppressor
BTF	Beam Transfer Function
CERN	European Laboratory for Particle Physics, Switzerland
CESR	Laboratory of Nuclear Studies, Cornell University, USA
DAPHNE	Accelerator at Laboratori Nazionali di Frascati, Italy
DAC	Digital to Analogue Converter
DESY	Deutsches Elektronen-Synchrotron laboratory in Hamburg, Germany
DSP	Digital Signal Processor
ECL	Emitter Coupled Logic
ESR	Experimental Storage Ring
ELETTRA	Elettra Synchrotron Light Source, Italy
FIR	Finite Impulse Response
FNAL	Fermi National Accelerator Laboratory, USA
GSI	Gesellschaft für Schwerionenforschung mbH
HERA	Hadron-Elektron-Ring-Anlage at DESY
JTAG	Joint Test Action Group (also known as IEEE 1149.1 (JTAG) or Boundary Scan)
KEK	National Laboratory for High Energy Physics, Japan
KEK B	An Asymmetric Electron-Positron Collider for B-Factory at KEK
LEAR	Low Energy Antiproton Ring at CERN
LEP	Large Electron Positron collider at CERN
NSLS	National Synchrotron Light Source, at Brookhaven National Laboratory,USA
PC	Personal Computer
PCB	Printed Circuit Board
PECL	Positive Emitter Coupled Logic
PETRA	Positron-Elektron-Tandem-Ring-Anlage at DESY, Hamburg
PLD	Programmable Logic Device
PS	Proton Synchrotron, CERN
PSB	Proton Synchrotron Booster, at CERN
RMS	Root Mean Square
SAW	Surface Acoustic Wave
SIS	Heavy Ion Synchrotron
SLAC	Stanford Linear Accelerator Center, USA
SPEAR	Storage Ring at SLAC
SPS	Super Proton Synchrotron, at CERN
TFS	Transverse Feedback System
UNILAC	UNIversal Linear ACcelerator
VLIW	Very Long Instruction Word

Contents

Chapter 1

Motivation

Accelerators are devices that control and manipulate the motion of charged particles. To describe the dynamics of a beam of particles, one considers the beam as a collection of non-interacting single particles moving in the environment prescribed by the accelerator design. The electric and magnetic fields of the various accelerator components specified in the design define the beam surroundings. Given these fields, intricate effects of linear and non-linear dynamics of a single particle can be studied.

Many accelerator applications, however, require beams of medium or high intensities. As the beam intensity is increased, the electromagnetic fields generated by the beam itself, particularly the fields generated by the beam interacting with its immediate surroundings, will perturb the external prescribed fields. When the perturbation becomes sufficiently strong, the beam can be unstable. The beam interacts with its surroundings and generates an electromagnetic field. This field has also an influence on the beam, perturbing its motion. The beam-surroundings interaction then can leads to an beam instability, known as a collective instability, and subsequently to a complete beam loss.

At the heavy-ion accelerator complex of the Gesellschaft für Schwerionenforschung mbH (GSI) an intensity-upgrade program is under way with the goal to fill the Heavy Ion Synchrotron (SIS) up to the space charge limit for all ions up to uranium. This project will increase the beam intensity especially for heavy ions by two orders of magnitude compared to the present situation. This upgrade program includes various steps: ion source development, combined electron cooling and multiturn-injection into the synchrotron SIS and the replacement of the UNIversal Linear ACelerator (UNILAC) prestripper structures by RFQs and IH-structures. Beside the described modifications, various additional activities will take place. SIS operation at high intensities should be further improved by the installation of new equipment. A new transverse feedback system for the compensation of coherent transverse instabilities will be installed [18, 20].

An increase of ion intensities at high energies is mainly demanded by the following experiments [18, 19, 20]:

- nuclear spectroscopy with rare isotopes at the fragment separator
- plasma physics with target temperatures above 10 eV.

Transverse feedback system: state-of-the-art

In modern electronic systems it is increasingly true that signals are transformed back and forth between analogue and digital forms. This is usually because some of the required manipulations cannot be done in digital processing because they must be

too rapid, whereas digital processing is preferred for certain slower operations because of *programmability* or *accuracy* requirements. Programmability has unquestionably been lacking in high-speed analogue signal processing systems. True digital programmability is highly desirable: just any electronic system can benefit from added intelligence or additional modes of operation. Up to now, most *wideband analogue devices* are either fixed or slightly "programmable" in analogue way, like the capacitance of a varactor diode is changed with a control voltage. Presently, "programmable" analogue systems often contain a number of fixed analogue devices that can be switched in and out.

From this point of view the hardware of a feedback loop can be implemented in one of two basic forms. **A digital feedback loop** first digitises the data from the pickups. This is typically done with an analogue to digital converter (ADC). The calculations are then done on either a general-purpose computer, which is a part of the control system, or on a special purpose computer or digital signal processor (DSP) devoted to the feedback task. The calculated signals are then converted to analogue form and, after amplification, applied to the exciter. This conversion is typically done with a digital to analogue converter (DAC) [51, 120, 124, 127]. **An analogue feedback loop** doesn't digitise the data. It simply uses filters, amplifiers, analogue multipliers, and so on to implement the feedback algorithm. This can cause a problem for wide band signal because of the non-linearity. Because each component introduces some noise the number of components used for signal processing should be limited. A single, small, simple feedback loop is typically best implemented in the analogue form. The hardware for an analogue loop is easier (hence faster and cheaper) to design and there is no software to write. Very fast loops are almost always done with analogue hardware because it is difficult to get enough processing power for such a fast digital loop [51, 60].

Nowadays the fast analogue to digital converters (because that is the first limiting part of using digital systems) are able to convert every 2 ns an analogue signal into an 8 bit word. Detector systems with such ADC's have been tested successfully [12, 16, 45, 48, 73]. To reduce digitising noise the 12 or even 14 bits ADC's can be used for transverse feedback system.

The required arithmetic operations processed by digital systems must be carried out within the bunch spacing (about 100 ns). There are a few measures to speed up the signal processing:

- *The phase-rotation technique* has been used in the transverse feedback of the CERN SPS [24, 62], PEP II [13] and ALS [9]. The correction signal is attained on the analogue level. So after digitising, the signal has *only to be properly delayed* which can be done at a rate of 500 MSPS/8 bits. A prototype of the PEP II factory transverse system has been successfully tested in the DAPHNE, ALS, and SPEAR [48, 49, 61].

- To speed up the signal processing the algorithm of the *filtering technique* can be simplified. For example a 2 tap filter (8 bit ADC) may be used as is done for instance in the KEK B feedback system [72, 74]. Their filter design requires only a subtraction of two 8 bit words which can be carried out rapidly. Usually it is also necessary to run filters in parallel so the error signal of some bunches is grouped with the help of fast multiplexors, and the data of a group of bunches is then processed by one signal processor. Once the feedback is running *the parameters of the digital system can not be changed.*

- The *parallel processing* is the other method to speed up the data processing. To convert the analogue signal with a frequency bandwidth of tenths of MHz one needs

to use a very high sampling frequency. Because the arithmetic operations must be carried out within the bunch spacing a parallel processing strategy is used for the digital system to spread the high sampling rate information among several slower computing blocks. As an example of the successful implementation of this method the fast digital transverse feedback in the CESR [96] for damping of the coupled bunch instabilities and the transverse multi-bunch feedback system in ELETTRA [30] can be listed.

Table 1.1 compares digital and analogue transverse feedback systems at different accelerator facilities. The most important parameters of the TFS such as number of harmonics, number of bunches, maximum frequency, frequency band, required amplifier power, and type of a TFS system are listed.

Machine	h	M	Mf_o [MHz]	Frequency range [MHz]	V, I, power	Digital (D) or analog (A)
SPS	4620	4620	200	0.003 – 10	3 kV	D
PSB	5	5	8	0.005 – 50	100 W	A
PS	20	20	9.5	0.06 – 2.5	2 kW	D
FNAL M	1113	1113	53	0 – 27	5 kW	D
FNAL B	84	84	53	0 – 27	100 W	A
SPEAR II	280	2	1.3	0 – 65	2.5 kW	A
NSLS B	5	1	10.5	10 – 250	–	A
PETRA	400	80	10.4	5 – 10	1 kW	D
LEP	31320	4+4	0.045	0 – 23	40 A	D
AA	1	1	1.85	0.1 – 25	10 W	A
LEAR	1-2	1-2	3.6	0.1 – 70	–	A
PEP	2592	6+6	0.816	9.4 – 10.2	20 A	A
ALS	328	328	500	0.15 – 250	300 W	A
PEPII	3492	1746	238	0.013 – 238	300 W	A

Table 1.1: Some parameters of various transverse feedback systems. Most of these systems are working at $\beta \approx 1$ [35, 85].

This work consists of the accelerator physics theory, theoretical analysis, and simulation of the signal processing system as well as its practical realisation. The complete analysis of the transverse coherent instabilities of intense coasting ion beams is given. The main goal is the investigation of an active feedback system to increase the maximum beam intensity of ions in the synchrotron SIS by damping coherent instabilities that lead to loss of the beam. To stabilise the beam, a feedback system has to produce a force that damps the increasing beam oscillations. The main topics are:

- to analyse transverse coherent instabilities in the SIS
- to identify most important parameters for the realisation of a transverse feedback system (TFS)
- to investigate and to construct an active TFS for the compensation of coherent transverse instabilities
- to improve the parameters of transverse feedback system for optimal operation

This thesis is organised as follows. The description of the experimental environment, in particular the SIS, and the basic concepts of accelerator physics with focus on beam dynamics in the transverse direction are given in Chapter 2. Problems occurring in accelerators at high energies are discussed in Chapter 3. The transverse coherent instabilities are analysed including application to the SIS. The influence of the transverse feedback system through the definition of feedback impedance is introduced. The different methods of damping oscillations as well as state-of-the-art of transverse feedback systems with focus on the programmable variable delays are described in Chapter 4. Because the transverse feedback system was planned to be installed in the SIS the demands on TFS for SIS are discussed. This chapter contains also simulation results and comparison of different damping strategies. The signal treatment by digital signal processing along with simulation and practical realisation are presented in Chapter 5. The novel method of integration the complete feedback system on a single chip together with methods for improvement of the delay step resolution are described in detail. Chapter 6 presents measurement results with the automatic digital feedback system 12 bits/100 MHz. In the course of that chapter, results of the measurements without and with beam are discussed.

Apart from the main part of this text, it is to be emphasised the importance of the appendices, which actually contain valuable information about the design of the TFS. Appendix B contains the complete design of the TFS for the ALTERA chip. The connection diagrams for the main board are shown in Appendix C, and connection diagrams for the control board are shown in Appendix D.

Chapter 2

Introduction to particle accelerators

This chapter is organised in two parts. In the first part the experimental environment of GSI will be described shortly, whereas the second part is a short introduction to the theory.

2.1 Experimental environment

The experimental environment of GSI, in which the measurements have taken place, will be described. The GSI operates a quite complex accelerator structure for heavy ions, which consists of the linear accelerator UNILAC, the synchrotron for heavy ions SIS, and the Experimental Storage Ring ESR. As the knowledge of the experimental environment is indispensable for the understanding of accelerator physics experiments, in this section we will essentially describe the accelerator facility. The measurements presented in this work have been carried out at the SIS as well as at the ESR. Because the feedback system is planned to be used for the SIS, a more detailed description of the SIS will be given in the following, with its most important properties and technical parameters, insofar as they will be needed for a full comprehension of this work.

2.1.1 Accelerator facilities at GSI

Since 1975 GSI has been operating an accelerator facility for all elements from protons to ions having masses spanning between ^{4}He and ^{238}U. The linear accelerator UNILAC delivers ion beams of all elements with specific ion energies between 2 and 20 MeV/u for low-energy experiments[6, 7]. After an extension of the facilities in 1989, the UNILAC serves in addition as injector for the heavy ion synchrotron SIS [17, 18, 50]. After acceleration and extraction from the SIS, it is possible either to guide the beam to one of the different experimental areas, inject it into the storage ring ESR or send it to the treatment area for cancer therapy with heavy ions [80]. Depending on the experiment, the beam can be extracted from the SIS either fast (within one revolution) or slow (over some seconds). There exist two possibilities of beam transfer from the SIS to the ESR or to the experimental areas: either the beam goes directly or it is guided through a fragmentation target and the following the FRagment Separator (FRS) [52]. In the ESR [22], ions suitable for experiments in the fields of atomic or nuclear physics, as well as for beam physics measurements, can be stored for quite long times (hours). After being stored in the ESR, the beam can be eventually re-injected from the ESR to SIS for further acceleration, or it might be as well ejected and directed to the experimental areas.

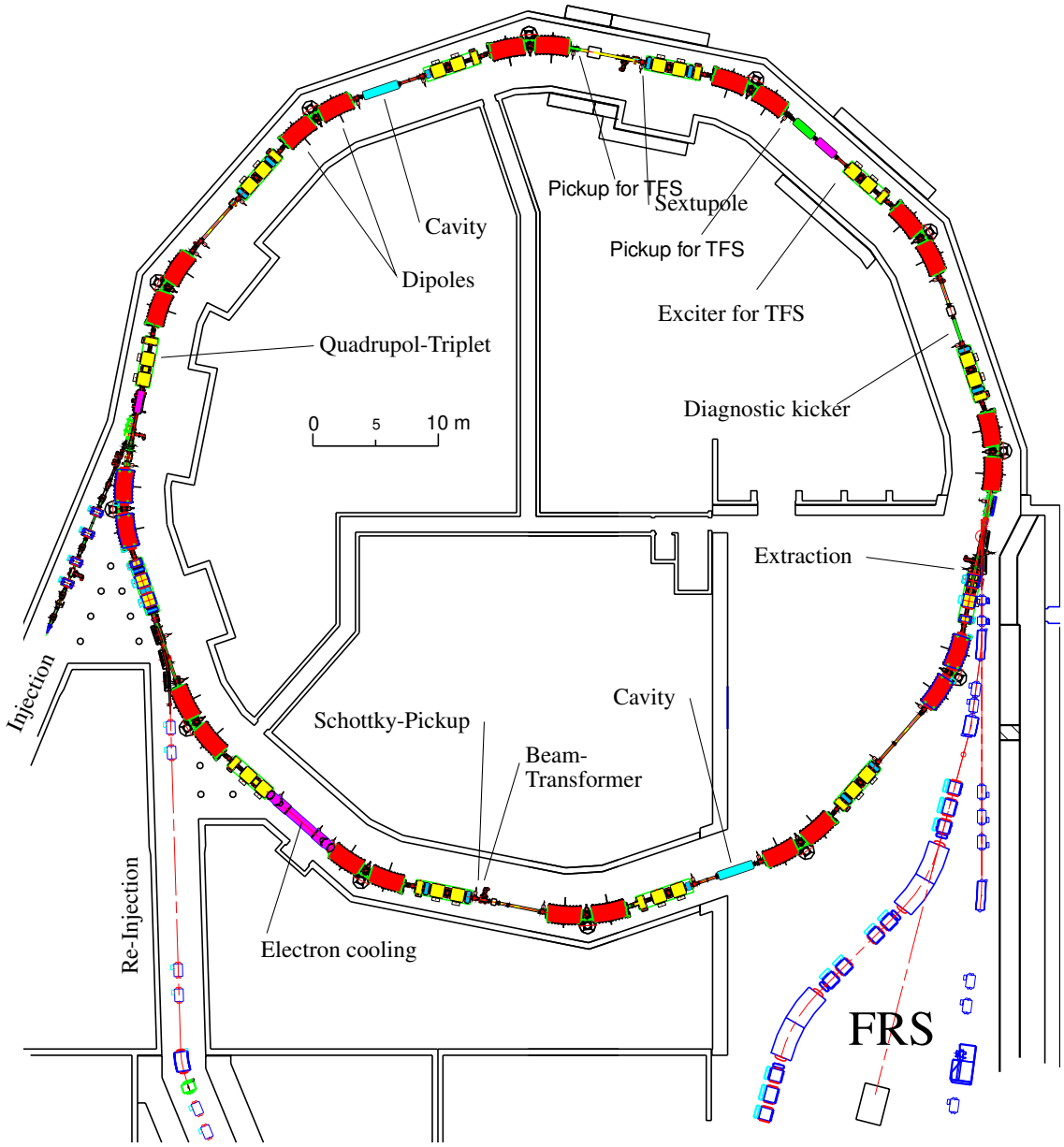

Figure 2.1: Overview of the heavy ion synchrotron SIS [50].

2.1.2 SIS - heavy ion synchrotron

The heavy ion synchrotron SIS was designed for operation at the space charge limit, i.e. for the acceleration of $2 \cdot 10^{11}$ Ne^{10+} ions and $4 \cdot 10^{10}$ U^{73+} or $2 \cdot 10^{11}$ U^{28+} ions at an injection energy of 11.5 MeV/u. At present, the UNILAC injector linac can provide an injection current of about 3 mA for neon and 20 mA for uranium ions. With neon ions the high intensity operation of the SIS could be tested during the last two years [20], while for uranium and all other heavy ions the beam intensities were restricted to about $1 \cdot 10^8$ heavy ions per machine cycle. In the first half year of 1999 the frontend part of the UNILAC with a total acceleration voltage of 34 MV was replaced by a new RFQ/IH - linac with 84 MV, which should boost the beam currents for heavy ion beams to about 3.5

Circumference of the SIS		216.720 m
Period length		18.060 m
Harmonic number		1 – 4
Accelerating frequency		
	at 11.4 MeV/u	0.858 MHz
	at 4.5 GeV/u	5.455 MHz
Maximal bending power		18 Tm
Magnet ramping rate		10 T/s
Working point (Q_x, Q_y)		4.17/3.29

Table 2.1: Beam and ring parameters [50].

mA for U^{73+} for SIS injection. Thus it will be possible to approach the SIS space charge limit also for heavy ions [14].

In addition, a low energy electron cooler has been installed in the SIS [108]. In May 1998 first tests of the new cooler have shown that even with the present low injection currents the beam intensities can be raised e.g. to about $1 \cdot 10^9$ Bi^{67+}-ions per SIS cycle by repetition of 50 multi-turn injections with about 100 ms electron beam cooling after each injection. This new SIS operation scheme proved especially useful for the direct transfer of heavy ion beams to the experimental storage ring ESR, which now can be filled with one single SIS pulse. It could be shown that with beam currents of about 10 mA in the SIS the limit is reached, where *coherent transverse beam instabilities* gradually appear, while without electron cooling high intensity neon beams of about 40 mA at injection and 120 mA at high energy did not cause *transverse coherent instabilities* [20].

The layout of SIS with its major components is shown schematically in figure 2.1 and the most important ring parameters are listed in table 2.1 [50].

2.1.3 Focusing

The quadrupoles of SIS form twelve triplets. With this type of focusing low and smooth amplitude functions can be obtained. Thus the transverse acceptance in a given vacuum chamber is maximum, which is important at injection energy. During the acceleration the beam shrinks and the acceptance becomes less important.

On the other hand the efficiency of correction elements and the extraction system demand high amplitude functions. They also should be different in both transverse planes. This can be realized best with doublet focusing which is used at higher energies.

Transition from triplet to doublet is done by keeping the field gradient of one lens at injection level. The other two lenses have to be programmed slightly different to the dipoles to keep the tune constant [50].

The betatron functions along the ring can be calculated by means of computer programs. Such calculated betatron characteristic along the one period in the SIS is shown in figure 2.2.

2.1.4 Beam diagnostics and exciter

When designing a new transverse feedback system, components already existing in the ring should be used as far as possible. In the SIS ring some components are installed for first turn diagnostics (e.g. Faraday cup, radial pickups) and diagnostics of the acceleration process (e.g. beam bunch monitors, RF pickup, beam transformer) [50]. In each of the twelve periods of the ring radial position monitors which are used for beam diagnostics are

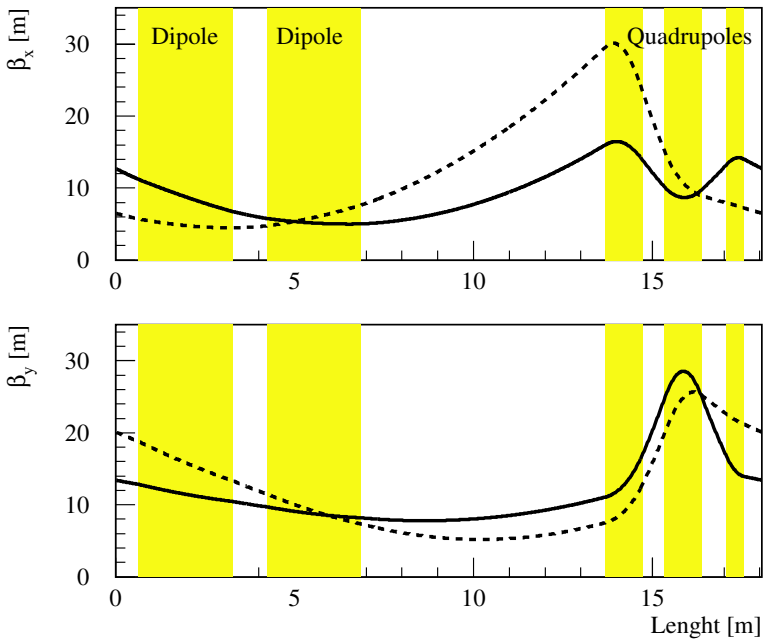

Figure 2.2: Horizontal and vertical $\beta_x(s)$ and $\beta_y(s)$ betatron functions along one period in the SIS. Dashed and solid lines indicate doublet and triplet focusing modes respectively [50].

installed. They are the candidates to be also used as monitors for the feedback system. For excitation of radial beam deflection there is no device available. Therefore, a new exciter had to be installed in SIS ring. This will be discussed in chapter 3.

2.2 Transverse beam dynamics

This section gives a short introduction to review of theory with some definitions, especially in relation to betatron functions. The basic principles of accelerator physics like accelerator optics, beam dynamics, and particularly the particle motion in circular accelerators and storage rings are described in detail in various publications like textbooks [37, 131, 132], proceedings of accelerator conferences, physics courses [28, 64, 99, 133] and review articles [26, 27, 87]. The reader is referred to the literature mentioned above regarding physical quantities and observable commonly used in accelerator physics and used also within this thesis.

2.2.1 Transformation in phase space

Liouville's theorem provides a powerful tool to describe a beam in phase space. Knowledge of the area occupied by particles in phase space at the beginning of a beam transport line will allow us to determine location and distribution of the beam at any other place along the transport line without having to calculate the trajectory of every individual particle. Because it is easy to describe an ellipse in phase space analytically, it has become customary to surround all particles of a beam in phase space by an ellipse called the *phase space* (figure 2.3) described by [131, 132]

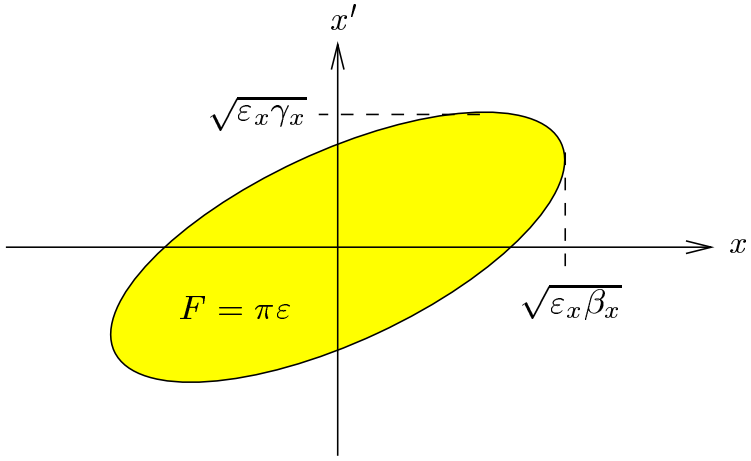

Figure 2.3: Phase ellipse of the particle movement in the horizontal direction [37, 131, 132].

$$\gamma x^2 + 2\alpha x x' + \beta x'^2 = \varepsilon \tag{2.1}$$

where β, α, γ and ε are ellipse parameters. The area enclosed by the ellipse is called the *beam emittance* ε defined by

$$\int_{\text{ellipse}} \mathrm{d}x\, \mathrm{d}x' = \pi\varepsilon \tag{2.2}$$

while the parameters β, α and γ determine the shape and orientation of the ellipse.

Since all particles enclosed by the ellipse stay within that ellipse due to Liouville's theorem, we only need to know how the ellipse parameters transform along the beam line to be able to describe the whole particle beam.

2.2.2 Betatron functions

The equation of motion for the transverse planes is a second order differential equation with a periodic driving term. It can be written in the form of Hill's equation [28, 133]

$$\begin{aligned} u'' + k(s)\, u &= 0 \\ k(s+L) &= k(s) \end{aligned} \tag{2.3}$$

where *u(s)* stands for the horizontal or vertical coordinate (*x(s)* or *y(s)*) and *k(s)* is an arbitrary function of s resembling the particular distribution of focusing along the beam. For a circular accelerator $k(s)$ is a periodic function with the period L (full circumference or length of a one cell for a periodic lattice). The form of (2.3) is valid for particles with nominal momentum and no coupling between the horizontal and vertical planes. The independent solutions of the Hill equation are

$$\begin{aligned} u(s) &= \sqrt{\varepsilon}\sqrt{\beta(s)}e^{\pm \mathrm{j}(\psi(s)-\psi_0)} \\ \text{with} \quad \psi'(s) &= \tfrac{1}{\beta(s)}\ . \end{aligned} \tag{2.4}$$

The *betatron function* $\beta(s)$ is a continuous function given by the lattice structure which depends on the longitudinal coordinate s. Properties of betatron functions can be

used to calculate the parameters of individual particle trajectories anywhere along the beam line. Any particle trajectory can be described by

$$u(s) = a\sqrt{\beta}\cos\psi + b\sqrt{\beta}\sin\psi \tag{2.5}$$

and the amplitude factors a and b can be determined by setting at $s = 0$

$$\begin{aligned} &\psi = 0, \quad \beta = \beta_0, \quad u(0) = u_0, \\ &\alpha = \alpha_0, \quad u'(0) = u'_0 \, . \end{aligned} \tag{2.6}$$

With these boundary conditions we get

$$\begin{aligned} a &= \tfrac{u_0}{\sqrt{\beta_0}}, \\ b &= \sqrt{\beta_0}u'_0 + \tfrac{\alpha_0}{\sqrt{\beta_0}}u_0 \end{aligned} \tag{2.7}$$

and after insertion into (2.5) the particle trajectory and its derivative are

$$\begin{aligned} u(s) &= \sqrt{\tfrac{\beta}{\beta_0}}\left(\cos\psi + \alpha_0\sin\psi\right) u_0 + \sqrt{\beta\beta_0}\sin\psi\, u'_0 \\ u'(s) &= \tfrac{1}{\sqrt{\beta\beta_0}}\left[(\alpha_0 - \alpha)\cos\psi - (1 + \alpha\alpha_0)\sin\psi\right] u_0 + \sqrt{\tfrac{\beta_0}{\beta}}\left(\cos\psi - \alpha\sin\psi\right) u'_0 \, . \end{aligned} \tag{2.8}$$

These equations can immediately be expressed in matrix form and the general transformation matrix is as follows

$$M = \begin{bmatrix} \sqrt{\tfrac{\beta}{\beta_0}}\left(\cos\psi + \alpha_0\sin\psi\right) & \sqrt{\beta\beta_0}\sin\psi \\ -\tfrac{1}{\sqrt{\beta\beta_0}}\left[(1 + \alpha\alpha_0)\sin\psi + (\alpha - \alpha_0)\cos\psi\right] & \sqrt{\tfrac{\beta_0}{\beta}}\left(\cos\psi - \alpha\sin\psi\right) \end{bmatrix} . \tag{2.9}$$

Any particle trajectory transforms from the starting point $s = 0$ to any other point $s \neq 0$ by the transformation

$$\begin{bmatrix} u \\ u' \end{bmatrix} = M \times \begin{bmatrix} u_0 \\ u'_0 \end{bmatrix} \tag{2.10}$$

where M is the general transformation matrix.

Knowledge of betatron functions along a beam line allows us to calculate individual particle trajectories. During acceleration, focusing is changing in the SIS from doublet to triplet and the focusing parameters of the ring (e.g. β, α, Q) are changing too. The change of the betatron functions for exciter and pickup positions of the feedback system can be seen in figures 2.4 and 2.5. τ_{focusing} is 1 for triplet focusing and 0 for doublet focusing. The 0 for doublet it is not exactly 0 because the current for the third lens can not be adjust to zero for technical reasons. The number between 0 and 1 means that focusing is continuously changing from triplet to doublet and vice versa. This change is very important for using feedback system because the betatron phase is varying as long as the tune in the ring is changing. This knowledge as well as the transport matrix will be used in the following for the automatic calculation of the vector summation coefficients.

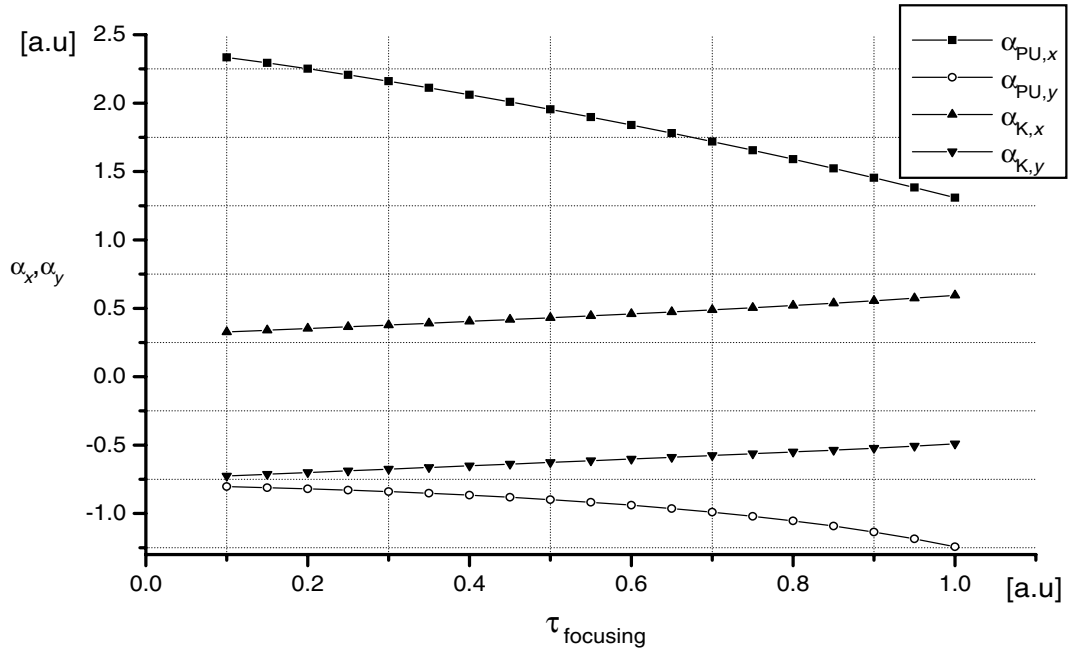

Figure 2.4: Calculated change of the α functions at the exciter (K) and pickup (PU) positions for both x and y directions as function of the parameter τ_{focusing} (τ_{focusing} is 1 for triplet focusing and 0 for doublet focusing.). These calculations were done for $Q_x = 4.290$ and $Q_y = 3.290$.

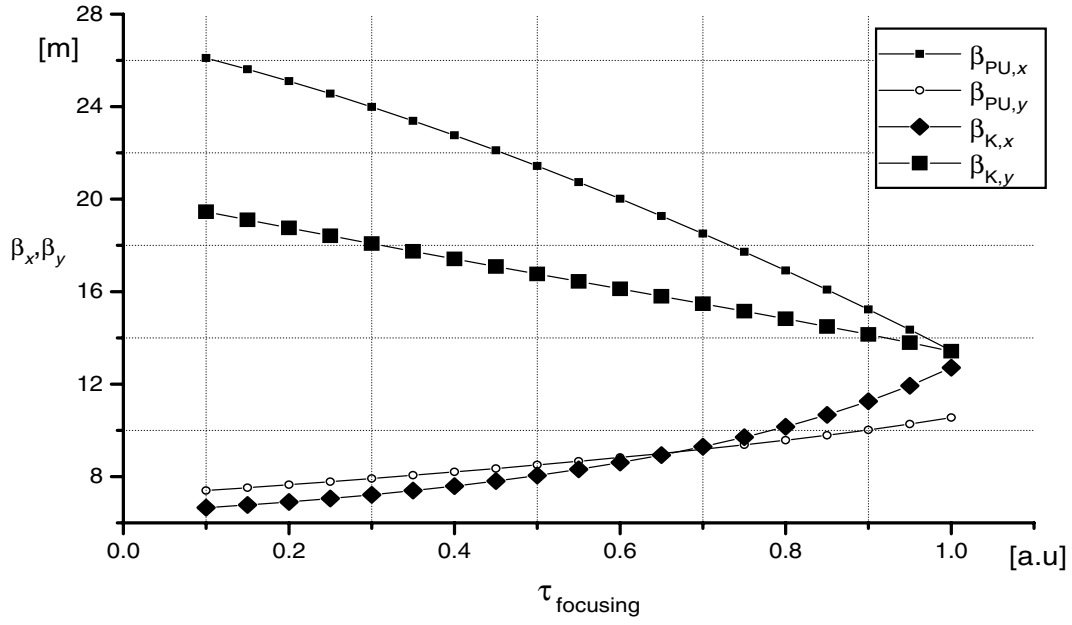

Figure 2.5: Calculated change of the β functions at the exciter (K) and pickup (PU) positions for both x and y directions as function of the parameter τ_{focusing} (τ_{focusing} is 1 for triplet focusing and 0 for doublet focusing.). These calculations were done for $Q_x = 4.290$ and $Q_y = 3.290$.

Chapter 3

Transverse instabilities and their cures

If a charged particle is locally displaced or kicked, it will start to oscillate around an equilibrium orbit ("betatron coherent oscillations") due to external focusing fields of an accelerator or storage ring. These oscillations will excite electromagnetic fields which are modified by the presence of the vacuum chamber walls or other material boundaries in the neighbourhood of the beam. This beam environment is represented by the *coupling machine impedance*. In practice, the total coupling machine impedance seen by the beam has to be added up (for each frequency) from the contributions due to the smooth chamber, bellows, cavities, other cross-section variations, pickup electrodes, kickers, etc. With the total value we can then calculate the beam stability.

The electromagnetic fields react back on the oscillating beam. If there is an out-of-phase component of the forces, such as caused by the finite resistivity of the walls, the original oscillations may be reinforced. Their amplitude will then grow exponentially, i.e. the beam is unstable. Linear theory is only concerned with the conditions for the onset of the instability, i.e. the thresholds and initial growth rates, or with the means to stabilise the beam, e.g. Landau damping or the feedback system [15, 29, 63, 139].

3.1 Forces on particle

A single particle is in interaction with forces due to three different effects [15, 50, 131, 132]:

- First, there are *magnets* which are designed to keep particles confined near the design orbit. The fields in these magnets are not time varying or are varying slowly.
- The second source of forces on the charged particle are *rf cavities*. These cavities are designed to accelerate the particles near the required energy and to keep the particles in bunches. They do this by using an electric field which is varying sinusoidal in time. The slope of the electric field with respect to time is such that a particle which is in the tail of the bunch will have its energy changed so as to move it forward in the bunch, and vice-versa.
- The third source of forces on the charged particles are *wake fields*. These are electromagnetic fields which are generated by particles which are (usually) in front of the particle in question, and act back on that particle. The existence of such fields is due to the fact that the particles are moving within a vacuum chamber which in general is not smooth or perfectly conducting. Currents persist in the vacuum chamber walls

for a time after the source particles pass, and thus can cause fields which act back on later particles.

That means that the wake field is an electromagnetic field resulting from the interaction of charged particles in the beam with the surrounding conductor elements (beam pipe, kickers, rf-cavities, etc.), and it can also be characterised by the associated impedance (Fourier transformation of the wake field). From the other hand, the wake forces described above cause motion of one particle to affect motion of other particles. Since all the particles are thus coupled to one another, the entire beam will execute *coherent oscillations*. Such oscillations may or may not be stable. The way of controlling such an oscillation is with a *feedback system*.

3.2 Transverse coupling impedance

A charged particle beam interacts electromagnetically with its vacuum chamber surroundings in an accelerator. The generated fields affect the dynamics of the charge itself, and may exert forces on any trailing particles. The fields are referred to as a *wake fields* due to the fact that they are left mainly behind the travelling charge. The Fourier transform of the *transverse wake function* is called the *transverse coupling impedance* [65, 66, 94, 130, 131, 132]

$$Z_{\perp}(\overline{r},\omega) = \frac{\mathrm{j}}{c}\int_{-\infty}^{\infty} W_{\perp}(\overline{r},s)e^{-\mathrm{j}\omega s/c}\mathrm{d}s\ . \tag{3.1}$$

Transverse wake function and coupling impedance are two descriptions of the same thing, the coupling between the beam and its environment. The transverse wake function is the time domain description, the transverse coupling impedance is the frequency domain description. The reason for the usefulness of the coupling impedance is that it often contains a number of sharply defined frequencies corresponding to the modes of the cavity or the long range part of the wake function. (see figure 3.1 and 3.2 [21])

Then the transverse coupling impedance can be defined as the integral of deflecting fields over one turn normalised by the dipole moment of the excitation beam current [36, 37, 131, 132],

$$Z_{\perp}(\overline{r},\omega) = \frac{\mathrm{j}}{\beta}\frac{\oint\left[\overline{E}\left(\overline{r},\omega,s\right)+\overline{v}\times\overline{B}\left(\overline{r},\omega,s\right)\right]_{\perp}\mathrm{d}s}{I_{\mathrm{B}}\Delta x}\ . \tag{3.2}$$

The transverse coupling impedance describes the Lorenz force averaged over the beam cross section acting on the beam due to surroundings. This impedance is a property of the beam environment, but not of the beam itself. In other words, $Z_{\perp}$ represents coupling between the beam and its surroundings and it is therefore called the *coupling impedance*. The transverse impedance depends on both electric and magnetic fields and the latter are generally more important.

The real (resistive) part is proportional to the imaginary part of the betatron frequency shift and for positive (negative) value is responsible for the growth (damping) of the coherent instabilities [36, 37, 131, 132].

The imaginary part is responsible for the incoherent tune shift and determines the maximum space charge density of the beam [36, 37, 131, 132].

Transverse machine coupling impedance

In qualitative terms, observations made on several machines agree with the following description for the transverse coupling impedance of an accelerator ring. There are following major components to the transverse coupling impedance of accelerator ring (transverse impedance has the dimension $[\Omega/m]$) [21, 36, 37, 41, 82, 98, 102]:

$$Z_\perp = Z_\perp^{\mathrm{SC}} + Z_\perp^{\mathrm{RW}} + Z_\perp^{\mathrm{BB}} + Z_\perp^{\mathrm{K}} + Z_\perp^{\mathrm{EC}} \tag{3.3}$$

Space charge impedance ($Z_\perp^{\mathrm{SC}}$) is due to the capacitive coupling of the beam with the chamber wall. The space charge contribution is pure imaginary and dominates at non-relativistic energy ($\gamma \approx 1$).

Resistive wall impedance ($Z_\perp^{\mathrm{RW}}$) is due to the finite resistive of the vacuum chamber and this impedance dominates the real part of the coupling impedance at low frequencies and is therefore the most important in determining beam stability.

Broadband impedance ($Z_\perp^{\mathrm{BB}}$) describes the interaction of particles due to the presence of abrupt changes of the beam pipe cross section as well as high frequency tails of resonant structures such as RF cavities, bellows, vacuum ports, etc.

Kicker impedance ($Z_\perp^{\mathrm{K}}$) describes the inductive interaction between the beam and the kicker magnets. The magnet type, e.g. window-frame magnet or C-magnet, and his external electric network are the most important quantities to identify the coupling impedance values below the cut-off (for waveguide modes) of the beam pipe.

Electron cooling impedance ($Z_\perp^{\mathrm{EC}}$) describes the effect of the electron cooling system. Because the electron cooling system is already installed in the SIS we should take its effect into account. Plus and minus signs indicate for fast and slow waves.

The basic relations to estimate coupling impedance values for some components are recalled in table 3.1. Here, only the real part contribution of the *calculated kicker impedance* to the SIS transverse coupling impedance at the injection energy level is shown in figure 3.1 and its imaginary part is shown in figure 3.2 [21]. The kicker impedance with value $\approx$ 800 kΩ/m for the frequency $\approx$ 14 MHz was measured as the most dangerous contribution to the SIS transverse coupling impedance[21]. The resonance peaks in measured kicker impedance were observed. These are due to cabling-resonances in the transmission cable. The distance between two relative maxims is proportional the cable length.

All contributions to the SIS transverse coupling impedance will be calculated in chapter 3.6 for given beam and ring parameters. Note that the cooler impedance is inversely proportional to the beam current, whereas “normal” coupling impedance values are current independent.

Impedance contribution	**Transverse coupling impedance $Z_\perp$**
Space charge	$Z_\perp^{\mathrm{SC}} = -\mathrm{j}\frac{Z_0 R}{\beta^2\gamma^2}\left[\frac{1}{r_{\mathrm{beam}}^2} - \frac{1}{b^2}\right]$
Resistive wall	$Z_\perp^{\mathrm{RW}} = (1+\mathrm{j})\,\frac{2R}{b^3}\sqrt{\frac{Z_0 c}{2\sigma\omega_0}}$
Broad band impedance	$Z_\perp^{\mathrm{BB}} = \frac{2R}{b^2\beta}\frac{R_{\mathrm{s}}}{1-\mathrm{j}Q_{\mathrm{cav}}\left(\frac{\omega_{\mathrm{r}}}{\omega}-\frac{\omega}{\omega_{\mathrm{r}}}\right)}$
Kicker impedance	$Z_\perp^{\mathrm{K}} = \frac{c\omega\mu_0^2 l_{\mathrm{k}}^2}{4d_{\mathrm{k}}^2 Z_{\mathrm{k}}}$
Electron cooling impedance	$Z_\perp^{\mathrm{EC}} = \pm\frac{1}{\tau_{\mathrm{cool}}}\frac{2\pi Q}{I_{\mathrm{B}}}\frac{A}{Z}\frac{E_0/e}{c}$

Table 3.1: Some formulas for contribution to the beam-environment transverse coupling impedance $Z_\perp$ [21, 36, 37, 41, 82, 98, 102]. The variables, constants and parameters used in the table can be found in the Appendix A Symbols and constants.

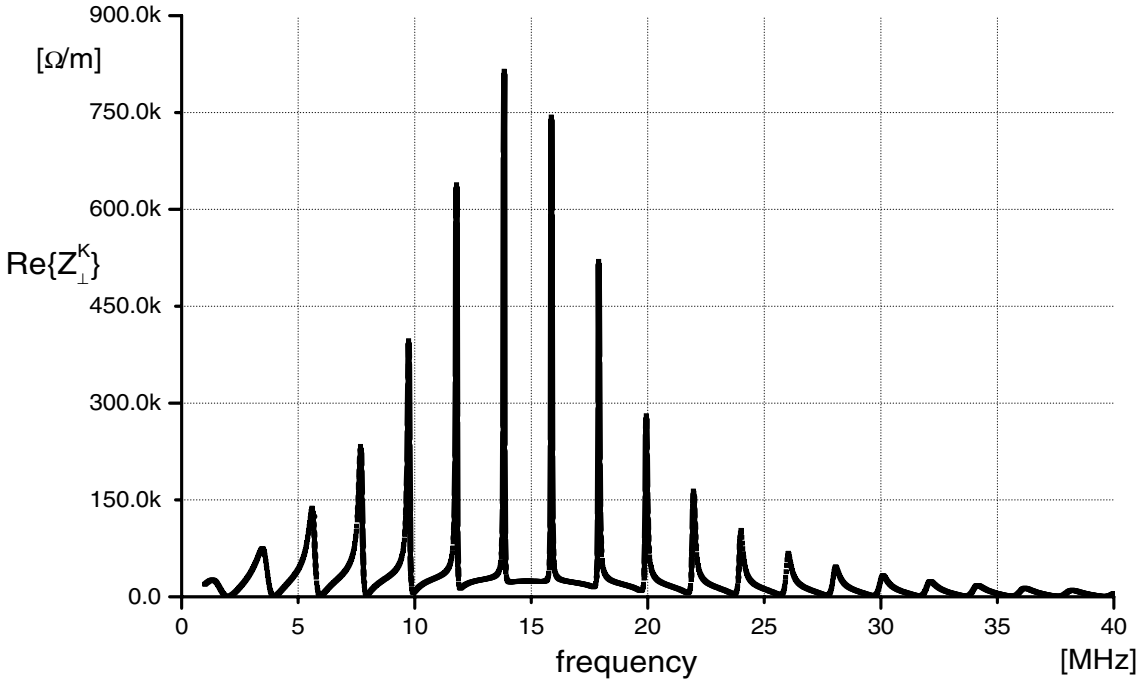

Figure 3.1: Real part of the calculated transverse kicker impedance in SIS [21].

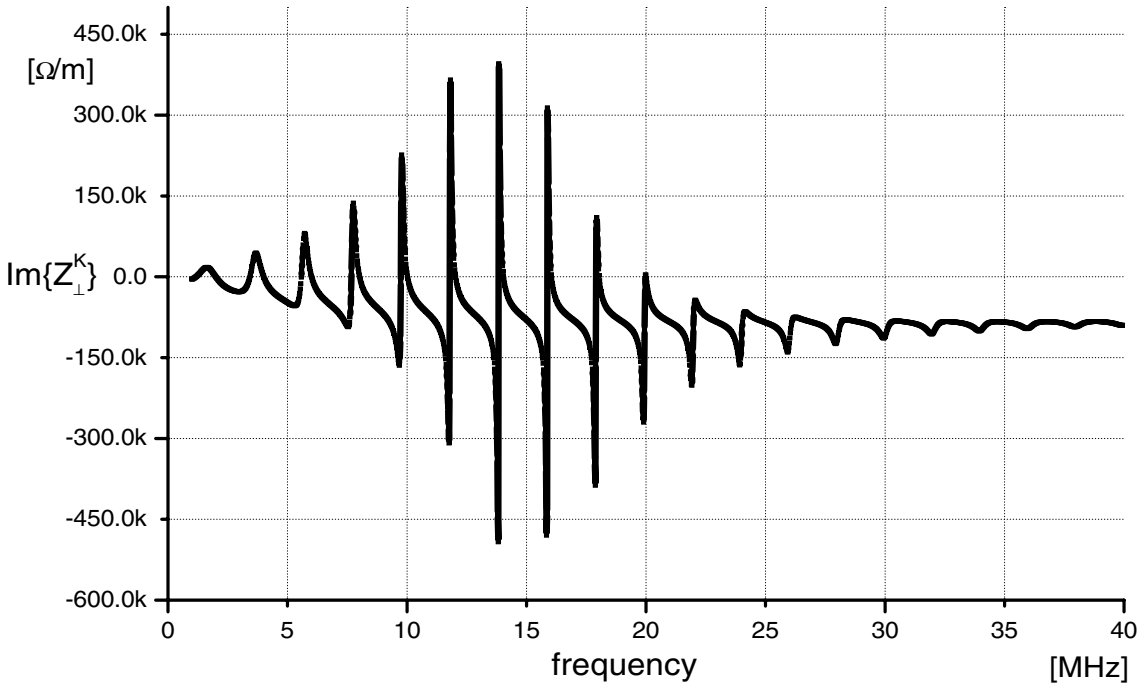

Figure 3.2: Imaginary part of the calculated transverse kicker impedance in SIS [21].

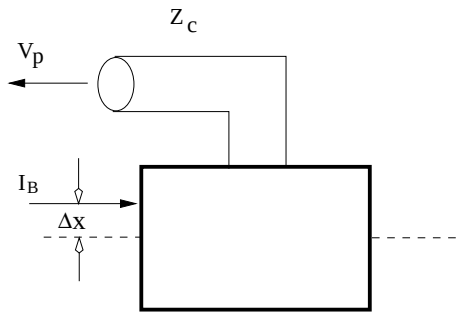

Figure 3.3: Schematic model of transverse pick-up (for horizontal direction).

3.3 Detection and excitation

Before introducing the feedback impedance it is important to describe basic parts of the system for deflection and detection of the beam. A charged-particle beam generates electromagnetic fields which in turn interact with the beam's surroundings. These interactions can produce fields which act back on the beam itself, or if the beam's surroundings - electrodes are of suitable designed form, can provide information on various properties of the beam. Such electrodes are generally known as *pick-ups*. Similarly, charged-particle beams respond to the presence of externally imposed electromagnetic fields; devices used to generate such fields are known as *kickers* or *exciters*. Systems which respond to the product of the current and the transverse displacement are called *transverse* devices, because they are sensitive to the transverse motion of the beam [54, 56, 83, 106].

As was already mentioned in chapter 2 for the TFS it is possible to use the 12 position pick-ups already installed in the ring [50, 111]. For observing the signals with the possible big amplitude it is required to select pick-up electrodes in position where the betatron oscillation amplitude $\beta(s)$ is big.

Due to the fact that there was no exciter for TFS available in the ring, a new exciter was installed in the ring.

3.3.1 Pick-up

A transverse pick-up (in the horizontal or vertical direction) can be schematically described as a "black box" as shown in figure 3.3. A beam of particles passing through the black box causes a signal to appear at the end of a signal cable which is connected to an internal beam-sensing electrode structure. For a transverse pick-up, the output signal is proportional to the product of the beam current and the beam's transverse displacement, i.e. to the dipole moment of the beam.

The signal obtained by *adding* the voltages on the upper and lower plates is proportional to the total charge of the beam pulse (i.e. the current), and to the first order is independent of the vertical position of the beam. On the other hand, the signal obtained by *subtracting* the voltages on the upper and lower plates is to the first order proportional to the vertical position of the beam.

Transverse frequency spectrum

A *transverse pick-up* (with a linear response to transverse displacement) will sense the particle's dipole moment, which can have both a time-independent part (due to a "dc"

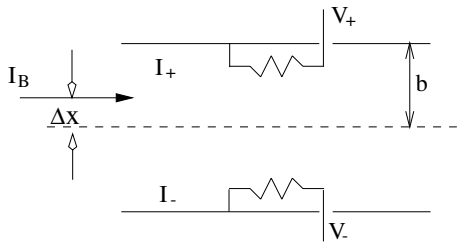

Figure 3.4: Schematic representation of transverse beam impedance by a two electrodes.

offset of the orbit relative to the center of the pick-up) as well as a time-varying part (due to particle's betatron motion).

If the particle's betatron motion is characterised by an amplitude A and tune Q (i.e. betatron frequency Qf_0), the pick-up will see a time-dependent dipole moment given by [54, 103]

$$d(t) = Aef_0 \left[\sum_{n=0}^{\infty} \cos\left[\omega_0 t(n+q)\right] + \sum_{n=1}^{\infty} \cos\left[\omega_0 t(n-q)\right] \right] \tag{3.4}$$

where q is the fractional part of Q. Hence, the betatron motion produces two lines per frequency interval f_0 in the transverse spectrum. Using communication theory language, the transverse pick-up observes a signal whose amplitude is modulated at the betatron frequency, producing a pair of amplitude modulated sidebands. In addition, if the particle's equilibrium orbit is displaced by an amount A_0 from the pick-up center, there will be additional lines of amplitude $2A_0ef_0$ at each integer multiple of f_0.

Transverse impedance

A simplified model for a transverse impedance such as a pick-up, is shown in figure 3.4. The image currents produced by the beam will divide between the two resistance values; if the beam is displaced from the centre of the device, the currents will divide *unequally*. In the following we will assume that this division varies *linearly* with the beam displacement [54], i.e.

$$I_+ = \frac{I_\mathrm{B}}{2} \cdot \left(1 + \frac{\Delta x}{b}\right) \tag{3.5}$$

$$I_- = \frac{I_\mathrm{B}}{2} \cdot \left(1 - \frac{\Delta x}{b}\right) \ . \tag{3.6}$$

If such a device is used as a pick-up, the difference of the output voltages V_+ and V_- will be proportional to $I_\mathrm{B} \cdot \Delta x$, the desired output for a transverse pick-up.

Electrostatic pick-up - capacitive type

We now consider the behaviour of the device we have been using as the illustrative model of a pick-up electrode, isolated plate(s) in the wall of the beam tube. If we imagine the pick-up plate in figure 3.5 (a) to be of length l_PU, then the image-current analysis will be valid at frequencies for which $l_\mathrm{PU} \ll \beta c/\omega$.

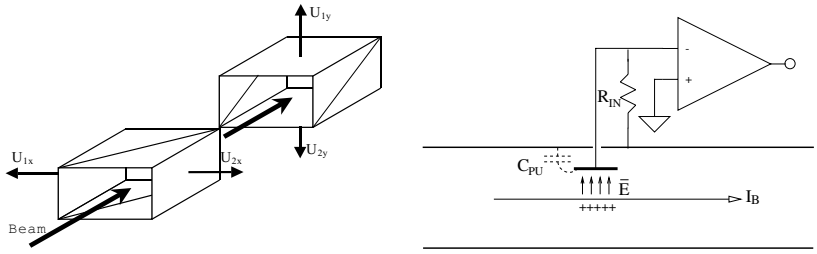

(a) (b)

Figure 3.5: Schematic design of the capacitive pick-up (a) and representation of single-plate (b).

When the capacitor plate is exposed to the electric field of the beam, the image charge on the plate will be related to the beam current I_{B} by [54, 83]

$$q = -\frac{g l_{\mathrm{PU}} I_{\mathrm{B}}}{\beta c} \,. \tag{3.7}$$

Associated with q is a charging current $I_{\mathrm{C}} = \partial q/\partial t = \mathrm{j}\omega q$ which flows through the series combination of $\mathrm{R_{IN}}$ and $\mathrm{C_{PU}}$, causing a voltage across $\mathrm{R_{IN}}$ of [83, 107]

$$V = \mathrm{j} \cdot I_{\mathrm{B}} \cdot g \cdot \frac{\omega l_{\mathrm{PU}}}{\beta c} \cdot \frac{\mathrm{R_{IN}}}{1 + \mathrm{j}\omega \mathrm{R_{IN}} \mathrm{C_{PU}}} \tag{3.8}$$

where I_{B} is an average beam current, $\mathrm{R_{IN}}$ is the input impedance of the preamplifier, and $g = \Delta x/b$ is a geometrical factor.

A few relevant data on the SIS pick-up electrodes are given in table 3.2.

Parameter	Pick-up	Exciter
length	$l_{\mathrm{PU}} = 12$ cm	$l_{\mathrm{K}} = 15$ cm
horizontal	$h_{\mathrm{PU}} = 20$ cm	$h_{\mathrm{K}} = 20$ cm
vertical	$w_{\mathrm{PU}} = 7$ cm	$w_{\mathrm{K}} = 7$ cm
impedance output	50 Ω	50 Ω
capacity	$C_{\mathrm{PU}} = 140$ pF	–

Table 3.2: Parameters of the pick-up and exciter.

3.3.2 Exciter

Charged particle beams respond to the presence of externally imposed electromagnetic fields; devices used to generate such fields are generally known as *exciters* or *kickers*. Schematically we can present a transverse exciter as a "black box" as shown in figure 3.6.

A (time-varying) voltage is injected onto an electrode structure internal to the black box as a result of a voltage V_{K} being impressed on an input signal cable of characteristic impedance Z_{C}. The resulting electrode voltage produces a change in the transverse momentum $p_{\perp}$ of the particles in the beam passing through the structure. If we apply an external signal to the plates we should be able to influence the beam's motion: if the

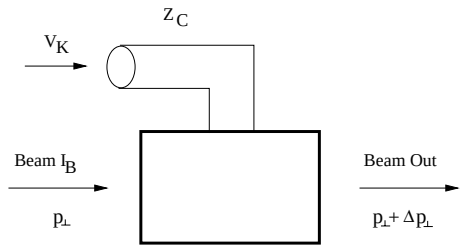

Figure 3.6: Schematic model of transverse exciter.

voltages were equal in magnitude but *opposite* in sign, the beam would receive a *transverse* kick.

The exciter used in the feedback system is realised as a pair of stripline electrodes, shown as a scheme in figure 3.7 and in reality in figure 3.8. This exciter was installed in the ring at the end of year 2000.

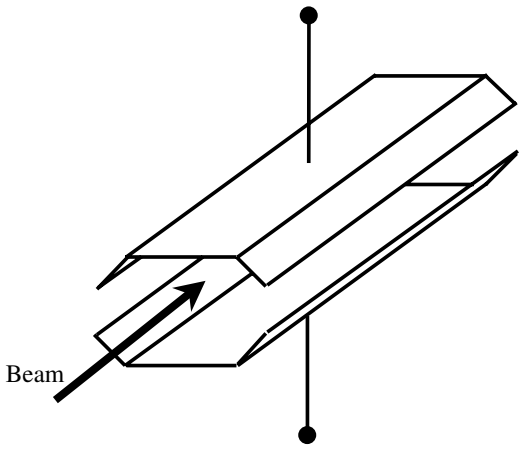

Figure 3.7: Schematic representation of a pair of stripline electrodes(vertical direction).

The basic difference from the capacitive electrodes is that striplines are travelling wave devices, and that results in different fields produced. Therefore, different force is exerted on particles at the exciter position. This feature is described with the relation including a momentum change of the particles [83]:

$$\frac{\Delta p_\perp \cdot \beta \cdot c}{e} = K_\perp \cdot V_\mathrm{K} \tag{3.9}$$

where $K_\perp$ is a figure of merit for the transverse exciter, defined as a ratio of the change in beam voltage (expressed as a change in energy per unit charge) to the input voltage of the exciter V_K. To power a pair of striplines of impedance Z_L at voltage V_L from some standard input impedance Z_C, using a matched transformer and splitter, requires an input voltage $V_\mathrm{K} = V_\mathrm{L}\sqrt{2Z_\mathrm{C}/Z_\mathrm{L}}$. Using the Panofsky-Wenzel theorem to connect longitudinal and transverse behaviour, we get the expression for $K_\perp$ [83]:

$$K_\perp = \sqrt{\frac{Z_\mathrm{L}}{2Z_\mathrm{C}}} \cdot 4 \cdot g_\perp \cdot \frac{v_\mathrm{B}}{h_\mathrm{K}\omega} \cdot \mathrm{e}^{-\mathrm{j}\theta} \cdot \sin\theta \tag{3.10}$$

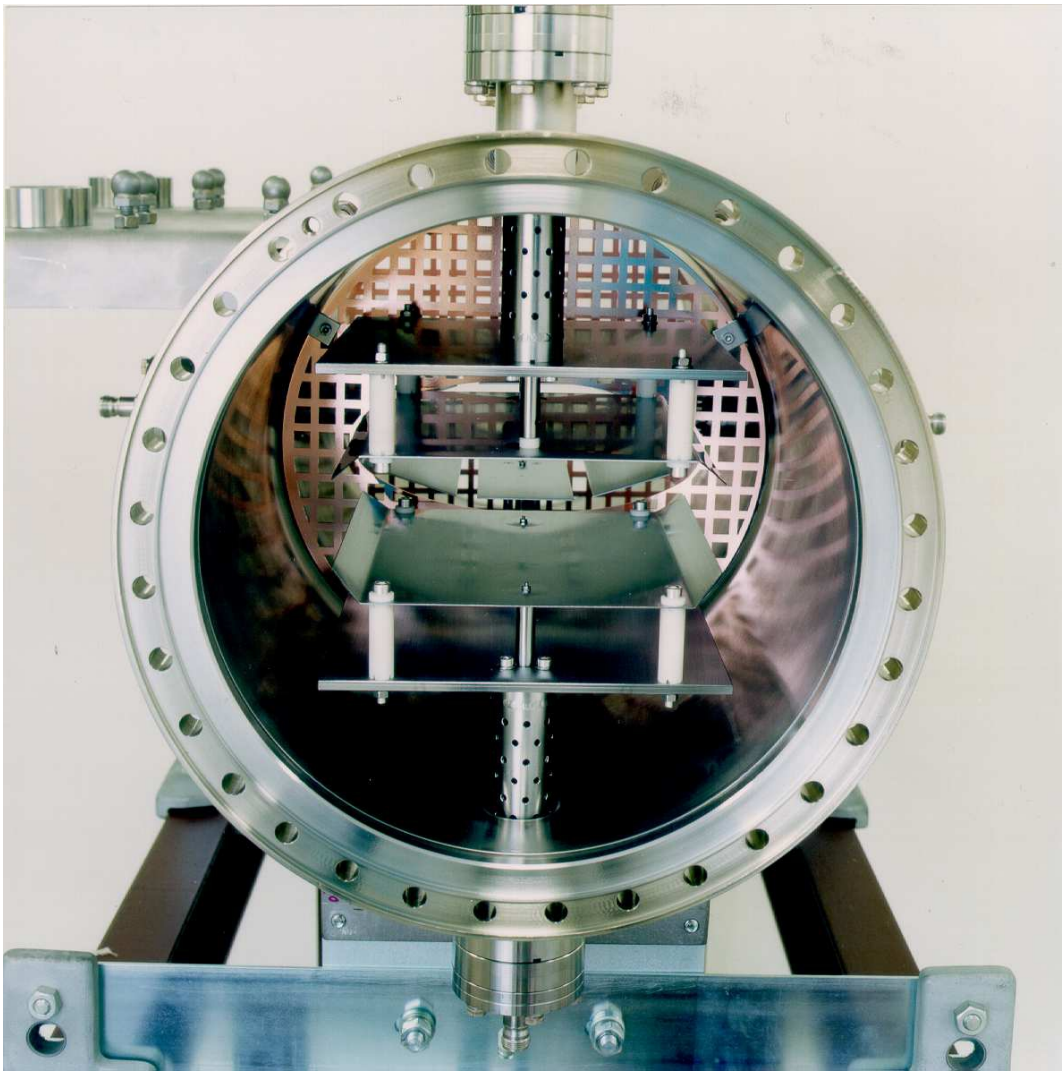

Figure 3.8: A photograph of SIS exciter in the beam pipe (vertical plane). The new exciter was installed in the ring at the end of year 2000.

where a closed-form expression $g_\perp = \tanh \frac{\pi w_\mathrm{K}}{2h_\mathrm{K}}$ is valid in linear approximation, near the center line and $\theta = (\frac{1}{v_\mathrm{B}} + \frac{1}{c})\frac{\omega l_\mathrm{K}}{2}$.

Using (3.9) and (3.10), it is now possible to find the transverse momentum change of the particle:

$$\Delta p_\perp = \frac{eV_\mathrm{L}}{\beta c \cdot h_\mathrm{K}\omega} \cdot 4 \cdot \tanh \frac{\pi w_\mathrm{K}}{2h_\mathrm{K}} \cdot \mathrm{e}^{-\mathrm{j}\theta} \cdot \sin\theta \; . \tag{3.11}$$

Because the effect of the kick is small compared to displacement it takes many repeated kicks to bring the beam on axis. A few relevant data on the exciter are already given in table 3.2.

3.3.3 Feedback impedance

Active feedback systems are frequently used in particle accelerators to damp transverse coherent beam oscillations. The principle of the transverse feedback system is described

in chapter 4. This kind of damping system is seen by the beam as an additional complex impedance, whose real part is different for the slow and fast waves.

The electromagnetic field in the exciter may be interpreted as a transverse coupling impedance [102]

$$Z_{\perp,x}^{\mathrm{FB}} = \mathrm{j}\frac{c}{I_{\mathrm{B}}e}\frac{\Delta p_{\perp}\sqrt{\beta_{\mathrm{K}}/\overline{\beta}}}{y_{\mathrm{PU}}\sqrt{\overline{\beta}/\beta_{\mathrm{PU}}}}\,. \tag{3.12}$$

$\beta_{\mathrm{PU,K}}$ are the lattice functions at the pick-up and exciter respectively, $\overline{\beta}$ is the average beta function, and y_{PU} is the amplitude of oscillations at the position of the pick-up. The effect of the pick-up is weighted with $\sqrt{\overline{\beta}/\beta_{\mathrm{PU}}}$ and the effect of the exciter is weighted with $\sqrt{\beta_{\mathrm{K}}/\overline{\beta}}$. The relationship between the oscillation amplitude at the exciter y_{K} and pick-up y_{PU} positions can be expressed as follows:

$$y_{\mathrm{K}} = y_{\mathrm{PU}}\sqrt{\beta_{\mathrm{K}}/\beta_{\mathrm{PU}}}\cdot \mathrm{e}^{-\mathrm{j}(\omega\tau_{\mathrm{p}}\mp\Delta\mu)} \tag{3.13}$$

$\Delta\mu$ is the betatron phase advance between the pick-up and the kicker, and τ_{p} is the particle flight time between pick-up and exciter.

The goal is to obtain an expression for the transverse feedback impedance in the case of an electrostatic pick-up and stripline exciter. (3.12) is taken as a starting point. Using (3.8) to get the V_{L} voltage, by multiplying V with G and a phase factor to account for the electronic signal time of flight, (3.11) and (3.13), the calculation yields:

$$Z_{\perp,x}^{\mathrm{FB}} = \mathrm{j}\frac{Gl_{\mathrm{PU}}}{\beta C_{\mathrm{PU}}h_{\mathrm{K}}w_{\mathrm{PU}}\omega}\cdot\sqrt{\frac{\beta_{\mathrm{PU}}\beta_{\mathrm{K}}}{\overline{\beta}^2}}\cdot 4\tanh\left(\frac{\pi w_{\mathrm{K}}}{2h_{\mathrm{K}}}\right)\cdot \mathrm{e}^{\mathrm{j}[\omega\Delta\tau\mp\Delta\mu-\theta]}\sin\theta \tag{3.14}$$

where G is the total gain in the feedback loop and $\Delta\tau = \tau_{\mathrm{p}} - \tau_{\mathrm{e}}$ is the difference between the particle time of flight and electronic delay.

Transversal feedback impedances given by (3.14) can be considered as functions of many parameters. However, important features are shown in the most transparent way when impedances are taken as functions of ω and $\Delta\tau$. Both real and imaginary parts of impedance's are shown in figures 3.9 and 3.10, respectively.

Obvious characteristic of the feedback impedance, which includes the performance of stripline kicker, is the decrease of amplitude with the increase of both ω and $\Delta\tau$. If there is an instability at high frequencies it is because of low feedback impedance. This impedance model describes more accurately the real situation, as the behaviour of the stripline exciter and electrostatic pick-up are taken into account.

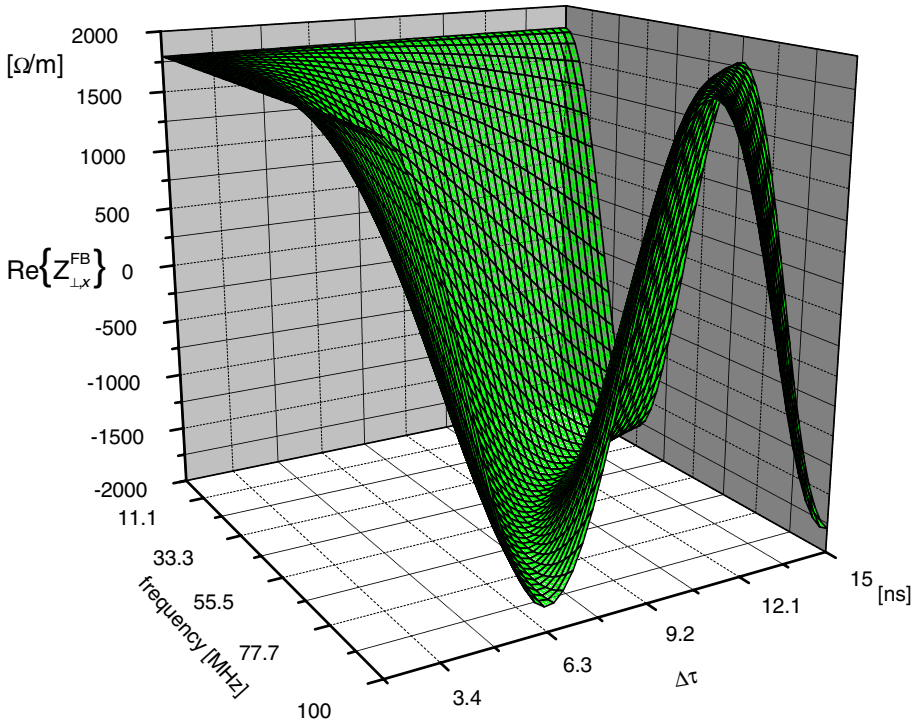

Figure 3.9: Real part of $Z_{\perp,x}^{\mathrm{FB}}$ in horizontal direction. Calculations were done for loop gain $G = 1$.

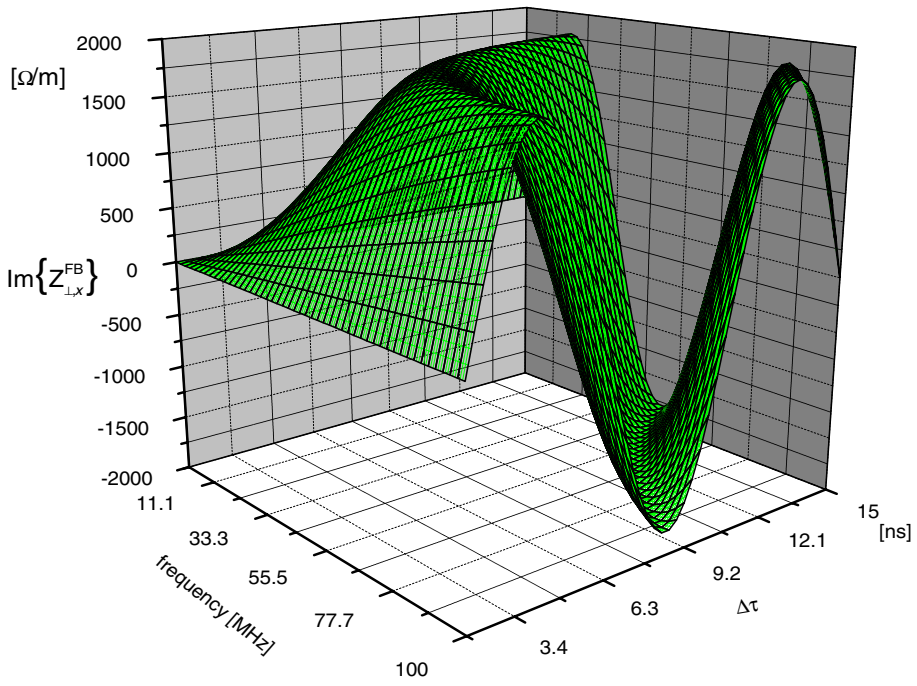

Figure 3.10: Imaginary part of $Z_{\perp,x}^{\mathrm{FB}}$ in horizontal direction. Calculations were done for loop gain $G = 1$.

3.4 Coasting beam stability diagrams

Now, when the coupling impedance values − machine and feedback − are known, it will be useful to determine the instabilities. Let us calculate the frequency range, in which one can expect appearance of instabilities as well as their rise times. These results are used for simulation and for determination of the basic parameters of the transverse feedback system.

When we are only interested in the conditions for stability, we can assume that the amplitudes of the oscillations are very small. All pertinent equations can be then linearised. As a consequence, the superposition principle is kept, and we can investigate each frequency component separately. In complex notation, we assume a time dependence of all perturbed quantities proportional to $\exp(-\mathrm{j}\omega t)$, where the frequency ω may be a complex number. If the imaginary part of ω is positive, we will have an instability. A more detailed description of the Vlasov equation and dispersion relation can be found in [37, 63, 64, 82, 98, 131, 132, 139].

3.4.1 Single particle transverse motion

The co-ordinates used to describe the motion of a generic beam particle are:

- τ is time delay between a generic beam particle and the synchronous particle. $\dot{\tau} = \mathrm{d}\tau/\mathrm{d}t$ is its time derivative.
- $\widehat{x}$ is maximum amplitude of transverse oscillation assumed to be one-dimensional. φ is the phase of an oscillation.

Analysing transverse signal of a single particle having revolution frequency ω and betatron tune Q in (3.4), we see that its spectrum is made up of single lines whose positions along the frequency axis are given by [37, 82, 98, 139]:

$$\omega_n^{\pm} = (n \pm Q)\omega \qquad \text{with} \quad n \quad \text{integer} \tag{3.15}$$

It is interesting to look for the incoherent frequency spread induced by a momentum spread and a betatron amplitude spread [82, 98, 139]

$$\delta\omega_n^{\pm} = [(n \pm Q)\omega \mp \omega_\xi] \cdot \dot{\tau} \pm \dot{\varphi}(\widehat{x}) \tag{3.16}$$

$$\omega_\xi \widehat{=} \frac{\xi}{\eta}\omega Q \qquad \text{and} \qquad \dot{\varphi}(\widehat{x}) \widehat{=} \omega Q(\widehat{x})$$

The spread arising from momentum via *chromaticity* varies with n. On the contrary, the spread due to amplitude spread is constant whatever the value n gets of the revolution frequency harmonic. For the lower sidebands, the incoherent spread due to momentum vanishes for [37, 82, 98, 139]

$$n = Q - \frac{\omega_\xi}{\omega_0}\,. \tag{3.17}$$

For this value of n the incoherent band is very narrow. Narrow bands corresponding to this harmonic number n are dangerous, since they are associated to minimum Landau damping. In order not to run into transverse instabilities one should always avoid to associate these betatron sidebands with large values of the transverse impedance.

Now, let us also define a distribution function for the beam, and write it as the sum of a stationary part and a perturbation on the n-th harmonic [37, 82, 98, 139]:

$$\psi(\varphi, \widehat{x}, \tau, \dot{\tau}, t) = \psi_0 + \Delta\psi_n =$$
$$= g_0(\dot{\tau}) f_0(\widehat{x}) + g_n(\dot{\tau}) f_n(\varphi, \widehat{x}) \exp \mathrm{j}(n\omega\tau + \omega_{\perp nc} t) \tag{3.18}$$

The frequency offset $\omega_{\perp nc}$ is a complex quantity. In general it may be written as [37, 82, 98, 139]

$$\omega_{\perp nc} = \pm Q\omega \pm \Delta Q_{nc}\omega$$

where two quantities are to be distinguished:

- the central incoherent betatron frequency $\pm Q\omega$
- the coherent transverse betatron frequency shift $\pm\Delta Q_{nc}\omega$

The stability is evaluated from the condition

$$\mathrm{Im}(\omega_{\perp nc}) < 0 \qquad \text{for an unstable beam}$$
$$\tau_{\mathrm{risetime}} = -\frac{1}{\mathrm{Im}(\omega_{\perp nc})} \tag{3.19}$$

3.4.2 Dispersion relation

The transverse driving term can be expressed by using the definition of transverse coupling impedance seen by a beam over the entire frequency range [37, 82, 98, 139]:

$$\left[\vec{E} + \vec{v} \times \vec{B}\right]_{\perp} [t, \theta] = \frac{-\mathrm{j}\beta}{2\pi R} \cdot \int_{-\infty}^{\infty} Z_{\perp}(\omega) S_{\perp}(\omega, \theta) \mathrm{e}^{-\mathrm{j}\omega t} \, \mathrm{d}\omega \tag{3.20}$$

where the $S_{\perp}(t, \theta)$ represents the transverse beam signal detected by a pick-up. After carrying out all the derivatives and limiting oneself to considering only linear terms, the following relation is received by integrating with respect to the variables $\dot{\tau}$ and $\widehat{x}$ [37, 82, 98, 139]

$$1 = -\frac{\pi(\mathrm{q}/\mathrm{A})\bar{I}\mathrm{c}}{(\mathrm{m_0c^2/e})\bar{\gamma}} \cdot \mathrm{j}Z_{\perp}[(n \pm Q)\omega] \iint_{\dot{\tau}\widehat{x}} \frac{g_0(\dot{\tau})[\partial f_0(\widehat{x})/\partial\widehat{x}]\widehat{x}^2}{(n\omega\dot{\tau} + \omega_{\perp nc})^2 - \dot{\varphi}^2} \, \mathrm{d}\dot{\tau} \, \mathrm{d}\widehat{x} \tag{3.21}$$

This relation is called the *dispersion relation* for coasting beams. For given beam parameters it defines for each value of the driving frequency ω the maximum coupling impedance $Z_{\perp}$ which still does not lead to an instability. In (3.21) the integral and the impedance are expressed in complex numbers. It is therefore convenient to visualise the stability criterion by mapping the impedance $Z_{\perp}$ in relation to the frequency ω.

3.5 Solutions of dispersion relation

The following sections give some examples on solving the dispersion relation.

3.5.1 Coasting beam without tune spread

The first simple solution for this equation might be found if we assume that the beam is monochromatic and that the machine tune does not depend on the betatron amplitudes of particle oscillations. In mathematical terms it can be written [37, 82, 98, 139]

$$g_0(\dot{\tau}) = \frac{\bar{\omega}}{2\pi}\delta(\dot{\tau}) \tag{3.22}$$

and

$$\dot{\varphi} = Q\omega\,[1-\dot{\tau}] + \omega_\xi\dot{\tau} + \dot{\varphi}(\widehat{x}) \qquad \text{with} \qquad \dot{\varphi}(\widehat{x}) = 0 \tag{3.23}$$

In this case, one may see through a simple computation, that the two roots of (3.21) are of the following kind [37, 82, 98, 139]:

$$\mathrm{Re}(\omega^{\pm}_{\perp nc}) = \pm\left(Q\omega - \frac{(\mathrm{q/A})\bar{I}\mathrm{c}\ \mathrm{Im}[Z_\perp((n\pm Q)\omega)]}{4\pi Q(\mathrm{m_0c^2/e})\bar{\gamma}}\right) \tag{3.24}$$

$$\mathrm{Im}(\omega^{\pm}_{\perp nc}) = \pm\frac{(\mathrm{q/A})\bar{I}\mathrm{c}}{4\pi Q(\mathrm{m_0c^2/e})\bar{\gamma}}\mathrm{Re}[Z_\perp((n\pm Q)\omega)] \tag{3.25}$$

If the impedance has a resistive part, the coherent motion is always unstable. It is possible to prove that both series of solutions lead to identical predictions about the beam stability and identical expected rise times. That is why one can concentrate only on one of these two series, for example on that associated to the lower bands (solutions of the slow wave type), and study the beam stability just for this case.

Principal possibilities for providing a tune spread will be discussed in two next sections below.

3.5.2 Landau damping by momentum spread

In order to study this effect, we first assume that the tune does not depend on betatron amplitudes. We will assume a parabolic distribution function in momentum or quartic one with smooth profile at the edges, which would be physically more realistic [37, 63, 64, 82, 98, 131, 132, 139]

$$g_0(\dot{\tau}) = \frac{3\omega}{8\pi\dot{\tau}_L}\left[1-\left(\frac{\dot{\tau}}{\dot{\tau}_L}\right)^2\right] \qquad -\dot{\tau}_L \le \dot{\tau} \le \dot{\tau}_L \tag{3.26}$$

$$g_0(\dot{\tau}) = \frac{15\omega}{32\pi\dot{\tau}_L}\left[1-\left(\frac{\dot{\tau}}{\dot{\tau}_L}\right)^2\right]^2 \qquad -\dot{\tau}_L \le \dot{\tau} \le \dot{\tau}_L \tag{3.27}$$

To simplify the double integral that appears in the dispersion relation (3.21) as the product of two simple integrals of single variables $\dot{\tau}$ and $\widehat{x}$ the denominator of the integral should be decomposed as the product of two terms [37, 63, 64, 82, 98, 131, 132, 139]

$$(n\omega\dot{\tau}+\omega_{\perp nc})^2 - \dot{\varphi}^2 = (n\omega\dot{\tau}+\omega_{\perp nc}-\dot{\varphi})(n\omega\dot{\tau}+\omega_{\perp nc}+\dot{\varphi}) =$$

$$= [\omega_{\perp nc} - Q\omega + ((n+Q)\omega-\omega_\xi)\,\dot{\tau}][\omega_{\perp nc} + Q\omega + ((n-Q)\omega+\omega_\xi)\,\dot{\tau}]$$

They are associated with the upper (for the first one) and lower (for the second one) sidebands. From the previous section we know that both waves lead to the same result, that is why we can concentrate only on the solutions of the type slow wave and thus approximate the first factor at the right side of the last equation with $-2Q\omega$. Besides, it is possible to show with an integration part-by-part that [37, 63, 64, 82, 98, 131, 132, 139]:

$$\int_{\widehat{x}} \frac{\partial f_0}{\partial \widehat{x}} \widehat{x}^2 \, \mathrm{d}\widehat{x} = -\frac{1}{\pi}$$

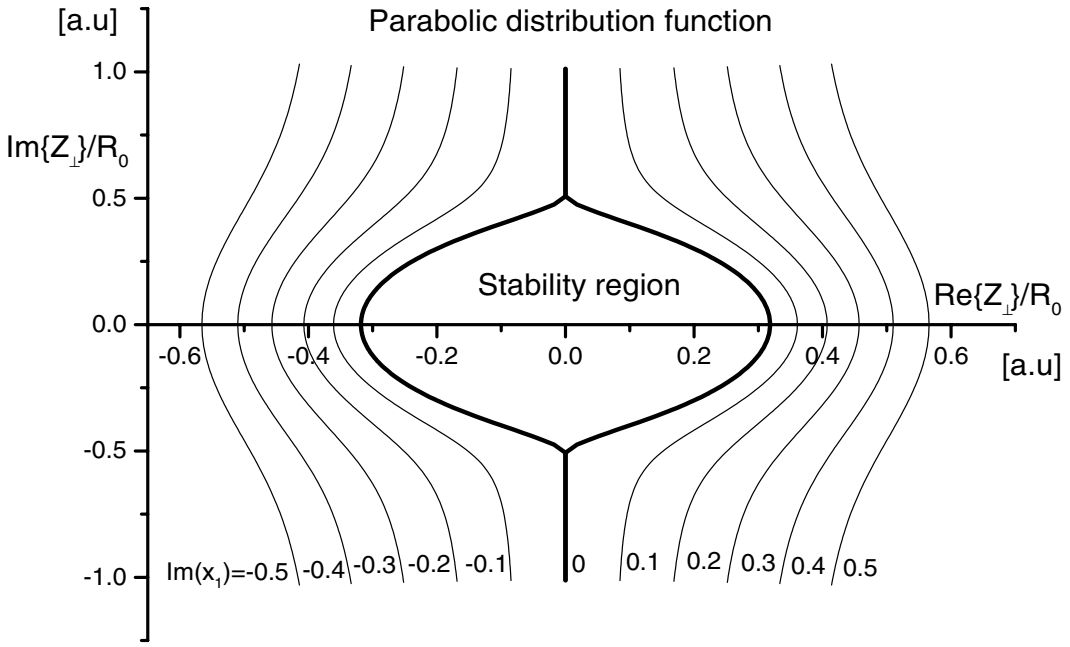

Figure 3.11: Stability boundary and rise time trajectories in an dimensionless impedance plane for a beam with a parabolic momentum distribution function.

By applying these observations to (3.21), the dispersion equation becomes for this case [37, 82, 98, 131, 132, 139]

$$1 = \frac{(\mathrm{q}/\mathrm{A})\bar{I}\mathrm{c}}{2Q\omega(\mathrm{m_0c^2/e})\bar{\gamma}[(n-Q)\omega+\omega_\xi]}\mathrm{j}Z_\perp[(n-Q)\omega]\int_{\dot{\tau}} \frac{g_0(\dot{\tau})\,\mathrm{d}\dot{\tau}}{\dot{\tau}+\frac{\omega_{\perp nc}+Q\omega}{(n-Q)\omega+\omega_\xi}} \; . \tag{3.28}$$

To simplify the latter we use the following definitions [37, 63, 64, 82, 98, 131, 132, 139]

$$\Delta\omega_n \widehat{=} \dot{\tau}_L[(n-Q)\omega+\omega_\xi] \; .$$

This quantity represents full width of half maximum of incoherent spread of frequency around the lower sidebands considered.

If we first give the following definitions [37, 63, 64, 82, 98, 131, 132, 139]

$$R_0 \widehat{=} a\frac{\Delta\omega_n \pi Q(\mathrm{m_0c^2/e})\gamma}{(\mathrm{q}/\mathrm{A})\bar{I}\mathrm{c}} \qquad a = \begin{cases} 16/3 & \text{parabolic} \\ 64/15 & \text{quartic} \end{cases}$$

$$x_1 \widehat{=} -\frac{\omega_{\perp nc}+Q\omega}{\dot{\tau}_L[(n-Q)\omega+\omega_\xi]} = -\frac{\omega_{\perp nc}+Q\omega}{\Delta\omega_n},$$

we might then rewrite our dispersion relation in form of [37, 63, 82, 98, 139]

$$Z_\perp[(n-Q)\omega] = \mathrm{j}R_0 \frac{1}{\int_{-1}^{1} \frac{(1-x^2)^n}{x-x_1}\,\mathrm{d}x} \tag{3.29}$$

where $n = 1$ applies for a purely parabolic distribution and $n = 2$ for the quartic one. Plotting the above equality gives the stability diagram. Figures 3.11 and 3.12 represent a graphical solution of (3.29) via a mapping of the complex plane x_1 into the plane $Z_\perp/R_0$. The diagrams consist of two sets of curves; at the right, the curves for the slow wave with positive values of the coupling impedance; at the left, the curves for the fast wave with negative values for the resistive impedance. The curves with $y =$Im (x_1) are plotted, starting from the stability boundary corresponding to $y = 0$ up to the rise time trajectory $y = 0.5$. The curves Im $(x_1) =$ const. yield lines of equal *frequency shift*, and Im $(x_1) =$ const. lines indicate equal *growth rate*.

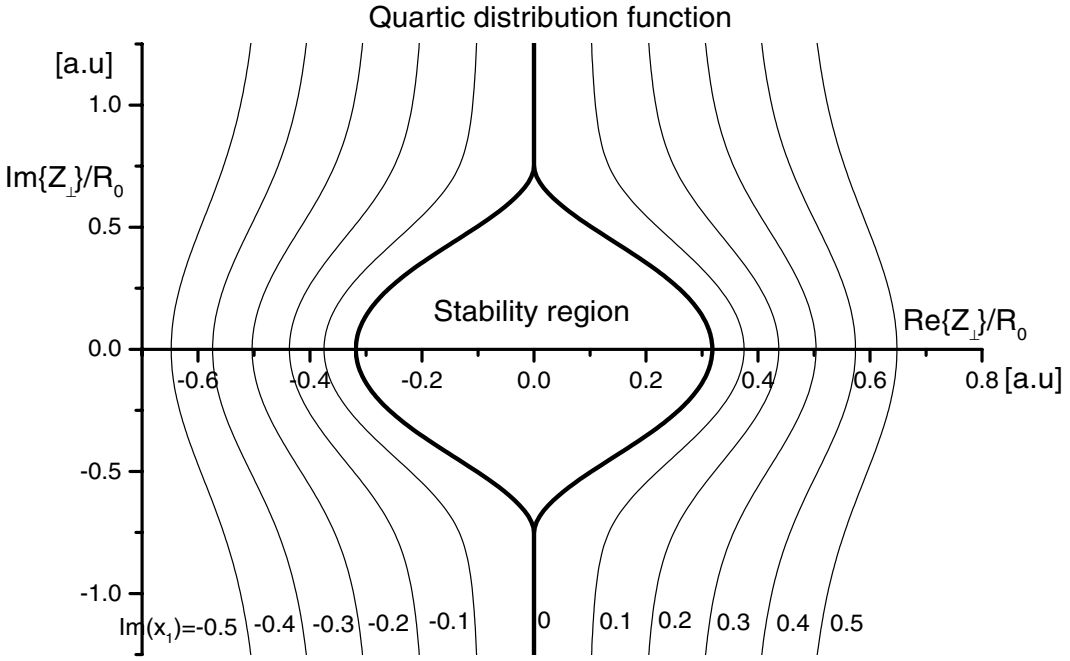

Figure 3.12: Stability boundary and rise time trajectories in an dimensionless impedance plane for a beam with a quartic momentum distribution function.

In order to evaluate the rise time corresponding to a working point lying on an instability curve associated to a certain value of y, we just apply [37, 63, 82, 98, 139]

$$\tau_{\mathrm{risetime}} = \frac{1}{y\Delta\omega_n}\,.$$

It is interesting to point out the following characteristics of the stability diagrams. As the size of the stability region is proportional to the parameter R_0, it also increases with increasing harmonic numbers: this means that the Landau damping is more effective for higher harmonic numbers and instabilities are more likely to arise at lower frequencies rather than at the higher ones. A dangerous line is that associated to the n corresponding to $-\omega_\xi \simeq (n-Q)\omega$, but this must be taken into consideration only if $\omega_\xi < 0$ (that means ξ and η should have different signs). The latter condition is generally avoided in designing a machine.

3.5.3 Landau damping by amplitude dependent tune

Now we consider the influence of a tune spread arising from a betatron amplitude spread in the beam. In order to write down the corresponding dispersion relation, we assume a monochromatic beam (3.22) and a parabolic distribution of betatron amplitudes [37, 82, 98, 131, 139]

$$f_0(\widehat{x}) = \frac{2}{\pi \widehat{x}_L^2}\left[1 - \left(\frac{\widehat{x}}{\widehat{x}_L}\right)^2\right] \qquad 0 < \widehat{x} < \widehat{x}_L \ . \tag{3.30}$$

As usual, we need to give some definitions so as to put the dispersion relation in form of equality between impedances [37, 82, 98, 131, 139]:

$$\Delta Q_L \hat{=} \frac{\partial Q}{\partial \widehat{x}^2}\widehat{x}_L^2 \qquad R_0 \hat{=} \frac{\Delta Q_L 2\pi^2 Q\omega(\mathrm{m_0c^2/e})\bar{\gamma}}{(\mathrm{q/A})\bar{I}\mathrm{c}}$$

$$\Delta Q_{nc} \hat{=} \frac{1}{\omega}(\omega_{\perp nc} + Q)\omega \qquad x_1 \hat{=} \frac{\Delta Q_{nc}}{\Delta Q_L} \ .$$

Under these assumptions, the dispersion relation takes the following form [37, 82, 98, 139] :

$$Z_\perp[(n-Q)\omega] = R_0 \frac{1}{\mathrm{j}\int_0^1 \frac{x}{x-x_1}\,\mathrm{d}x} \ . \tag{3.31}$$

From the definition of the parameter R_0, we note that the size of the stability region does not depend on harmonic number n. Figure 3.13 shows stability boundary and rise time trajectories in the dimensionless plane $Z_\perp/R_0$. The rise time of an instability associated to a working point lying on a curve parameterised in y will be $\tau_{\mathrm{inst}} = 1/(y\Delta Q_L)$.

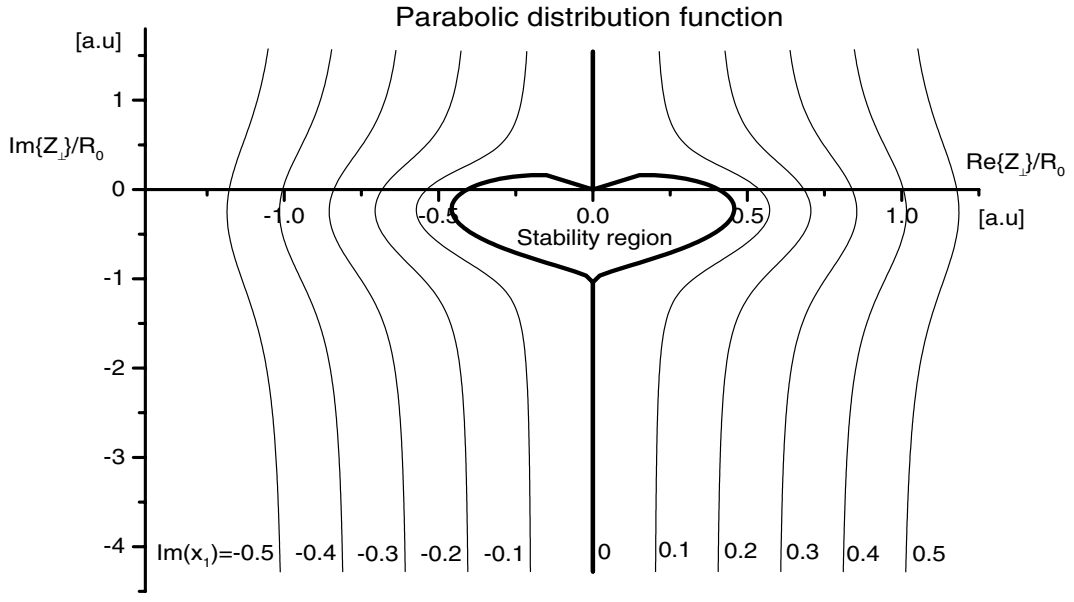

Figure 3.13: Stability boundary and rise time trajectories in an dimensionless impedance plane for a beam with a parabolic amplitude distribution function.

Parameter	without cooling		with cooling	
Ion species	Ne_{10+}	U_{72+}	Ne_{10+}	U_{72+}
ε_x [mm mrad]	160 π	160 π	3 π	3 π
ε_y [mm mrad]	40 π	40 π	4 π	4 π
Max particles	$2 \cdot 10^{11}$	$4 \cdot 10^{10}$	$1 \cdot 10^{10}$	$1 \cdot 10^{9}$
Laslett tune shift	0.3		0.25	
$r_{\mathrm{beam},x}$ $r_{\mathrm{beam},y}$	$r_x \approx 3.5$ cm, $r_y \approx 2$ cm		$r_x \approx 1.75$ cm, $r_y \approx 1$ cm	
$\delta p/\bar{p} \leq$	$1 \cdot 10^{-3}$	$6.5 \cdot 10^{-4}$	$3 \cdot 10^{-4}$	$3 \cdot 10^{-4}$
Injection energy	11.4 MeV/u			
Extraction energy	2 GeV/u	1 GeV/u	2 GeV/u	1 GeV/u
β	$0.16 - 0.95$	$0.16 - 0.88$	$0.16 - 0.95$	$0.16 - 0.88$
transition γ_{T}	$\gamma_{\mathrm{T}} = 4.79$			
	Horizontal		Vertical	
ξ_{t}	-0.94		-1.83	
ξ_{d}	-1.51		-1.41	
Q_x, Q_y	$4.1 - 4.4$		$3.1 - 3.4$	
η_{t}	0.9308 at max energy			
η_{d}	0.9407 at max energy			
revolution frequency	$0.23 - 1.385$ MHz			

Table 3.3: Specific beam and machine parameters.

3.6 Application to SIS

In general, when we deal with practical applications of the theory of transverse instabilities to real accelerators or storage rings (as it will be later the case), it is customary to represent the stability diagrams not in an dimensionless plane but in the impedance plane $Z_\perp$ so that the parameter R_0 relates directly to the size of the stability region and immediately gives a rough idea of the order of magnitude for tolerable impedances. This is undertaken to keep the beam stable and not let it blow up.

To be able to place a working point in the stability diagrams considered above, we need to know the impedance seen by a certain beam circulating in a given machine. For this purpose, the machine transverse coupling impedance according to table 3.1, figure 3.1 and 3.2 will be used. To apply the previous theory to the SIS of GSI, a set of SIS parameters is shown in table 2.1. Beam parameters are listed in table 3.3. The transverse coupling impedance was approximated and calculated as shown in figure 3.14. The impedance of the machine will vary with frequency. The resistive wall as well as the kicker impedance are shown in detail. These are the most important impedance values in the low frequency range, where the Landau damping is insufficient. The broadband impedance is dominant for higher frequency. As it can be seen in figure 3.15, where the imaginary part of the machine impedance is shown, the most important contribution to the imaginary part of the coupling impedance is the space charge impedance. In qualitative terms, observations made on several machines agree with this description for the transverse coupling impedance of an accelerator ring.

The heavy ion synchrotron SIS was designed for a space charge limit of $2 \cdot 10^{11}$ for Ne^{10+} ions and of $4 \cdot 10^{10}$ for U^{72+} or of $2 \cdot 10^{11}$ for U^{28+} ions at an injection energy of 11.4 MeV/u. The analysis for these species will be performed. In addition, the stability

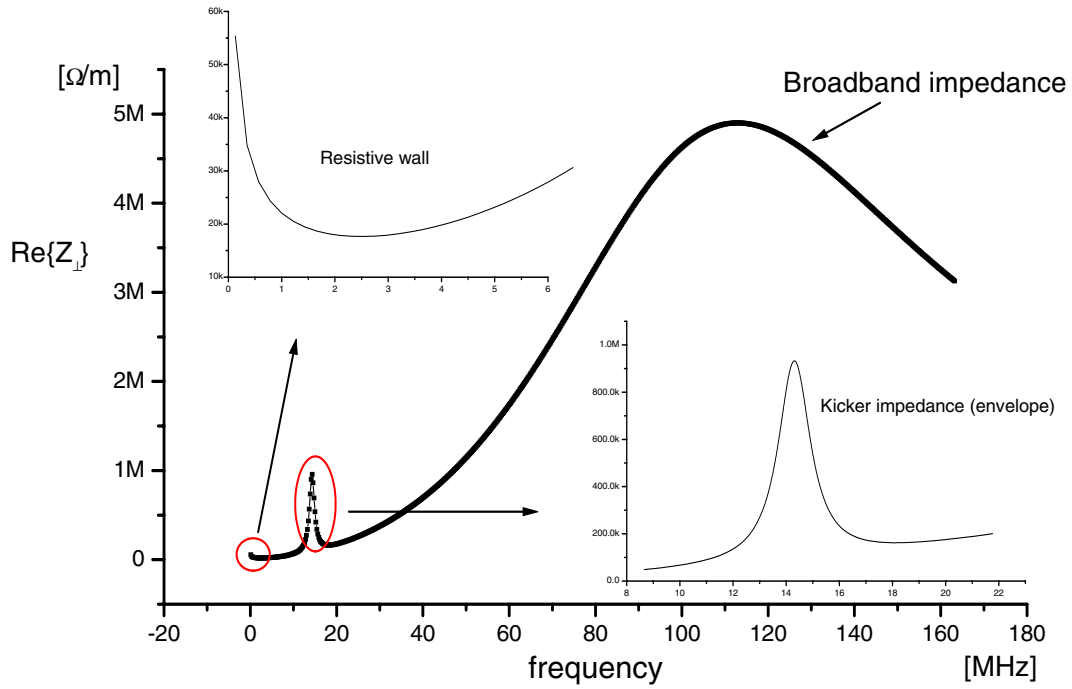

Figure 3.14: Real part of the transverse coupling impedance seen by the beam at injection energy 11.4 MeV/u ($\beta = 0.156$).

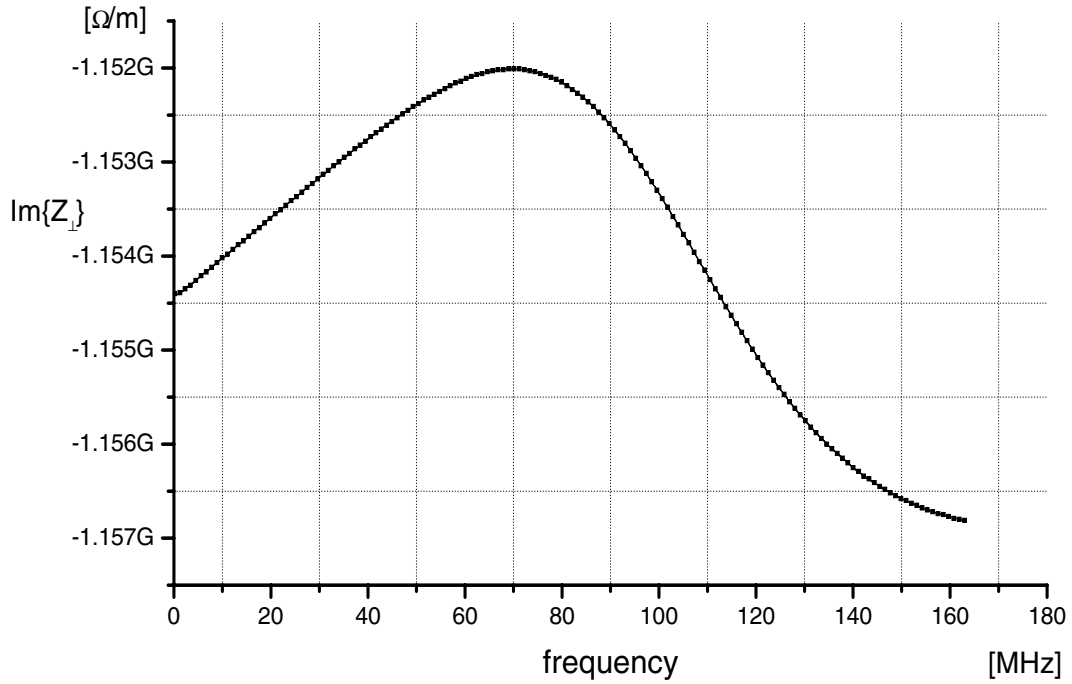

Figure 3.15: Imaginary part of the transverse coupling impedance seen by the beam at injection energy 11.4 MeV/u ($\beta = 0.156$).

diagram of the $1 \cdot 10^{11}$ Ne^{10+} ions and $3 \cdot 10^{10}$ U^{72+} and $1 \cdot 10^{11}$ U^{28+} ions will be given below.

In the following we will study first the transverse stability of an uncooled beam of $3 \cdot 10^{10}$ particles of $^{238}U^{72+}$ at injection energy, and then the stability of the same beam after acceleration. Let us assume the shape of the momentum distribution function to be a quartic one. The parameters ω_ξ, $\Delta\omega_n$ and R_0 must be estimated for the four different cases that come out if we consider the two possible focusing modes of the SIS (doublet and triplet) and both the horizontal and vertical particle motions. After checking the characterising instability parameters for the transverse beam motion in all these cases, we will find out that the worst case, that means the case for which the Landau damping from momentum spread is minimal, is associated to the vertical motion when the SIS works in the doublet focusing mode. The related parameters can be found in table 3.3.

3.6.1 Stability at injection energy level

At the injection level the beam parameters for $3 \cdot 10^{10}$ particles of U^{72+} are:

$$E_{\text{kin}} = 11.5 \text{ MeV/u} \qquad \gamma = 1.013 \qquad \beta = 0.158$$

$$f = 0.2186 \text{ MHz} \qquad I = 75 \text{ mA} \qquad \left(\frac{\delta p}{\bar{p}}\right)_{\text{HWFL}} = 1 \cdot 10^{-3} \qquad \eta_2 = -0.941 \; .$$

Because the transverse instability is low frequency mechanism where the Landau damping is at least effective, we should first check the stability for $n = 4$ (the case providing the minimum value for $(n - Q)$). For $n = 4$ we have then

$$\omega_\xi = 7.0 \cdot 10^6 \text{ rad/s} \qquad \Delta\omega_{n=4} = 7.36 \cdot 10^3 \text{ rad/s} \qquad R_0(n = 4) = 47 \text{ M}\Omega/\text{m}$$

and the transverse stability diagram shown in figure 3.16. The working point must be located down as indicated by an arrow, because of the very high space charge contribution. The coupling impedance associated to this harmonic number $n = 4$ can be evaluated from figures 3.14 and 3.15

$$Z_\perp[(p - Q)f = 0.13 \text{ MHz}] = (0.06 - \text{j } 1154) \text{ M}\Omega/\text{m} \; .$$

As the working point lies outside the stability region as can be seen from figure 3.16, we expect the beam to become unstable at the $n = 4$ harmonic with a rise time that is connected to the real part of the coupling impedance. Now we are interested to find out the harmonic number, for which the working point is placed inside the stability region and therefore is covered by Landau damping. To evaluate such a harmonic number one should check the working point, which crosses the stability boundary and enters the stable region. We take the identity

$$\delta\omega_n = \frac{15}{0.8 \cdot 64} \cdot \frac{(\text{q/A})Ic}{\pi Q(\text{m}_0\text{c}^2/\text{e})\gamma} \cdot \text{Im}[Z_\perp((n - Q)\omega)] \; . \tag{3.32}$$

To be sure, that the Landau damping is sufficient, only 80 % of the stability region is taken into account.

$$\Delta\omega_n = 227 \cdot 10^3 \Longrightarrow n \simeq 174 \qquad f(n = 174) = 37.3 \text{ MHz} \; .$$

This means that the whole frequency range up to 40 MHz can give problems for the beam stability.

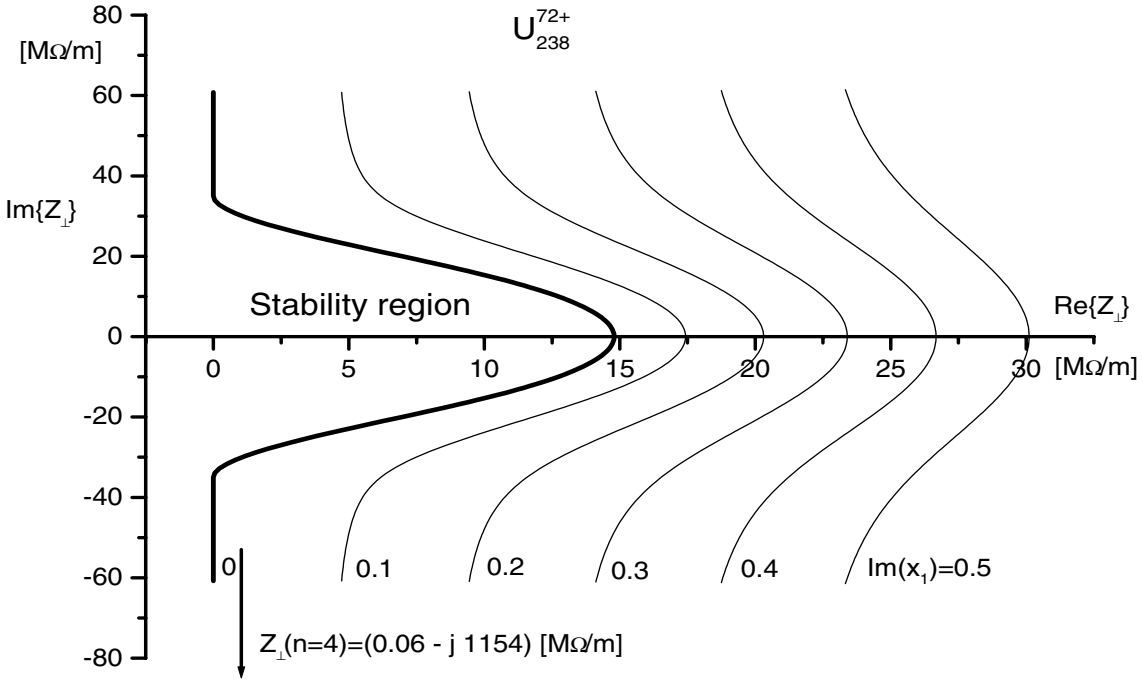

Figure 3.16: Stability boundary and rise time trajectories for the SIS $^{238}U^{72+}$ beam with $3 \cdot 10^{10}$ particles at the injection energy level and without electron cooling.

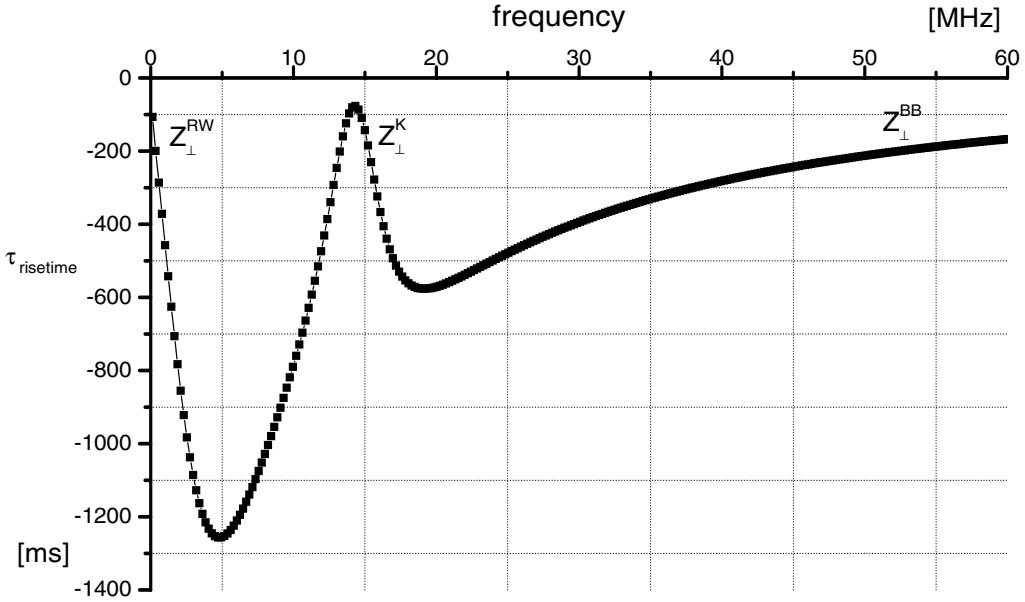

Figure 3.17: The rise times for the SIS $^{238}U^{72+}$ beam with $3 \cdot 10^{10}$ particles at the injection energy level and without electron cooling.

For every harmonic number smaller than $n < 174$ we should determine the rise time of the instabilities associated to the real part of the transverse impedance. Using (3.19) and (3.25) one can calculate the rise times for the $^{238}U^{72+}$ at injection energy. This is done for the whole frequency range in figure 3.17. The most critical is the contribution from the resistive wall impedance within the low frequency range

$$\tau_{\mathrm{rw}} = 107 \text{ ms} \qquad \text{for } f(n=4) = 0.13 \text{ MHz} .$$

The other impedance peak laying outside the stability diagram is the contribution from the kicker impedance

$$\tau_{\mathrm{k}} = 77 \text{ ms} \qquad \text{for } f(n=72) = 15.0 \text{ MHz} .$$

The last transverse impedance component is the broadband impedance which can provoke some coherent instabilities in the high frequency range where, on the other side, the Landau damping starts to be active

$$\tau_{\mathrm{bb}} = 307 \text{ ms} \qquad \text{for } f(n=174) = 37.3 \text{ MHz} .$$

In table 3.4, some other species, for which the same method for calculating the stability diagrams and rise times was used, are listed.

Species	N	I[mA]	τ_{rw}[ms]	τ_{k}[ms]	τ_{bb}[ms]	f_{Landau}[MHz]
$^{238}U^{72+}$	$3 \cdot 10^{10}$	75	107	77	307	37, n=174
$^{238}U^{28+}$	$1 \cdot 10^{11}$	98	212	152	1126	18, n=87
$^{20}Ne^{10+}$	$1 \cdot 10^{11}$	35	140	100	550	28, n=133
$^{238}U^{28+}$	$2 \cdot 10^{11}$	196	106	76	300	37, n=176
$^{238}U^{72+}$	$4 \cdot 10^{10}$	101	80	58	180	45, n=212
$^{20}Ne^{10+}$	$2 \cdot 10^{11}$	70	70	50	115	57, n=268

Table 3.4: Calculation of the growth rate and stability at injection energy ($\beta = 0.158$) for coasting beam.

3.6.2 Stability after acceleration

Similarly to the previous case, we consider the stability of the vertical beam motion when the SIS works in the doublet focusing mode. The new beam parameters are:

$$E_{\mathrm{kin}} = 214 \text{ MeV/u} \qquad \gamma = 1.228 \qquad \beta = 0.58$$

$$f = 0.8024 \text{ MHz} \qquad I = 278 \text{ mA} \qquad \left(\frac{\delta p}{\bar{p}}\right)_{\mathrm{HWFL}} = 5 \cdot 10^{-4} \qquad \eta = -0.63 .$$

The change in the transverse emittance causes the beam vertical size to get smaller ($r_{\mathrm{beam}} \approx 10$ mm) and consequently, the value of the space charge impedance reduces the value of the imaginary part of the transverse coupling impedance. The parameters ω_ξ, $\Delta\omega_n$ and R_0, if we still assume a quartic distribution function for the accelerated beam, are

$$\omega_\xi = 38.37 \cdot 10^6 \text{ rad/s} \qquad \Delta\omega_{n=4} = 13.04 \cdot 10^3 \text{ rad/s}$$

$$R_0(n=4) = 27.18 \text{ M}\Omega/\text{m} .$$

As usual, we represent the mapping of the dispersion integral on the plane of complex impedance's with our working point:

$$Z_\perp[(n-Q)f = 0.4701 \text{ MHz}] = (0.03 - \text{j}\,279)[\text{M}\Omega/\text{m}] \; .$$

Stability boundary and rise time trajectories for the SIS $^{238}\text{U}^{72+}$ beam after acceleration is shown in figure 3.18.

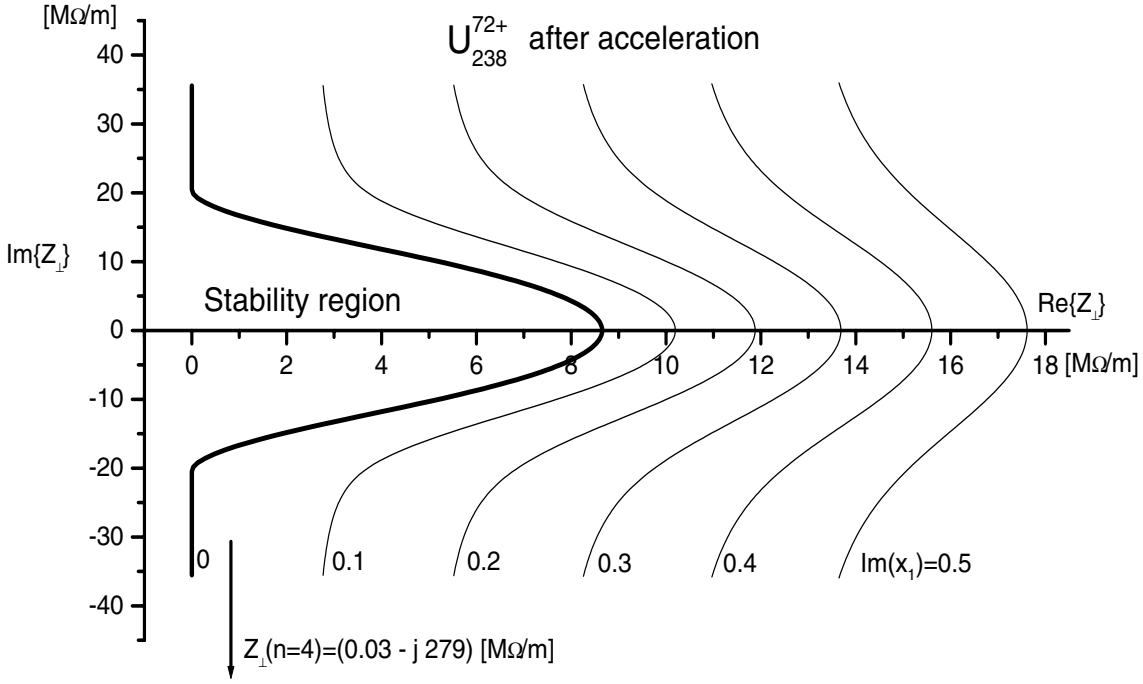

Figure 3.18: Stability boundary and rise time trajectories for the SIS $^{238}\text{U}^{72+}$ beam with $3 \cdot 10^{10}$ particles after acceleration.

Our working point is placed far outside of the stability region and we expect the beam to get unstable on the $n = 4$ harmonic with a rise time

$$\tau_{\text{rw}} = 65 \text{ ms} \qquad \text{for } \; f(n=4) = 0.481 \text{ MHz} \; .$$

A more dangerous impedance peak laying outside the stability diagram can represent the contribution from the kicker impedance with $\tau_{\text{k}} \approx 8$ ms. To check whether the frequency interval with the kicker impedance can be dangerous or not, we calculate like in the previous case for which harmonic number the working point ends up into the stability region. Using (3.32) it can be calculated that the harmonic numbers up to $n = 105$ can be dangerous. This is related to the frequency

$$(n-Q)f = 78 \text{ MHz} \; .$$

Due to the fact that the kicker impedance with a related rise time of ≈ 10 ms lies in this frequency range for the accelerated beam, it can be the main reason of the coherent instabilities to arise. This can lead to beam blow up or beam loss. The rise times for the $^{238}\text{U}^{72+}$ beam after acceleration for all dangerous frequencies are shown in figure 3.19.

To compare the different species the parameters like number of particles, current, rise time of the resistive wall, kicker rise time, broad band rise time as well as the frequency range with harmonic number are listed in table 3.5.

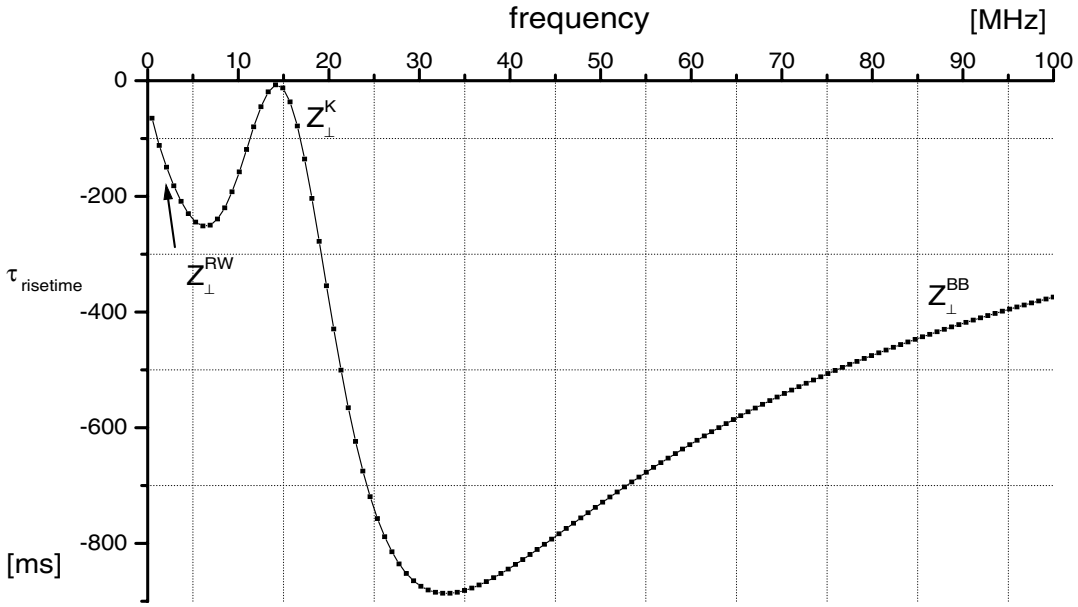

Figure 3.19: The rise times for the SIS $^{238}U^{72+}$ beam after acceleration.

Species	N	I[mA]	τ_{rw}[ms]	τ_k[ms]	τ_{bb}[ms]	f_{Landau}[MHz]
$^{238}U^{72+}$	$3 \cdot 10^{10}$	267	65	8	473	78, n=105
$^{238}U^{28+}$	$1 \cdot 10^{11}$	359	129	15	1740	36, n=48
$^{20}Ne^{10+}$	$1 \cdot 10^{11}$	110	87	12	760	60, n=89
$^{238}U^{28+}$	$2 \cdot 10^{11}$	719	65	7	476	79, n=102
$^{238}U^{72+}$	$4 \cdot 10^{10}$	370	49	6	283	100, n=127
$^{20}Ne^{10+}$	$2 \cdot 10^{11}$	247	43	5	190	123, n=163

Table 3.5: Calculation of the growth rate and stability after acceleration of the beam ($\beta = 0.58$).

3.7 Conclusions

The transverse coupling impedance for the SIS was analysed in detail. There are following major components to the transverse coupling impedance of accelerator ring: space charge impedance, resistive wall impedance, broadband impedance, kicker impedance and electron cooling. The basic relations to estimate transverse coupling impedance values for all components are recalled in table 3.1. The kicker impedance with magnitude ≈ 800 kΩ/m for the frequency ≈ 14 MHz was calculated as the most dangerous contribution to the SIS transverse coupling impedance[21].

The pick-up as a basic part for detection of the beam and the exciter as a basic part for deflection of the beam are described. The mathematical analysis was performed for the transverse feedback impedance. Transverse feedback impedance given by (3.14) can be considered as function of many parameters. This impedance model describes more accurately the real situation, as the behaviour of the stripline exciter and electrostatic pick-up are taken into account. Obvious characteristic of the feedback impedance, which includes the performance of stripline kicker, is the decrease of amplitude with the increase of both ω the angular frequency and $\Delta\tau$ the difference between particle flight time and electronic delay time. If there is an instability at high frequencies it is because of low feedback impedance.

The beam may become stable when the frequency spread is large enough for Landau damping to be effective. Landau damping is especially efficient for long bunches, what is usually the case with protons or heavy particles, for which synchrotron radiation is non existent.

The transverse stability of an uncooled beam of $3 \cdot 10^{10}$ particles of $^{238}U^{72+}$ at injection energy, and then the stability of the same beam after an acceleration was calculated. After checking the characterising instability parameters for the beam transverse motion in all cases, we find out that the worst case, that means the case for which the Landau damping from momentum spread is minimal, is associated to the vertical motion when the SIS works in the doublet focusing mode. To compare the different species the parameters like number of particles, current, rise time of the resistive wall, kicker rise time, broad band rise time as well as the frequency range with harmonic number are listed in the table 3.4 (at injection energy for the coasting beam) and in the table 3.5 (after acceleration of the beam).

From the stability diagrams presented in this chapter one can see that the Landau damping is active from about 50 MHz upward. The rise times at this frequency are approximately 0.5 s and therefore are not dangerous since coherent instabilities coming from the kicker have a rise time of about 20 ms. Such coherent instabilities might become a problem after ≈ 100 ms and therefore especially at a frequency of 15 MHz where the maximum of the transverse coupling impedance is supposed to be.

To avoid coherent instabilities the active transverse feedback is installed. The TFS should work up to the higher frequencies where the instabilities with rise times < 100 ms are present and fast, i.e. up to 40 MHz. We shall concentrate on the analysis of such a system in the following chapter.

Chapter 4

Transverse feedback system

Transverse feedback systems exist for the purpose of damping coherent betatron oscillations at frequencies much lower than those of transverse stochastic cooling systems, and transverse feedback systems correct the coherent motion of the beam (macroscopic) opposite to stochastic cooling systems which correct the incoherent motion of the particles in the beam (microscopic) reducing "temperature" [32, 35, 81, 82].

4.1 Method description

What is a feedback system in accelerators and why do we need it in accelerators? Feedback systems in accelerators serve for different purposes [36, 39, 41]:

- **Correction of the injection errors.**

  At injection there are errors in the beam position, angle, energy and phase. These errors can lead to beam emittance growth if not corrected. Because these errors are relatively large compared with other types of perturbations described below, an important requirement to a feedback system is to have *enough power to kick the beam to the orbit.*

- **Damping of the resistive wall instabilities**

  The transverse impedance of the wall of the beam tube increases as the frequency decreases. It can lead to fast beam blow-up in the transverse planes, a feedback system with *a large gain* is needed.

- **Damping of the coupled-bunch instability**

  Higher order modes (HOM) of the rf cavities, if not properly damped, may cause an unstable beam. The bandwidth of the feedback system depends on the number of circulating bunches in the ring. The feedback system needs *a wide bandwidth.*

- **Control of emittance growth from above and/or other mechanisms**

  Any external perturbation will be remembered by the beam and may eventually lead to emittance growth. A feedback system that keeps the coherent motion of the beam below a certain tolerable amplitude can effectively reduce the emittance growth rate. This feedback system must have *very low noise level.*

It is seen that each purpose imposes different requirements on feedback systems. This, of course, does not mean that a total of four systems would be required. One system may well serve several different purposes.

A classical transverse feedback system, shown in figure 4.1, consists of a pickup, which senses coherent betatron oscillations, an appropriate delay to match the pickup signal to the transit time of the beam, an amplification system followed downstream by an exciter which is located an odd multiple of 90° away from the pickup and applies a correcting force on the beam by an angular kick. The exciter corrects the beam angle according to the beam deviation from the closed orbit in the pickup . The variable delay is used for adjusting such a synchronisation during acceleration. The value of the variable delay is used normally less than one turn and the exciter corrects the beam angle at every turn. But sometimes the value of the variable delay may be more than one revolution period. Such situation can occur for a synchrotron with a short length of circumference or for a feedback circuit with a special digital filter where procedures for signal transformations are realised with signal processors.

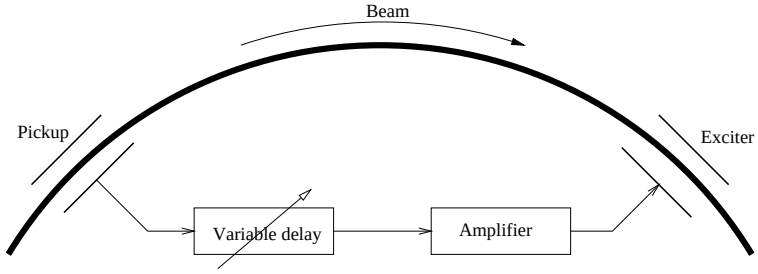

Figure 4.1: Principal scheme of a classical transverse feedback system. The phase advance of the betatron oscillation is n x 90° (n is odd integer) between pickup and exciter.

The transverse feedback system can be explain on a system making a harmonic-oscillator-like motion. The trajectory in the transverse phase space $(x, x^{'})$ of such system is an ellipse. The simplest method to realize a transverse feedback system is:

1. to observe the position error x
2. to give a kick to the transverse momentum $p_{\perp}$ after a quarter of the oscillator period, where the kick-strength is proportional to the observed position x
3. to repeat step 1 and 2 many times.

The scheme in figure 4.1 has some disadvantages. *The problem* is adjusting of the required phase advance between pickup and exciter as the lattice optics are changed. *The second problem* is that the phase of the bunch is uncertain, and instead of full cancellation, damping of the betatron oscillation is provided only in some number of turns, which depends on the lattice tune.

4.1.1 Phase advance adjusting methods

Due to the above mentioned reasons, there are the following methods for adjusting of phase advance between pickup and exciter:

Phase-rotation technique. The phrase "*after a quarter of the oscillator period*" should be read as "after the phase rotation of $\pi/2$ in the betatron (or synchrotron for longitudinal feedback system) oscillation". A bunch performs this phase rotation when it travels from a pickup to an exciter. Practically, due to some reasons, it is hard to adjust the phase rotation from the pickup to the exciter to $\pi/2$ in the transverse plane, particularly in a large ring. Thus, we have to be satisfied to choose a rotation-angle of $2\pi n+\pi/2$ instead of $\pi/2$, where n is some integer. However, since the fractional part of the tune is not necessarily 0.25, we must devise a technique for adjusting the phase-rotation angle to the desired value. The usual technique is to prepare two monitors that are separated from each other by roughly 90° in the betatron phase. By vectorial combining of the signals from these two monitors, we can create an oscillator with arbitrary phase offset. The rotation angle can be easily adjusted using this technique [10, 11, 12, 13, 38, 39, 40].

Multi-turn technique. There is another technique for adjusting the phase angle to $2n\pi + 2\pi$. For the above-defined integer n we do not necessarily need to adopt the integer part of the tune. Instead, we can permit a bunch to rotate several times in the ring from position monitoring to kicking. Of course, in this case, we should carefully choose the number of turns so that the phase-rotation angle is $\pi/2$ (mod 2π) in total. If this technique is employed, it is not necessary to prepare two sets of monitors, and a vector combining device is not required. That contributes to a simplification of the hardware. The disadvantage of this method is that between measuring and kicking we need to wait a number of revolutions. During this time, the beam signal in the ring may change and thus the correction applied may not match the beam signal measured before a number of revolutions [77, 92, 93].

Filtering technique. To achieve damping, an overall phase shift of 90° is necessary. Such a phase shift can be realised with a so-called n tap FIR (finite impulse response) filter. For example, with a three tap filter a phase shifter with arbitrary phase shift can be realised. The correction signal is then properly delayed so that it is applied to the corresponding bunch [71, 76, 121, 122, 123, 137, 138].

The methods described above are well-known and they are used in different proton accelerators all over the world for the constant particle velocity. In our case we have to use a **well adjusting method for vector summation with coefficients changing automaticaly during the acceleration process**.

The first reason for using of the vector summation is a **variable** fractional part of the tune. This value can change from one acceleration cycle to an other. Also vector summation coefficients should be recalculated and changed automatically.

The second reason is alternation of the focusing from triplet to doublet and focusing parameters of the ring (e.g. β, α, Q) during the acceleration process. Also, vector summation coefficients are not constant during the acceleration cycle.

4.1.2 Damping methods

We shall consider two possible kick schemes [68, 79, 88, 136]:

Proportional scheme – the kick is proportional to beam displacement (exponential damping with time). The pickup signal is used to drive a linear amplifier that powers the exciter.

"Bang-bang" scheme – the kick magnitude is constant, above a certain threshold, and depends only on the sign $(+/-)$ of the beam displacement (linear damping with time). This scheme is very simple: the exciter is powered by a constant supply, whose output polarity is adjusted each time to damp the oscillations.

In reality a time sequence of kicks is a combination of kicks with a constant amplitude and kicks with a amplitude proportional to the beam displacement. Both damping methods will be studied and discussed in chapter 4.5.

4.1.3 TFS in frequency and time domain

We can understand the betatron oscillations as quasi-harmonic oscillations [44, 78]:

$$x_i'' + \omega_0^2 x_i = F^{\mathrm{W}}, \tag{4.1}$$

where x_i is transverse position-error of the i-th bunch and ω_0 is the betatron frequency. The driving term F^{W} in this case is the wake force due to the trapped energy in the structure. The usual way to damp a motion governed by (4.1) is to add a term proportional to the velocity, x':

$$x_i'' + 2\eta x_i' + \omega_0^2 x_i = F^{\mathrm{W}} \tag{4.2}$$

with η being the damping coefficient. It is, however, hardly possible to know the "velocity" in the case of betatron oscillations. Instead, we can use the "delayed position", $x(t - \Delta t)$. For the sinusoidal functions, differentiation and origin-point displacement by $\pi/2 + 2n\pi$, with negation after that, are mutually equivalent. Then the equation of motion can be expressed as

$$x_i''(t) - 2\eta x_i'(t - (2n + 1/2)\pi/\omega_0) + \omega_0^2 x_i(t) = F^{\mathrm{W}}. \tag{4.3}$$

This equation tells us that the function of the feedback system is to create a force corresponding to $\eta x(t - \Delta t)$. This statement implies that we are not concerned with the detailed characteristics of F^{W}; whatever F^{W} is, we can damp the oscillation via the term $\eta x(t - \Delta t)$, if the gain of the damping $(\propto \eta)$ is high enough. Feedback systems designed as based on (4.3) are called **bunch-by-bunch (time-domain) feedbacks**. In designing bunch-by-bunch feedback systems, designers implicitly ignore the nature of the term F^{W} except for its total strength. Consequently, they must prepare a system which can handle any frequency range of oscillation sources. In this sense, the term bunch-by-bunch feedback is sometimes used for the full-range feedback system.

Now we consider cases where we have some knowledge of F^{W}, in particular its frequency response. We move to the frequency domain by making the Fourier transform of (4.1) [44, 78]:

$$-\omega^2 X_i(\omega) + \omega_0^2 X_i(\omega) = \widetilde{F}^{\mathrm{W}}(\omega), \tag{4.4}$$

where $X_i(\omega)$ and $\widetilde{F}^{\mathrm{W}}(\omega)$ are the Fourier transforms of x_i and F^{W}. As a simple example, we assume $\widetilde{F}^{\mathrm{W}}(\omega)$ has a sharp peak at ω_1. The task of the feedback designer is to add a feedback term $\widetilde{F}_1^{\mathrm{FB}}(\omega_1)$ to the (4.4) in order to cancel out $\widetilde{F}_1^{\mathrm{W}}(\omega)$. Then the equation of motion including feedback is

$$-\omega^2 X_i(\omega) + \omega_0^2 X_i(\omega) = \widetilde{F}_1^{\mathrm{W}}(\omega) - \widetilde{F}_1^{\mathrm{FB}}(\omega_1). \tag{4.5}$$

Feedback systems designed using this equation are called **mode-by-mode (frequency domain) feedbacks**. Note that the feedback term is created from the signal from all the bunches in a ring, while that in the bunch-by-bunch system is made of signal of only one bunch.

Based on the above analysis the feedback system may be understood:

1. in the frequency domain – mode-by-mode feedback system
2. in the time domain – bunch-by-bunch feedback system

In a *mode by mode* feedback each mode is identified with help of a special narrow band filter centred around one of the revolution harmonics. Each mode is then processed individually leading to a feedback that consists of many narrow band systems running in parallel. In the case of HERA [59] and the B factories [69, 84, 125] the number of potentially unstable modes is very high and the amount of electronics for a mode-by-mode feedback would be extremely large. So a mode-by-mode feedback is an appropriate choice, if only a few coupled bunch modes have to be damped. For example, such a system has been in operation in the PS booster at CERN [8, 40, 139].

The time-domain approach treats each bunch as an independent oscillator coupled to its neighbours through an external driving term. Such a *bunch-by-bunch* system implements a logically separate feedback system for each bunch in a multi-bunch accelerator. It is therefore possible to implement a parallel processing strategy and spread the high sampling rate bunch information among several slower computing blocks. Since very fast digital signal processing electronics like digital to analogue, analogue to digital converters, and fast microcomputers have been developed and are commercially available, the signal processing unit of many bunch-by-bunch feedback systems has been constructed using digital electronics [9, 12, 13, 43, 45, 55, 57, 58, 59, 70, 85, 96, 101, 104, 110, 120, 126].

4.2 Demands on TFS for SIS at the GSI

The goal of this chapter is not only to design the transverse feedback system but to answer basic questions that will be raised inevitably when hardware and technology choices have to be made.

- What is the frequency bandwidth ?
- What is the gain ?
- What is the required delay step value ?
- What is the deflection strength and it is needed over the full bandwidth ?
- What is the limit of the pickup resolution ?
- What is the required power ?

Without good knowledge of the machine impedance one can not to answer the above mentioned questions. From this reason it is very important to know the frequency dependence of the impedance behaviour for all components in the ring.

Some relevant machine and beam parameters were already mentioned in table 2.1 and 3.3 and the sum of the relevant feedback parameters are shown in table 4.1. The coupling impedance was presented in figure 3.14 and 3.15. In the following these parameters will be used for the calculation of all important TFS parameters.

Bandwidth of the TFS

The performance and the efficiency of the feedback system depends on every component used in the feedback system such as pickup, the electronic of the feedback system (filter, delay, amplifier, etc.) and the exciter. Their gain and phase characteristics limit the bandwidth available for feedback stabilisation. For this reason optimisation of the hardware components for the feedback system requires an estimate of the frequency range, which should be covered by the TFS, to prevent that the beam becomes unstable.

The lower frequency limit is determined by the lowest sideband frequency at which the beam can become unstable. By using the following equation the *lower frequency limit* is thus

$$f_{\min} = \mathrm{Min}|(n-q)f_0| \approx 60 \text{ kHz} . \tag{4.6}$$

The instabilities in the lower frequency range are caused by the resistive wall impedance, because in this frequency range it is the most important contribution to the machine coupling impedance.

The upper frequency limit depends on many factors. This value was calculated from the stability diagram in chapter 3.6. Landau damping determine this frequency as well as the growth rates of the instabilities.

The frequency range, which should be covered by the TFS, is from 20 kHz to 40 MHz. The above calculated values are only an *estimation* of the frequency range and there may be a difference between values for the coasting and bunch beam.

Calculation of the feedback gain

In order to calculate the feedback gain G one should calculate the feedback impedance by means of (3.14) and parameters from tables 2.1, 3.2 and 4.1. The resulting feedback impedance for the horizontal plane is:

$$Z_{\perp,x}^{\mathrm{FB}}[\Omega/m] = 1852\ G[\pm\sin(\Delta\mu) + \mathrm{j}\cos(\Delta\mu)]\ e^{\mathrm{j}[\omega\Delta\tau]} \tag{4.7}$$

and for the vertical plane

$$Z_{\perp,y}^{\mathrm{FB}}[\Omega/m] = 1059\ G[\pm\sin(\Delta\mu) + \mathrm{j}\cos(\Delta\mu)]\ e^{\mathrm{j}[\omega\Delta\tau]} \tag{4.8}$$

where G is the total gain in the feedback loop and $\Delta\tau = \tau_{\mathrm{p}} - \tau_{\mathrm{e}}$ is the difference between the particle time of flight and electronic delay.

From (4.7) and (4.8) it is evident that the feedback system is represented by an complex impedance. The real (resistive) part of the feedback impedance with positive (negative) value is responsible for the growth (damping) of instabilities and the imaginary part is responsible for the incoherent tune shift.

In the case that the phase advance $\Delta\mu$ between pickup and exciter is an odd multiple of 90° degree and $\Delta\tau = 0$, the feedback impedance will be purely real. Then such a feedback system is called *resistive feedback system.* That means that a kick changes the transverse momentum of the beam, not the offset. Thus, the kick should occur $\pi/2$ in phase later in the oscillation, so that the measured offset is transformed into momentum.

The effect of the focusing on the feedback impedance during the acceleration process when the focusing is continuously changing from triplet to doublet, as shown in figure 2.5, is negligible. The difference between feedback impedance for the triplet (at the begin of the acceleration process) and doublet (at the end of the acceleration process) is only $\approx 100\ \Omega$. That means a difference in the gain loop of about 0.5 dB.

Now, the gain necessary to stabilise the beam can be estimated by means of (4.7) in the horizontal plane and (4.8) in the vertical plane. For a stabilising effect by the feedback system, the real part of the feedback impedance (4.7) and (4.8) must be larger than the real part of the machine coupling impedance (3.3):

$$-\mathrm{Re}\left(Z_{\perp}^{\mathrm{FB}}\right) > \mathrm{Re}\left(Z_{\perp}\right)\ . \tag{4.9}$$

Because the value of the machine coupling impedance depends on the harmonic number n, it is suggested to take the maximum value of the impedance in the estimated frequency range where the feedback system should work. The values for the machine coupling impedance can be calculated by means of equations shown in table 3.1 or can be read out from figure 3.14 and 3.15

$$Z_{\perp,x;y}[\Omega/m] = 800\ \mathrm{k} - \mathrm{j}\ 1046\ \mathrm{G}\ . \tag{4.10}$$

The calculated values are shown in the table 4.1. The minimum gain necessary to cancel the real part of the machine coupling impedance is 52.6 dB in the horizontal plane and 37.5 dB in the vertical plane. The minimum gain in the horizontal plane is about 15 dB bigger than in the vertical plane. The first reason is that the distance of the pickup plates in the horizontal plane is bigger than in the vertical plane and for this reason the difference signal from the pickup is smaller. The second reason is that the beta-functions at the pickup positions and exciter position are in the vertical and horizontal planes different.

For illustration the minimum gains in the case of the purely reactive feedback system are shown in table 4.1. A reactive feedback system is conceptually the same as a resistive one except that the phase advance between pickup and exciter must be an even multiple

Triplet		Doublet	
Pickup	Exciter	Pickup	Exciter
$\beta_x = 12.71$ m	$\beta_x = 13.45$ m	$\beta_x = 6.65$ m	$\beta_x = 26.10$ m
$\beta_y = 13.42$ m	$\beta_y = 10.55$ m	$\beta_y = 19.46$ m	$\beta_y = 7.39$ m
$\overline{\beta}_x = 8$ m		$\overline{\beta}_y = 10.4$ m	
Min. gain for resistive TFS			
$G^{\mathrm{FB}}_{\mathrm{resistive},x} = 52.6$ dB		$G^{\mathrm{FB}}_{\mathrm{resistive},y} = 37.5$ dB	
Min. gain for reactive TFS			
$G^{\mathrm{FB}}_{\mathrm{reactive},x} = 115.5$ dB		$G^{\mathrm{FB}}_{\mathrm{reactive},y} = 100.3$ dB	

Table 4.1: Specific parameters of the transverse feedback system.

of $\pi/2$ rather than an odd multiple. These gains are much higher than for the resistive feedback.

Time constants important for the TFS

One operation cycle of the SIS with injection, acceleration and extraction phase is shown in figure 4.3. In this figure two ramps are shown: the first one (top) is for the main dipol field B of the bending magnets and the second one is for the HF frequency. When one takes into account that the time of the acceleration process is more than 180 ms and the growth rates (see chapter 3.6) can be about 10 ms one need effective damping during the acceleration process.

Now, because the TFS should work during the injection and extraction as well as during the acceleration process some important parameters such as *delay times, step* and *setting times* of the variable delay should be specified.

The delay time depends on the revolution time in the SIS ring. This revolution time is derived from HF frequency of the accelerator cavity. The TFS system needs at least this one information for the correct and accurate work.

Delay times, as was mentioned already above, represent delay of the signal in the electric path. These delays can be calculated as follows

$$T_{\text{revolution time, PU}\rightarrow\text{K}} = T_{\text{system, PU}\rightarrow\text{K}} + T_{\text{variable delay, PU}\rightarrow\text{K}} \tag{4.11}$$

where $T_{\text{revolution time, PU}\rightarrow\text{K}}$ is the particle time of flight between pickup and exciter, $T_{\text{system, PU}\rightarrow\text{K}}$ represents the inherent delay time of the TFS due to connection cables, electronics, and $T_{\text{variable delay, PU}\rightarrow\text{K}}$ represents variable delay time needed for a synchronisation. The minimum and maximum delay times are listed in table 4.3.

$T_{\text{revolution time, PU}\rightarrow\text{K}}$ time is very important because the TFS should work with bunched beam where the number of bunches is changing. In this case the HF frequency will be multiplied by harmonics number Because the new ramp (this ramp coressponds to the $T_{\text{revolution time, PU}\rightarrow\text{K}}$ time) will be generated for the TFS the number of the bunches will be included in this time constant and no other constant is demanded to calculate the delays.

The next parameter of the TFS is *step of the variable delay.* This delay step value represents the resolution accuracy, or the programmability of the variable delay. This is

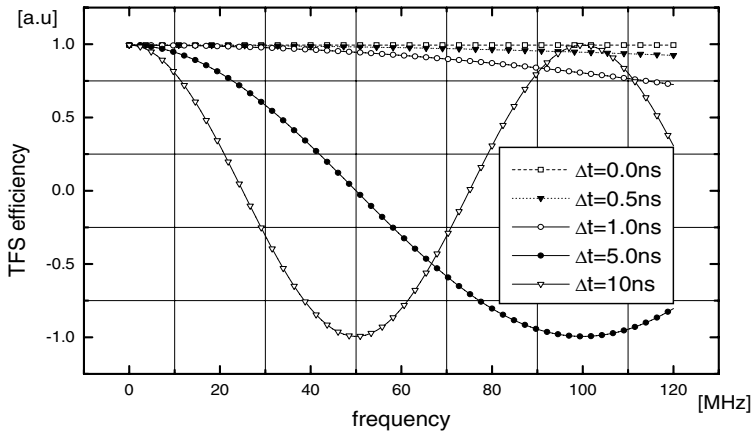

Figure 4.2: Step identification: efficiency of the feedback system for different times between the particle flight time and electronic delay time in the range from 0 ns to 10 ns for the frequency range from DC to 120 MHz. This calculation is based on (3.14) provided that $\Delta\mu$ is well adjusted.

shown in the figure 4.2 and it should be chosen considering the frequency range of the TFS. As it can be seen from figure 4.2 for higher frequency and delay step values the TFS efficiency is decreasing and at a specific value crosses zero. From this specific value upwards the TFS can not damp the coherent instabilities, but on the contrary it speeds the growth rate of the instabilities. In order to work the TFS with high efficiency in the entire frequency range (broadband system), the *step of the variable delay* should be better then 1 ns.

The lower limit of the delay step value can be calculated from the motion of particles with momentum deviation. A particle with momentum

$$\frac{\delta p}{\bar{p}} > 0 \tag{4.12}$$

travels on a revolution a longer distance than the reference particle with nominal momentum $\bar{p}$. Then the change of the circumference for this particle is [99]

$$\Delta L = L \cdot \alpha \cdot \frac{\delta p}{\bar{p}} \, . \tag{4.13}$$

The quantity α is the relative change in orbit length divided by the relative momentum deviation. It is called "momentum compaction factor" and a rough estimate in terms of the horizontal Q-value is given by $1/Q_x^2$. Then (4.13) can be rewritten for the time delay change of the particle as follows

$$\Delta t \approx \frac{\Delta L}{\beta c} \cdot \frac{1}{Q_x^2} \cdot \frac{\delta p}{\bar{p}} \, . \tag{4.14}$$

The calculated values of time delay change of the particle for injection $\beta = 0.15$ and extraction ($\beta = 1$) energy are shown in the table 4.2.

The setting time, needed for the setting the TFS delay, can be calculated from the maximum slope of the acceleration phase. In the worst case scenario the SIS cycle time is 180 ms (see figure 4.3). To change the delay in the whole range during the acceleration process with a delay step value of approximately 1 ns the variable delay value has to be changed every 44 μs.

Q_x	$\frac{\delta p}{\bar{p}}$	Δt ($\beta = 1$)	Δt ($\beta = 0.15$)
4.2	$6.5 \cdot 10^{-4}$	28 ps	190 ps
4.2	$1 \cdot 10^{-3}$	36 ps	240 ps

Table 4.2: The time delay per turn for a particle with releaive momentum deviation $\frac{\delta p}{\bar{p}}$ for two different β values and momentum deviations.

The most important parameters for the variable delay system are listed in table 4.3.

Parameter	Value
Min delay ($\beta = 1$)	722 ns
Max delay ($\beta = 0.15$)	4820 ns
Step	< 1 ns
Frequency range	20 kHz – 40 MHz
Impedance	50 Ω

Table 4.3: Key parameters for the variable delay system.

Deflection strength of the exciter

In order to calculate the deflection strength of the exciter, one should calculate the transverse momentum change of particle (conversion of the displacement in transverse momentum). For this purpose one can use (3.9) taking into account the phasor representation of both the beam voltage V_B and the input voltage at the exciter V_K. Then the definition for the transverse exciter constant which is the dimensionless ratio of change in the beam voltage to the input voltage

$$K_\perp = \frac{V_\mathrm{B} \mathrm{e}^{-\mathrm{j}\omega\tau_\mathrm{p}}}{V_\mathrm{K} \mathrm{e}^{-\mathrm{j}\omega\tau_\mathrm{e}}} = \frac{\Delta p_\perp \cdot \beta \cdot c}{e V_\mathrm{K}} \mathrm{e}^{-\mathrm{j}\omega\Delta\tau}, \tag{4.15}$$

where the $\mathrm{e}^{-\mathrm{j}\omega\tau_\mathrm{p}}$ describes the phase change between pickup and exciter for the τ_p particle time of flight and the $\mathrm{e}^{-\mathrm{j}\omega\tau_\mathrm{e}}$ describes the phase change for the τ_e electrical time of flight. The transverse exciter constant in this form includes the influence of the different time flights between the particle time of flight and electronic delay. Using the same principle like in section 3.3.2 it is now possible to find the transverse momentum change of the N particles using

$$\Delta p_\perp = \frac{N e V_\mathrm{L}}{\beta c \omega h_\mathrm{K}} \cdot \left(1 + \frac{c}{\beta c}\right) \cdot \frac{l_\mathrm{K}}{h_\mathrm{K}} \cdot 4 \tanh \frac{\pi w_\mathrm{K}}{2 h_\mathrm{K}} \cdot \mathrm{e}^{-j(\omega\Delta\tau \pm \theta)} \cdot \frac{\sin\theta}{\theta} \,. \tag{4.16}$$

As it can be seen from (4.16) the transverse momentum change is a $\sin\theta/\theta$ transit-time response. Then the kick angle received by an ion going through the exciter is given by

$$\Delta x' = \arctan\left[\frac{Re\Delta p(\omega)}{2\gamma m_0 \beta c}\right] \,. \tag{4.17}$$

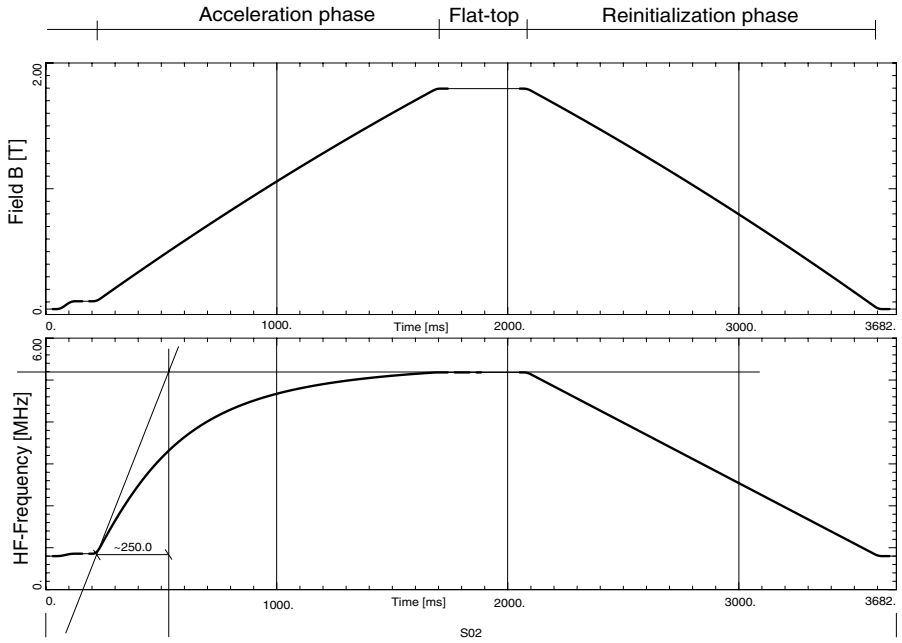

Figure 4.3: Example of full operation cycle of the synchrotron. Dipol field (top) and acceleration frequency (bottom) for $n = 4$. In this scenario the slope is about 250 ms [The figure was kindly provided by B.Franczak].

(4.16) and (4.17) describe the effect of the power connected to the exciter. From this equation it is possible to calculate the maximal power given to an ion and estimate the required power. In figure 4.4 is shown the kick angle received by an ion for the $\Delta\tau = 0$ ns, 1 ns and 5 ns and $\Delta\mu = 90°$ (achieved by vector summation). The effect of the exciter length can be calculated and the feedback efficiency can be estimated. From figure 4.4 can be concluded that the wavelength of the signal in the exciter should be larger than the exciter length ($l_{\mathrm{K}} = 0.15$ m), otherwise the beam can blow-up. Videlicet the carrying high frequency limits the length of the exciter. A decrease of the exciter length requires, naturally, an increase of the total power of the wide band amplifier for the TFS.

The limit of the pickup resolution

The practical achievable limit of the pickup resolution is one of the most important parameters for the accurate operating of the TFS.

The signal obtained by *adding* the voltages on the upper and lower plates is proportional to the total charge of the beam pulse (i.e. the current), and to first order is independent of the vertical position of the beam. On the other hand, the signal obtained by *subtracting* the voltages on the upper and lower plates is to first order proportional to the vertical position of the beam:

$$\frac{\Delta}{\Sigma} = \frac{\Delta y}{b} \tag{4.18}$$

Theoretically the sensitivity of a rectangular pick up system is given by $\frac{\Delta x}{b}$, where Δx is the beam displacement and b is half of the aperture. For the horizontal system of SIS

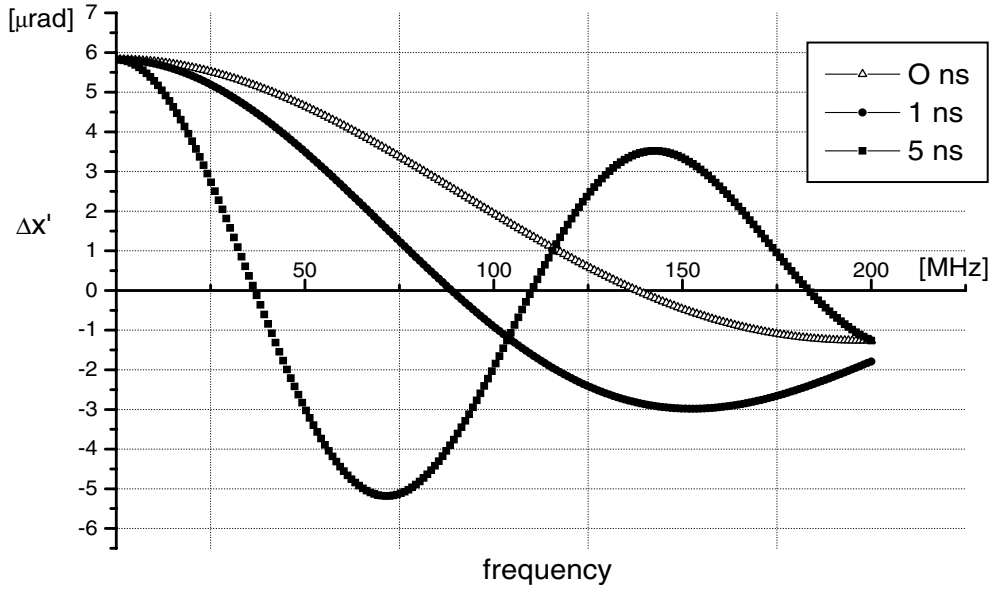

Figure 4.4: The kick angle received by an ion going through the exciter system. The different curves represent different time errors for the $\Delta\tau = 0$ ns, 1 ns and 5 ns and $\Delta\mu = 90°$.

with an aperture of $b = 200$ mm (theoretical) has been determined by test measurements to be 174 mm (effective).

The precision of the measurements of the coherent oscillations is specified by the symmetry of both channels from which the difference signal will be evaluated. The variation of the signals in the whole frequency range, in which the TFS should be active, should be taken into account. From this point of view the head-amplifiers are the most critical parts of the signal processing system. The symmetry of the both channels for creation of the difference signal is adjustable to match a pair of amplifiers to within ± 0.02 dB $= 2.3 \cdot 10^{-3}$ in the frequency range from 10 kHz to 50 MHz [111]. Then, based on (4.18), the achievable pickup resolution in the horizontal direction $\frac{b}{2} = 100$ mm is

$$\Delta x_{\min} = \frac{b}{2} \cdot \frac{\Delta}{\Sigma} = 115\ \mu\text{m} \tag{4.19}$$

and in the vertical direction $\frac{b}{2} = 70$ mm

$$\Delta y_{\min} = \frac{b}{2} \cdot \frac{\Delta}{\Sigma} = 80.5\ \mu\text{m}\ . \tag{4.20}$$

The required power

Because the gain of the whole system is known, one can estimate the power needed for the TFS. The power required for the damping of the coherent instabilities can be calculated from the maximum detected amplitude and from the minimum gain of the over all system. Using (3.8) one can calculate $V_{pp} = 140$ V. Then the required value for the power amplifier is 56 dBm.

4.3 Programmable variable delay

This section gives an overview of various techniques applicable for the programmable variable delay. The optimum method to choose then depends on the signal type, constraints on time resolution, overall delay range, power consumption, and processing data of the available technology. For a better understanding of programmable variable delay problems in case of *analogue signal*, table 4.3 gives some basic parameters of such delays.

Due to change of $T_{\text{revolution time}}$ throughout the acceleration cycle in the SIS, the TFS delay needs to be varied in exactly the same way. If the phase term (in (3.14) for feedback impedance) does not vanish completely due to unavoidable errors in tracking, this will cause the argument of the sine function to run out of the "stable" band beyond a certain frequency. This is already shown in figure 4.2. This effect is very important for *higher frequencies* and especially for *broadband systems*.

It is very important to have an accurate delay line with a precision better than < 1 ns. This variable delay will be used for the programmable variable delay as well as for the variable notch filter. The purpose of this circuit is to ensure that the total loop delay will remain equal to the variable revolution period $T_{\text{revolution time}}$ during the whole acceleration process.

There exist the following possibilities for the variable (digital, programmable) delay [91]:

1. Real-Time Digital Signal Processing [5, 10, 16, 47, 91]
2. Programmable analogue signal processor, ACT technology [5, 89, 90, 91]
3. Surface acoustic wave, SAW [89, 91]
4. Bulk acoustic wave, BAW [89, 91]
5. Electromagnetic Transmission Line (Switchable delay lines) [53, 91, 102]
6. Fibre optics [91, 105]

Table 4.4 compares technologies suitable for delay lines. Key performance parameters considered include dynamic range, maximum delay or processing time, precision, power dissipation, and size.

	ACT	Fibre optics	SAW	BAW	Real-time digital signal processing	Electromagnetic transmission line
Center frequency range	DC to 500 MHz	DC to 120 MHz (5 MHz - 4 GHz)	10 MHz to 2.5 GHz	300 MHz to 18 GHz	DC to 50 MHz	> 20 GHz
delay	20 ns to 10μ s	$\approx$ ms	to 100 μ s max	100 ns to 30μ s	indefinite	< 2 μ s
Device programmability	good	switchable delay lines	poor	switchable delay lines	good	switchable delay lines
Dynamic range	< 60 dB	< 65 (90) dB	-	-	< 65 dB (12 bit ADC)	-
Setup time	> 1 μ s	> 0.2 ms	$\approx \mu$ s	$\approx \mu$ s	$> 1/f_{\text{clock}}$	> 50 ns
Delay resolution	$\approx$ 5 ns	$\approx$ ps	$\approx$ 200 ns	$\approx$ 100 ns	$> 1/f_{\text{clock}}$	$\approx$ ps
Active or Passive	active	passive	passive	passive	active	passive
Size	small	middle	middle	middle	small	big
Temperature stability	temperature coefficient	depends on O/E and E/O	depends on material	depends on material	depends on f_{clock}	depends on circuit elements
Signal power handling cap.	small	small	high	high	small	small
RF-power	Yes	Yes	No	No	Yes	No

Table 4.4: Comparison of delay line technologies [5, 8, 35, 89, 90, 91].

4.4 Noise considerations in TFS

A variety of mechanisms can lead to an increase in the transverse beam size. Transverse feedback system with finite noise properties can be one of these mechanisms. A high noise level in the feedback system or a poor pickup resolution will lead to a fast emittance blow-up. Therefore, in addition to the general requirements of a transverse feedback system (such as the power or exciter voltage, the bandwidth, the gain, etc.), one needs in particular to specify the noise level or, equivalently, the pickup resolution of the feedback systems for the purpose of controlling the emittance growth [39].

Quantization noise

In any feedback system, one must make sure that the sensor noise (error in a sensor reading due to the properties of the sensor and its electronics, not the beam motion) is small enough so it does not significantly degrade the loop performance. Any errors in the sensor readings pass through the feedback controller equations, affect the actuator setting calculated and hence perturb the beam.

In a digital loop there is an additional source of noise. The quantization noise is typically one half of the least significant bit of the ADC. If the ADC does not have enough bits, loop performance will be degraded. This occurred for example, in the transverse feedback at the CERN SPS [24]. The implementation of this feedback is mostly analogue. However, a long delay time is needed (corresponding to the time it takes the beam to go around the ring) so that the kicked bunch will be the same one that was measured. This delay is accomplished by digitising the signal with an 8 bit ADC and then later putting it back through a DAC. It turns out that the single bit noise introduced by the digitisation is significantly larger than the analogue noise of the system. In fact the digital noise is large enough that the feedback loop would disrupt the stored or accelerated beams.

The variance, or noise power added to a signal, due to n+1 bits of quantization (including sign) is given by [24, 39]

$$B_{\mathrm{D}} = \frac{q_{\mathrm{D}}^2}{12} = \frac{2^{-2n}}{12} \tag{4.21}$$

where the q_{D} is the quantization level. The effective noise value is then given by [24, 39]

$$A_{\mathrm{D}} = \sqrt{B_{\mathrm{D}}} = \frac{q_{\mathrm{D}}}{\sqrt{12}}\,. \tag{4.22}$$

4.5 Theoretical consideration

To help guide the feedback design processes and to understand better the instability phenomena a computer simulation of the oscillations and the corresponding feedback system can be used. The importance of the simulation was shown clearly in the LEP CERN where the first operation of the TFS was done without the support of simulation studies. The beam became systematically unstable as soon as the feedback system was switched on. With better insight obtained from simulation studies a second experiment was carried out using improved parameters (phase errors, maximum kick strength, pick-up noise) [23, 46, 100]. The simulation addresses issues such as required feedback power and gain, noise (quantization noise, pickup resolution), bunch offsets and varying initial bunch conditions as well as the all timing parameters. One of the most important issues in the simulation are to determine if the specified power (the gain of the feedback system) is adequate to damp the beam oscillations under a variety of conditions.

As it was already mentioned in section 4.1.1 the method with two pickups will be used as a promising method for exact adjusting the phase advance between "virtual" pickup and exciter. Use of two monitors provides phase insensitivity.

4.5.1 System model

Because the detected signal at the pickup is the center of charge of the beam, we shall use the single particle model (rigid bunch) of coherent beam motion and linear optics to illustrate the working of the system and derive its properties. Figure 4.5 shows the essential components of a transverse feedback system where a fully decoupled motion in both horizontal and vertical plane is assumed, and the motion is restricted to a single plane. Assume, a source of the oscillation with a growth rate which represents our instability is simulated by means of an exponentialy growing function. Two pickups PU1 and PU2 (SIS devices S04DX5H and S05DX5H) were chosen because of their position near to the electronic room where the entire TFS hardware is installed. These pickups detect the amplitude of the coherent oscillation and from these two signals the signal for the "virtual" pickup PU3 is calculated. The obtained signal is delayed and then used for the exciter. For simplicity, the exciter (SIS device S04TFH) is taken as a thin element that changes only the phase but not the displacement at its location. Due to power limitation of the exciter, the phase is reduced a small amount each revolution, and many kicks are required. As the direction of the phase can be different each time, the kick direction has to be adjusted accordingly. The transfer function of the stripline exciter based on the (4.17) is being used in the simulation.

4.5.2 Vector summation

By combining the signals from PU1 (x_1, x_1') and PU2 (x_2, x_2') it is possible to calculate the signal for the "virtual" pickup PU3 (x_3, x_3') which has 90° phase advance to the exciter. The signal from the PU1 position will be transferred to the PU3 position by the transport matrix (2.9)

$$\begin{bmatrix} x_3 \\ x_3' \end{bmatrix} = \begin{bmatrix} A_1 & B_1 \\ C_1 & D_1 \end{bmatrix} \times \begin{bmatrix} x_1 \\ x_1' \end{bmatrix} \tag{4.23}$$

and the signal from the PU2 position by

$$\begin{bmatrix} x_3 \\ x_3' \end{bmatrix} = \begin{bmatrix} A_2 & B_2 \\ C_2 & D_2 \end{bmatrix} \times \begin{bmatrix} x_2 \\ x_2' \end{bmatrix} . \tag{4.24}$$

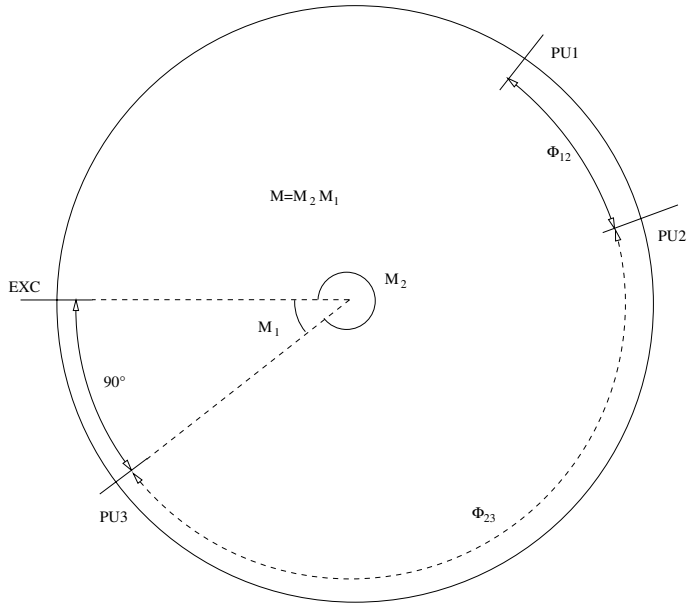

Figure 4.5: Parameters definition for simulation of the TFS damping rate.

Because in (4.23) and (4.24) both phases of the detected signals (x_1', x_2') are unknown, one must combine both equations to calculate the correct signal for the exciter. Combining (4.23) and (4.24) one gets the parameters for the 'virtual' pickup PU3 (x_3, x_3') only as a function of the measured signals x_1 and x_2 from the both pickups

$$\begin{bmatrix} x_3 \\ x_3' \end{bmatrix} = \frac{1}{B_2D_1 - D_2B_1} \cdot \begin{bmatrix} (A_1B_2D_1 - B_1C_1B_2) & (B_1C_2B_2 - B_1D_2A_2) \\ (D_2A_1D_1 - D_2B_1C_1) & (C_2B_2D_1 - D_2A_2D_1) \end{bmatrix} \times \begin{bmatrix} x_1 \\ x_2 \end{bmatrix} . \tag{4.25}$$

The coefficients of the transport matrix are complicated functions of the lattice functions. If one of these parameters is changing then the transport matrix will be changed. That happens for instance during the acceleration process or due to tune changes.

The (4.25) can be written as follows

$$x_3' = g_1(\beta, \alpha, \mu)\, x_1 + g_2(\beta, \alpha, \mu)\, x_2 . \tag{4.26}$$

The pickups PU1 and PU2 detect the amplitude of the coherent oscillation. The obtained signal (x_3, x_3') for the "virtual" PU3 will be used after delay and amplification of the signal as correction signal for the exciter.

4.5.3 Simulation studies

In the following simulations are presented for $^{238}U^{72+}$ with $dp/p = 1 \cdot 10^{-3}$ and for the horizontal plane. The input parameters for the simulation are listed below:

$\Delta\mu$ - betatron phase advance is adjusted by means of vector summation. In ideal case it should be 90°.

y_A - is the initial amplitude of the betatron oscillation.

q_D - is the quantization level or resolution of the ADC.

noise - represents the maximum noise level in the system. This is simulated by a random function with maximum noise amplitude.

$\tau_{risetime}$ - depends on the harmonic number n. The rise times are calculated automatically for each mode from the real part of the coupling impedance.

$Q_{x,y}$ - is the machine tune. This value influences the phase advance between virtual pickup and exciter and it is compensated by vector summation.

G - is the total TFS gain. From this value the maximum useable voltage at the exciter is calculated. If this value is bigger than $V_{pp} = 140$ V then a constant kick will be generated. This represents the saturation of the power amplifier.

$\Delta\tau$ - is the effect of the time difference between particle flight time and electronic signal transit time. It represents the synchronisation between the measured signal at the pickup and the applied signal at the exciter.

Furthermore, in the simulation program it is possible to chose the number of revolutions *without* instabilities and *without* TFS, the number of revolutions *with* instabilities and *without* TFS, the number of revolutions *with* instabilities and *with* TFS.

The program starts with the input of all parameters of the beam and the feedback system. Then the initial conditions are defined. For all calculations we arbitrary set $y_0 = y_A$ and $y_0' = 0$. At first program calculates the transverse coupling impedance using equations from Table 3.1 and transverse feedback impedance from (3.14). For the boundary conditions the rise times from (3.19) and (3.25) for every harmonics are calculated. Then the minimum gain of the system is calculated and its value is compared with given input gain. In the range of the allowable input amplitude of betatron oscillation using (3.8) multiplied by calculated gain the output voltage at exciter is tested if within this range its value is exceeded or not. If such an input amplitude is found the program takes it into account during the simulation. Then using (4.17) calculation is done for the kick angle received by an ion going through the exciter system in the whole frequency range for each harmonics. During the simulation the pickup resolution defined by (4.19) as well as the noise power added to a signal due to quantization defined by (4.22) are taken into account.

The program calculates the vector (y_{n+1}, y'_{n+1}) in the betatron phase space at the end of the (n+1) revolution. From this vector we derive the oscillation amplitude. Finally the program defines new initial conditions for the next revolution setting and starts the same procedure again.

After one revolution, including the effect of the exciter with the one turn matrix (M), the vector (y_{n+1}, y'_{n+1}) in the betatron phase space at the end of the (n+1) revolution is

$$\begin{bmatrix} y_{n+1} \\ y'_{n+1} \end{bmatrix} = e^{\left[\frac{-\mathrm{L}}{\beta c \tau_{\mathrm{risetime}}}\right]} \cdot \mathrm{M} \begin{bmatrix} y_n \\ y'_n \end{bmatrix} + \begin{bmatrix} 0 \\ \Delta y'_n \end{bmatrix} . \tag{4.27}$$

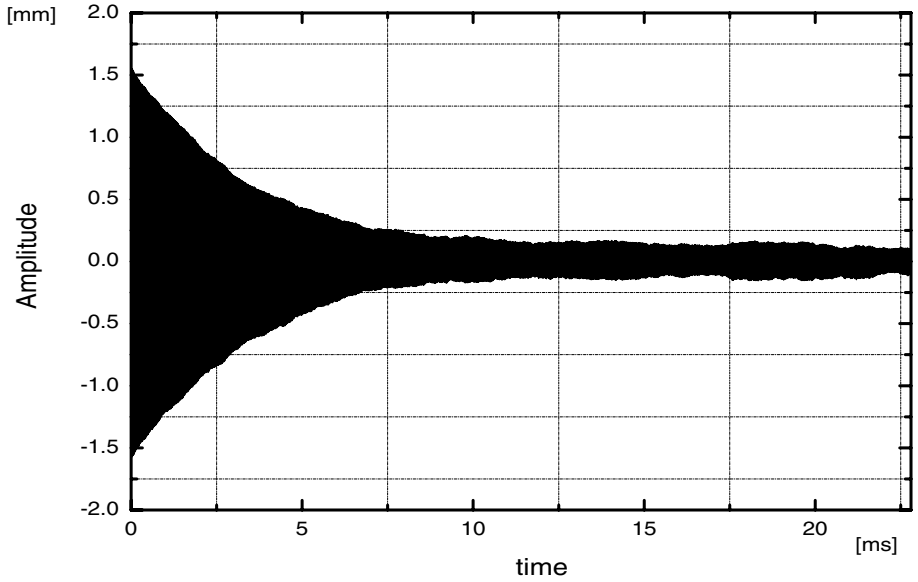

(a) kick with the power proportional to the pickup amplitude

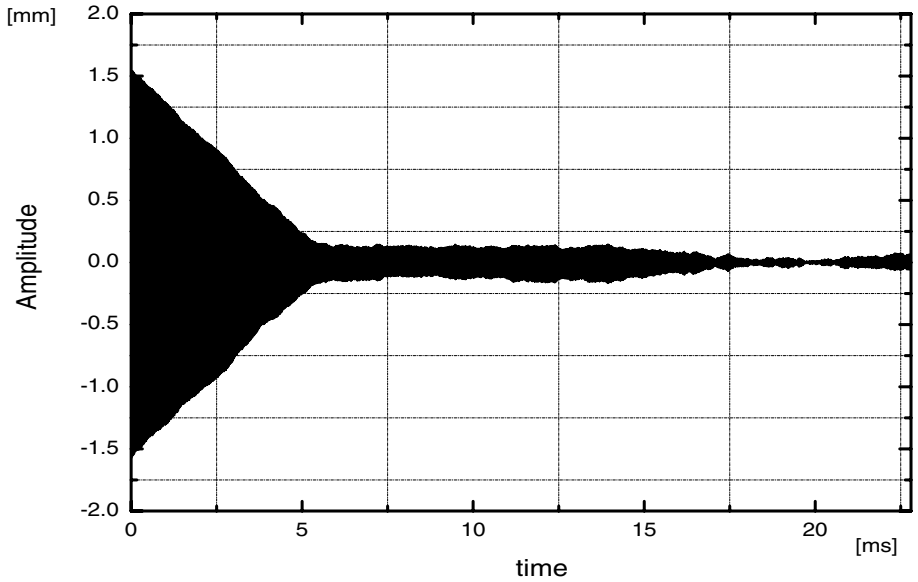

(b) kick with constant power

Figure 4.6: Simulated damping methods (for injection and coasting beam) with different kicking methods. The calculated amplitude at virtual pick-up position PU3 is displayed vs time.

The hardware limitations which can affect the feedback performance are the accuracy of the pickup system and the maximum deflection which can be delivered by the exciter. For what concerns the pickup system, the main problems are the errors affecting the measurement of position at each pickup, and the deviations of the pickup gains g_1 and g_2 (4.26) from a perfect setting, i.e. the one corresponding to a 90° phase advance between

the virtual pickup and the exciter. In the following the influence of the above mentioned input parameters on the TFS damping rates will be studied.

TFS with linear and exponential damping

In the following results from simulations for the comparison between the proportional damping and damping with constant kick amplitude are given (figure 4.6).

The proportional scheme is the typical method used in the accelerators. In this case we neglect throughout the possibility that the requested exciter voltage exceeds the hardware capability. In order to damp the transverse coherent oscillations by the feedback system with proportional damping the $\Delta y'_n$ has to be controlled by a measured signal which is proportional to the transverse deviation of the beam. The beam deviation from the equilibrium orbit at the electrodes is calculated as follows

$$\Delta y'_n \left(e^{\left[\frac{-\mathrm{L}}{\beta c \tau_{\mathrm{risetime}}}\right]} \cdot \begin{bmatrix} 1 & 1 \\ 0 & 0 \end{bmatrix} \cdot \mathrm{M}_2 \begin{bmatrix} y_n \\ y'_n \end{bmatrix} \right) . \tag{4.28}$$

The second method considered is using the same equation for the calculation of a “virtual” pickup amplitude at PU3. In this case the kick amplitude is constant and depends only on the sign of the beam displacement. During the simulations the following boundary conditions were considered

$$G = 250 \qquad \Delta\tau = 0 \text{ ns} \qquad \beta = 0.158$$

$$\tau_{\mathrm{risetime}} = 115 \text{ ms} \qquad q_{\mathrm{D}} = 100\ \mu\mathrm{m} \qquad \text{noise} = 115\ \mu\mathrm{m}\ .$$

In order to compare the damping rate of both kicking schemes the simulations shown in figure 4.7 were done. Three different simulations were performed: proportional kick, constant kick with 10% and with 100% of maximum power.

As it can be seen from figure 4.7, under certain condition the kick with constant magnitude is faster than the conventional proportional damping. The proportional damping produces an exponential damping with time and ’bang-bang’ damping (constant kicking) provides a linear damping of the magnitude with time. In reality under certain conditions both presented methods can be used together.

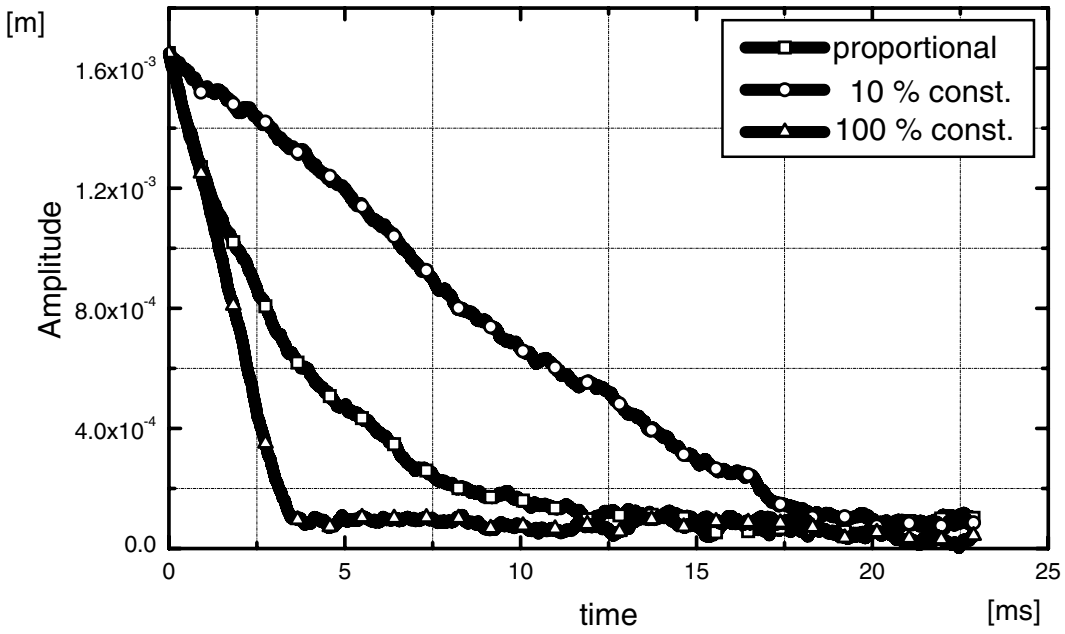

Figure 4.7: Simulations for different kicking methods. The amplitude was simulated at virtual pickup position PU3.

Phase errors

In the following the effect of the phase errors is simulated. Because the vector sum is calculated on-line in real time, some errors during this calculation should be taken into account. The possible errors can be caused by the short delay between both pickups, the calculated coefficients and the multiplication function. The ideal phase advance between the 'virtual' pickup PU3 and exciter is 90° and the active phase is within the range from 0 to 180°. The results of these simulations are shown in figure 4.8. The three different simulations were done for $n = 4$ harmonic number with $\tau_{\text{risetime}} = 115$ ms.

The following simulation was performed for two different harmonic numbers $n = 4$ and $n = 200$ as a function of the phase advance $\Delta\mu$. During these simulations the following boundary conditions were considered:

$$G = 250 \qquad \Delta\tau = 0 \text{ ns} \qquad \beta = 0.158$$

$$\tau_{\text{risetime}} = 115 \text{ ms} \qquad q_{\text{D}} = 100\ \mu\text{m} \qquad x_{\text{A}} = 1.6 \text{ mm} .$$

The results of this simulation are shown in figure 4.9. For $n = 4$ is the feedback working up to 20° and for $n = 200$ it is working up to 28°. The damping times are for $n = 200$ higher than for the $n = 4$ due to the transfer function of the exciter (4.17).

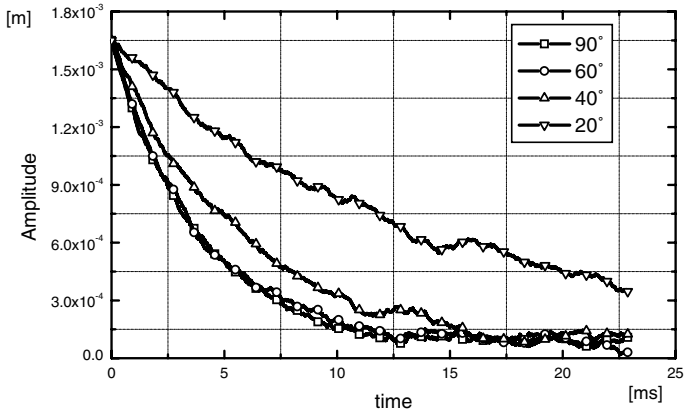

(a) proportional kicking

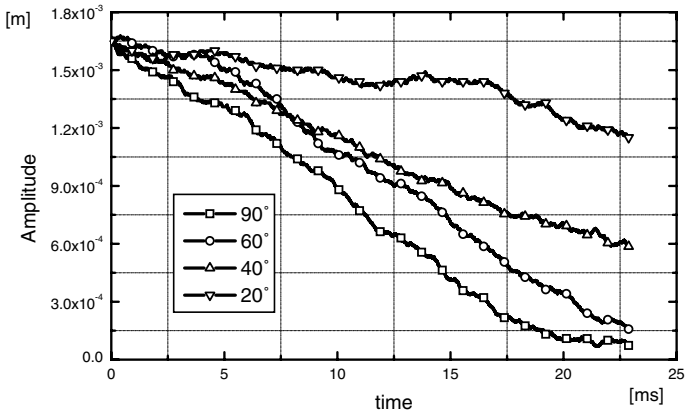

(b) constant kick with 10 % of power

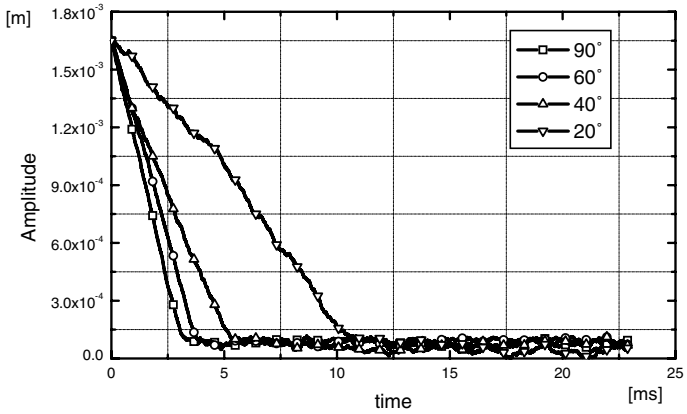

(c) constant kick with 100 % of power

Figure 4.8: Simulation of the damping rate for $\Delta\mu = 90°, 60°, 40°$ and $20°$ for a) proportional kick, b) constant kick with 10% of maximum power and c) constant kick with 100% of maximum power.

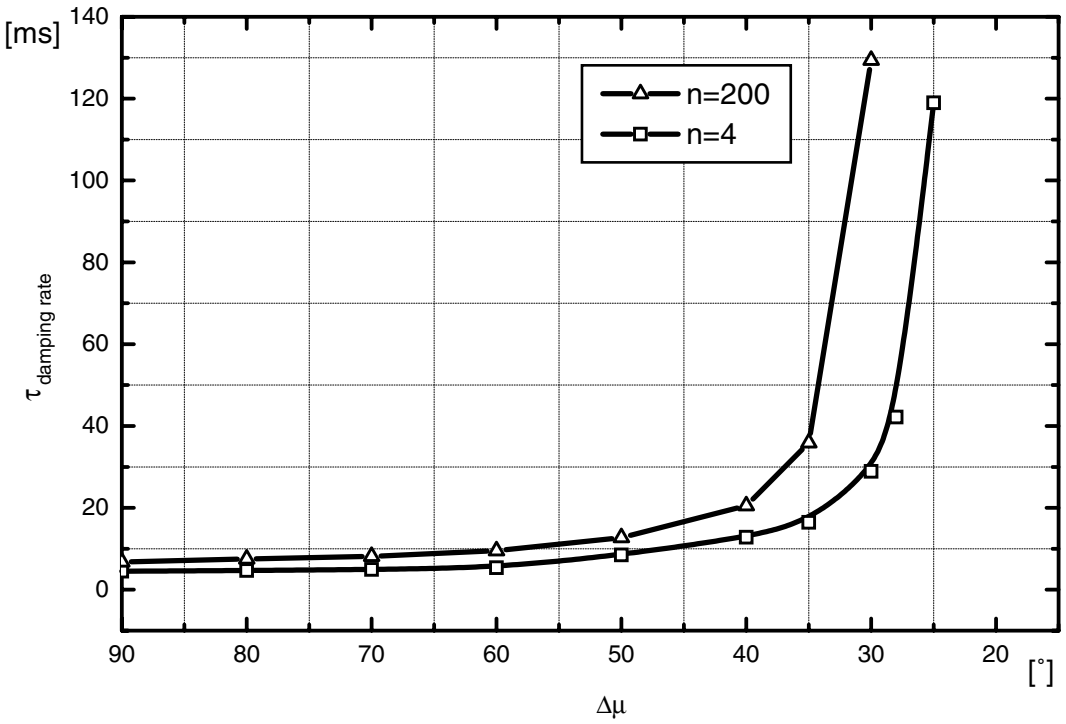

Figure 4.9: Simulation of the damping rate for $n = 4$ and $n = 200$ for different $\Delta\mu$ with proportional kicking.

Variable delay errors

The influence of the variable delay errors was investigated. This error means that for higher frequencies the TFS system is not able to damp any instability, because the "correct" signal for the exciter is coming earlier or later. In this case the measured signal does not correspond to the applied signal at the exciter. In order to demonstrate the influence of this phase error on the damping rate, figure 4.10 shows two different cases.

These simulations were performed for two different times $\Delta\tau = 10$ ns and $\Delta\tau = 5$ ns as a function of frequency. The following boundary conditions were considered:

$$G = 250 \qquad \beta = 0.158$$

$$q_{\mathrm{D}} = 100\ \mu\mathrm{m} \qquad x_{\mathrm{A}} = 1.6\ \mathrm{mm}$$

The corresspondig τ_{risetime} were calculated for each harmonic number independently. The calculated maximum frequency for two different exciter lenghts as a function of different times between the particle flight time and electric transit delay time are shown in figure 4.11. For certain adjusting "time-error" the TFS does not work from this limit frequency and the system can speed up the coherent instabilities. The reason is, that the transfer characteristic of the feedback system is crossing zero. It corresponds with plots shown in figure 4.10. In this figure maximum frequencies for two different exciter lengths $l_{\mathrm{k}} = 15$ cm and $l_{\mathrm{k}} = 75$ cm as a function of different times between particle and electronic flight transit delay time are shown.

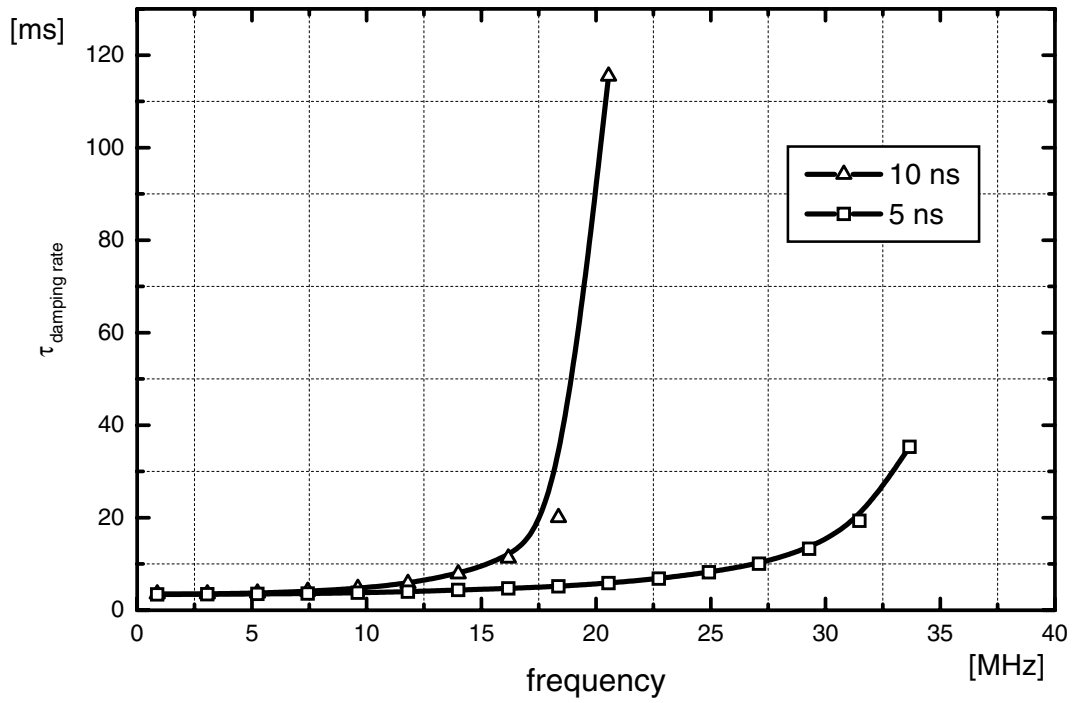

Figure 4.10: Simulation of the damping time as a function of frequency for two values of time difference between particle flight time and electronic signal transit time from pickup to exciter.

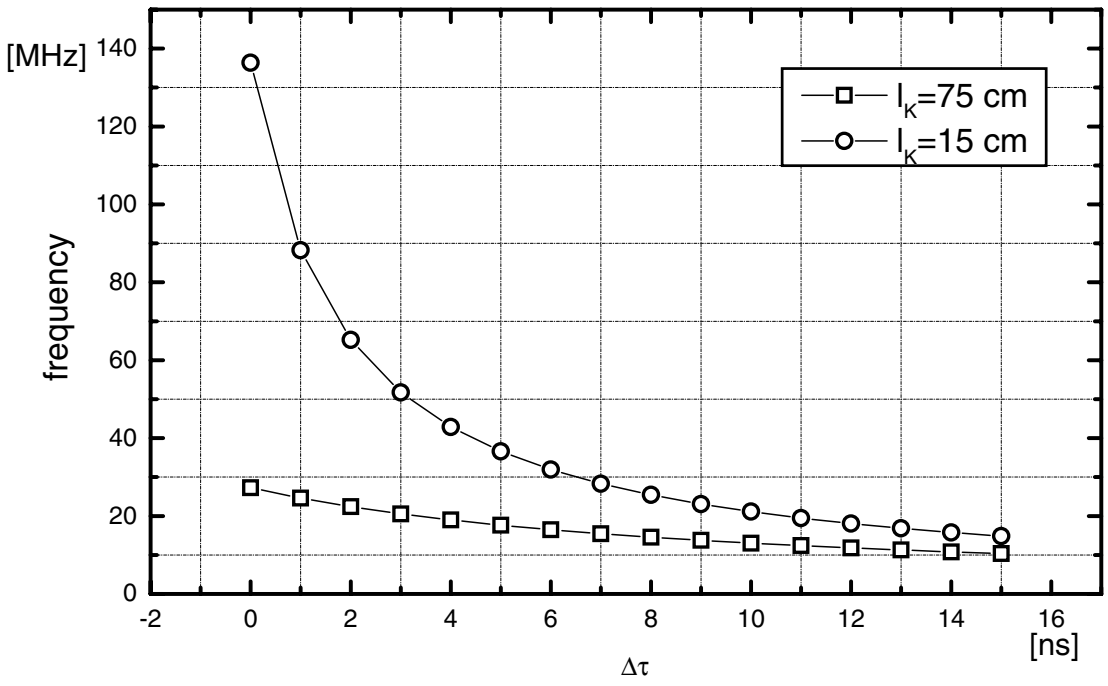

Figure 4.11: Calculation of the maximum frequency for damping action of the TFS for two different exciter lengths $l_\mathrm{k} = 15$ cm and $l_\mathrm{k} = 75$ cm as a function of time difference between particle flight time and electronic signal transit time from pickup to exciter.

System gain

The simulation was done for harmonic number $n = 4$ as a function of the system gain with following boundary conditions

$$\Delta\tau = 0 \text{ ns} \qquad \beta = 0.158$$

$$\tau_{\text{risetime}} = 115 \text{ ms} \qquad q_{\text{D}} = 100\ \mu\text{m} \qquad x_{\text{A}} = 1.6 \text{ mm} .$$

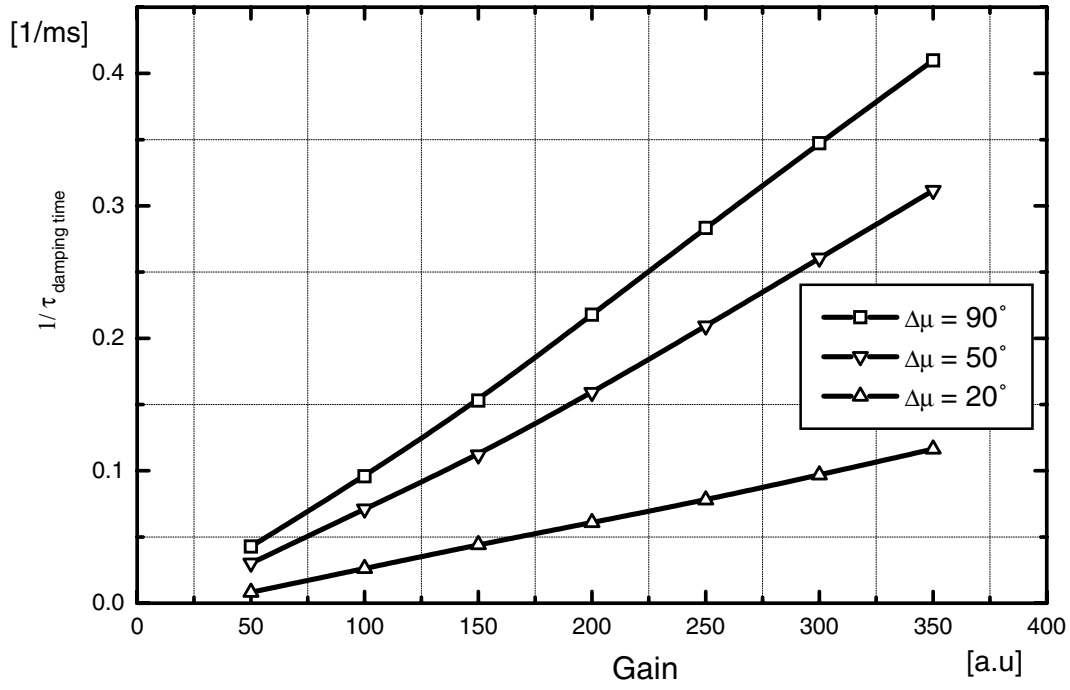

Figure 4.12: Simulation of the damping rate as a function of the system gain for different phase advances $\Delta\mu$ between "virtual" pickup PU3 and exciter.

The reciprocal value of damping time as a function of system gain was simulated. Three different curves are shown in figure 4.12.

4.6 Comparison and conclusions

In this chapter we discussed and listed different methods and technologies for transverse feedback systems and for the programmable variable delay and its comparison. The following methods for adjusting of phase advance between pickup and exciter were compared and discussed in detail: *phase-rotation technique*, *multi-turn technique* and *filtering technique*. The theoretical description and simulation results were presented for the two different damping methods. Their advantages and disadvatages were analysed. The mathematical analysis were performed for the transverse feedback system working in the time and frequency domains.

Analogue systems were successfully installed and commissioned in many accelerator facilities. On the other hand, the programmability of the most wideband analogue devices

has been lacking. The analogue loops are more difficult to change as one learns more about the problem and usually include fewer built-in diagnostics.

The digital systems were used only for some special parts (delay, notch filter with subtraction) of the feedback system and not for the entire feedback system. To process wideband analogue signals without distortion, the digital systems with 8 bits were only implemented with very simple mathematical operations. Because of the dynamic range of the feedback system the digital systems with more than 8 bits are desired particularly for the notch filter. The changing of the parameter (FIR coefficients, variable delay) was not possible during the acceleration process or it was possible only in the very small range. In the case that the RF revolution frequency was changed only in the small range, the clock signal for the digital system could be directly connected to this RF frequency multiplied by a constant. When changing the RF frequency the sampling frequency is changing too. In this case the frequency bandwidth of the processed wideband analogue signal is changed.

Until now the other limiting parameter of digital systems was the very high demand on the data processing throughput (> 500 MBytes/s). Because the new signal is delivered from detectors every clock signal and in the same time, the required calculation should be done delivering such processed signal to the exciter. Systems with very high data rate are desired. In this case parallel systems can be implemented. The disadvantage of a such system is a decrease of the time resolution.

Maintaining a proper delay is one of the most difficult problems in designing a wideband damper system for a beam with changing velocity during acceleration. This is the essential difference to high energy proton synchrotrons. The revolution period gets shorter as the beam is accelerated, and the total electrical delay from pickup to exciter must match the varying beam flight time. One way to solve this problem is to sample the beam digitally and delay the digital signal for a number of clock pulses. The most important disadvantage of the digital system for the variable delay is the achievable resolution which is very much limited by the maximum clock rate. Every frequency component of the delayed signal should be eqally delayed without dispersion. If there is some dispersion in the system the signal at the exciter is not correct and can cause the beam or for some frequency components can invoke to speed up coherent instabilities. The possibilities for variable delays were investigated and compared in detail. Concerning the design of a new TFS, we conclude that the main problems are to realise broadband non-dispersive variable delay in the range up to 10 μs (for correction in the second turn) and to allow mathematical operations in real time.

From the figure 4.2 can be seen that the frequency band of the analogue signal and the delay step value defining the circuit's resolution are coupled. Both parameters determine the efficiency of the TFS.

In order to understand the effect of some parameters (noise, pickup resolution, rise times, gain, phase advance and different times between particle flight time and electronic time) simulations were done. A comparison of different working methods (proportional and constant kick) under different conditions was also presented. The results obtained from these simulations shows which parameters are important for the design of a new TFS. We demonstrated, for instance, that:

- the damping time for 40° phase advance between "virtual" pickup PU3 and exciter is by factor 2 bigger than for 90°.
- the reciprocal value of the horizontal damping time is linearly dependent on the system gain.

- for a certain exciter length and time difference between particle flight time and electric transit delay time, an upper limit of the frequency exists above which the feedback system does not damp.
- a constant damping scheme provides a linear damping of the beam amplitude and additionally, for the same peak power it is faster than the conventional proportional damping scheme which produces an exponential damping in time.

There is no doubt that digital signal processing has gained its widest acceptance because of *programmability* and *accuracy*. The digital feedback system is more useful than the analogue feedback on both sides of research and operation, since the reproducibility in the operation is excellent. The digital approach has the advantage that economical and flexible systems can be built.

Chapter 5

Signal treatment using digital processing

The main parameters of a feedback system were specified in previous chapters. The challenging problem is to be able to vary parameters of a feedback system when a TFS system is running, without interrupting the analogue signal processed. To ensure such high demands on a system some novel methods for data processing are presented. Data transfer rate of the technology to be chosen has to be very high because the system should work on-line in real-time with changing parameters. Basing on chapter 4 and taking into account the choices described in table 4.4, *real-time digital signal processing* is the most promising data processing method for that [8, 13, 16, 47, 86, 95]. This signal processing method is discussed here.

5.1 Digital implementations

Due to the required high dynamic range and high resolution, a 12 bit system was implemented. For the frequency range up to $\approx$ 40 MHz, the 100 MHz minimal system clock frequency based on Niquist criteria should be chosen. According to the Niquist criteria, the sampling frequency has to be more than two times higher than the highest frequency in the processed analogue signal.

A digital signal processing system satisfying the requirements for a TFS system running with 12 bits/100 MHz was not available up till now. For this reason such a system is investigated and studied in the following.

Before starting "real" implementation one should choose the relevant technology. Nowadays, from all accessible and applicable digital technologies only *PLD - programmable logic devices* [4, 112, 135] and *DSP - digital signal processors* are available for such a purpose [30, 113, 117]. Because of the high clock frequency and high data rate to be processed other technologies cannot be used [112, 134, 135].

A *PLD* is a programmable logic device that can be programmed in situ. For our application it is important to have the possibility to simulate both logic functions and delays. One disadvantage with these devices is the fixed point arithmetic, but this problem can be partially solved [4, 135].

On the other hand, the main advantages of the *DSP* are flexibility, floating point operation and simple integration of control and diagnostic functions [112, 113, 115].

Both PLD and DSP digital processing technologies will be applied together - **ALTERA PLD will be used as DSP co-processor due to the fact that the PLD can handle repetitive functions with extremely high performance and the DSP processor can perform remaining functions**.

System analysis will be divided into the two parts:

main card with PLD – data processing from both pickups and signal calculation for the exciter. This part interacts directly with the measured signal and, hence, represents a more time-critical part of the system.

control card with DSP – data processing from the *main control room* as well as a "watch-dog" for the main card. Since signals from both pickups are available on each clock pulse, the processed signals from the *control card* have to be send into the *main card* without interrupting pickup data processing.

Both main and control card are shown in figure 5.1 [97].

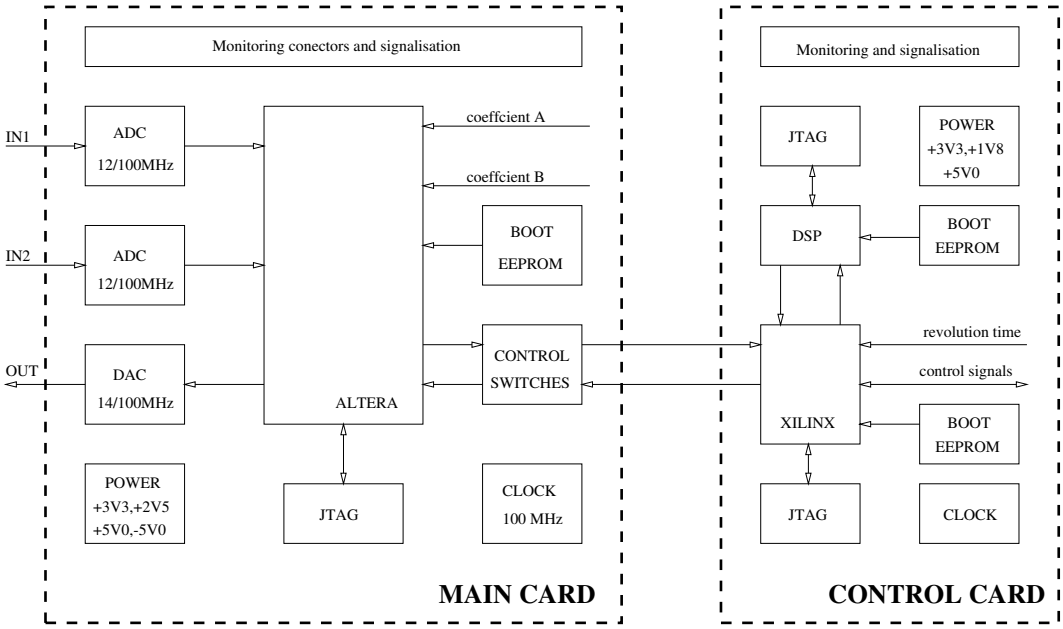

Figure 5.1: Principal scheme of the main and control card [97].

5.1.1 Main card

In order to process the data measured, the following tasks should be implemented in the ALTERA chip:

short delay – the delay between both pickups PU1 and PU2. This delay can vary from 60 ns to 400 ns. It is realised as a digital dual port memory ($12 \cdot 40$ bytes ≈ 480 ns).

long delay – the delay between pickup PU2 and exciter EXC. To evaluate this delay one should take into account the possibility to use a correction signal in the second turn. Then the delay can vary from ≈ 700 ns to 9.64 μs. For this task, a digital dual port memory is used ($14 \cdot 1000$ bytes ≈ 10 μs).

both multiplication's – since the new signal is coming every new clock signal (10 ns) and in the same time the calculated signal has to be ready for use at the exciter on each clock signal, the only possibility to multiply online is pipelining.

summation – two signed 24 bit words are to be added each new clock signal. The special care should be taken for the signed summation.

data encoding – due to different data coding used by ADC and DAC.

The complete block design of all functions implemented in the chip are shown in figure B.1, B.2 and B.3.

Multiplication

Due to the vector summation, two multiplications 12·12 bit words are to be implemented in the chip. Design of one sign multiplication together with data encoding for the converters is shown in figure B.3. The results of simulations with a 30KE chip for different optimization methods are shown in figure 5.2. System-clock frequency dependence on output latency shows that the clock frequency of 100 MHz cannot be achieved without pipelining. In the worst case, the variable delay is about 600 ns. Thus the optimum 4 or 5 clock cycles output latency (40 or 50 ns) can be used.

In figure 5.2 three different simulations are shown: with optimisation for speed (30KE SPEED) and for area (30KE AREA), and without optimisation (30KE NORMAL) [1, 4].

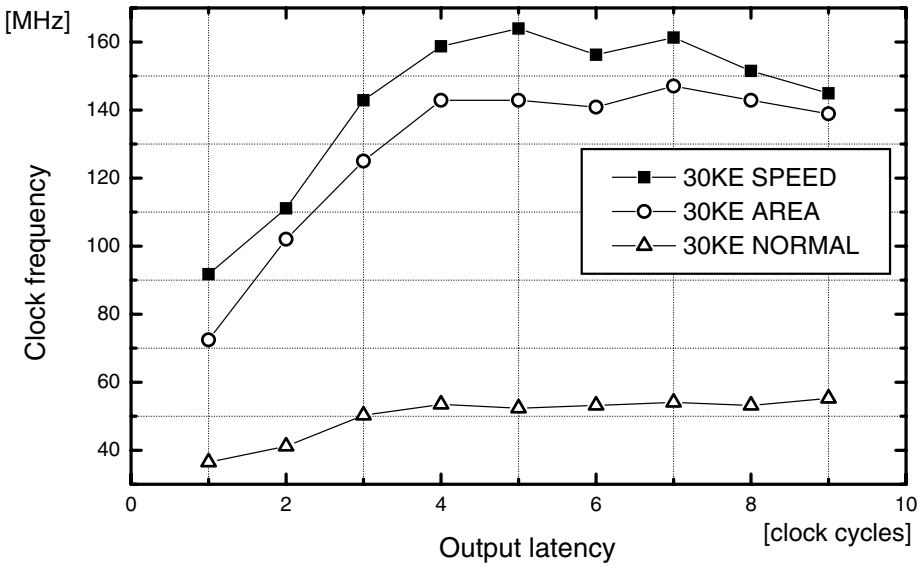

Figure 5.2: Simulation results for real-time floating sign multiplication $12 \cdot 12$ bit words with coding for converters.

A system without optimisation is able to work only up to approximately 50 MHz. With speed optimization method, it is possible to achieve a maximum system clock frequency about 15% higher than for area optimization method. The maximum achievable frequency is 164 MHz for 5 clock cycles output latency. This is very important because

the other part of the TFS systems should be implemented in the same chip and, therefore, the clock frequency will be decreased [4].

If the coefficients for multiplication are constant during the acceleration process, the look-up-table method for multiplication can be used to increase the maximum system clock frequency. Constant multiplication coefficients can be used with look-up-table method in memory and can be precalculated. Then the digital word from pickup represents the address in the look-up memory.

Switching

Until now, systems of variable delay have some disadvantages. The switching time depends on the length of the delay required. Setting up a new delay time value goes along with generating an "error" signal for the exciter. Since the acceleration process is characterised by monotonicity and continuous slope, the delay can be changed without interruption of the processed analogue signal. The exciter receives always the correct signal, and by this way the efficiency of the TFS can be increased.

This is done in the dual port memory with automatically running counters (see figure B.2). At power-up or at the beginning of the new accelerator cycle, the dual port memory addresses are initialised and the memory contents are filled with zeros. The left side address – input – is set up with a value corresponding to the value of the delay (the address represents a delay for injection energy level). The right side address – output – is filled with zero. Once the counters are loaded with correct value corresponding to delay control, the processor starts "free" running of counters. From this moment the processor on the control card monitors only the operation of the main card. Then, a new delay time value during acceleration process is setting up only by means of one digital signal – stop signal. It depends on requirements (acceleration or deceleration), whether we need to increase or decrease the delay time value. Control processor stops the appropriate counter for one clock cycle. Because other counter is running, its content will be increased with 1. The new difference between counters will be changed and will correspond to the new delay value.

5.1.2 Delay step value increasing

Because of using two pickups for a vector summation, both delays should be implemented in the system with a resolution better than 1 ns. The achievable digital-system time resolution is given by the system clock frequency. A novel method is used for its increase.

Two solutions can be commonly used to solve the problem of increasing the *delay step resolution*:

- implementation of a digital phase shift into the clock signal
- combination with the analogue technique

Both methods will be analysed below in detail.

Digital fine delay

To delay a digital signal with a resolution higher than the system clock frequency each digital input from one pickup and output signal for the exciter should run through the fine

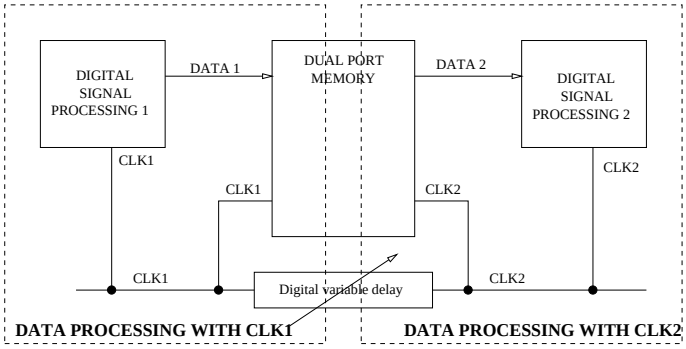

Figure 5.3: Dual port memory used for the clock signal splitting.

digital delay. Since of each delay needs to be programmable, problems with synchronisation such a large number of control bits arises.

In order to solve this problem only clock signal is delayed. This is possible to do only with dual port memory as shown in figure 5.3. Both "write" and "read" clock signals are separated. To use this technique the **digital signal should stay in one chip** like a dual port memory. This is a very important condition, otherwise all bits coming in the next cycle will be mixed with bits from the previous cycle. After splitting the clock signal, all signals on the right side of the dual port memory should run with read clock. The results of simulations with ALTERA are shown in figure 5.4.

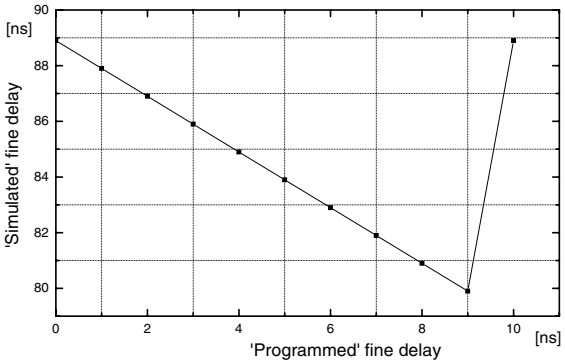

Figure 5.4: The clock splitting simulation for dual port memory.

Analogue fine delay

The analogue version for the time resolution increase is shown in figure 5.5. In this case the fine delay resolution depends on the LSB (last significant bit) bit. A delay with resolution of 25 ps and with the total length 12.5 ns (9 bits) was used. The analogue signal is switched to go through the delay (1.bit, 2.bit, etc.) or to run through the short connection without delay time. Due to very high damping in the signal path, a longer delay is not possible to implement [53].

Long, Short, and Fine delays

As implication of two pickups two variable delays need to be used. *Short delay* is the delay between both pickups. The time value of this delay depends on the position of

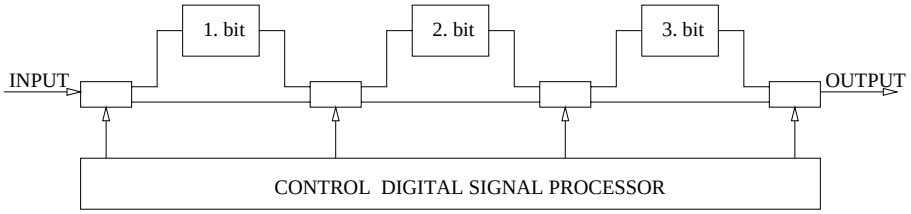

Figure 5.5: Delay line switches with three bits.

both pickups in the ring. *Long delay* is then the entire delay needed for a synchronisation between pickup and exciter.

In order to use only one digital system for both the short and the long delay, two fine delays have to be used. One fine delay is inserted ahead of a ADC and it works together with short delay, and the second fine delay is used for adjusting delay together with the long delay. The practical realisation of delays is shown in figure 5.6. A combination with an analogue *fine delay* is presented. Such an implementation on a single chip is feasible and only one analogue digital conversion is required. Both short and long delay values as well as both fine delays vary with revolution frequency. In order to ensure the overall synchronisation, the control card calculates the necessary information on-line.

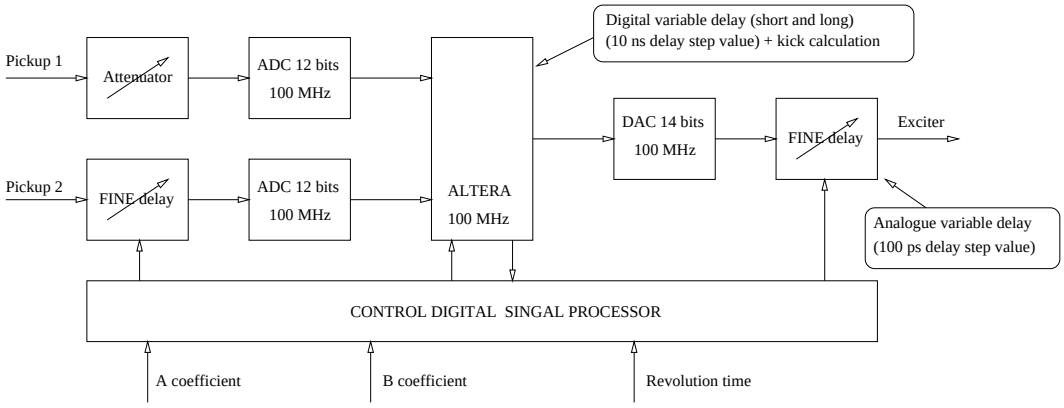

Figure 5.6: Practical realisation of long, short, and fine delays.

Implementation on a single chip

In order to increase the maximum working frequency and clock synchronisation inside and outside the chip as well as to improve the stability of the system, it is important to implement the whole design into a small chip. Such a system was simulated with optimum adjusted multiplication.

The results of this simulation are shown in figure 5.7. The 30KE NEW version was simulated with flip-flops at each digital input and output for better synchronisation. A different output latency corresponds to different output latency for the summation part. Simulation was done with 4 clock cycles output latency for multiplication. If the delay path is controlled by inverted clocks, the system can become unstable. The 30KE version is stable only for the output latency in the range from 2 to 5 clock cycles with maximum clock frequency 129.8 MHz. 30KE NEW version become a problem with synchronisation and

the system became unstable for the 4 output latency. The maximum simulated system clock frequency was 131.5 MHz. The project was compiled using new faster and more efficient Quartus fitter technology [2].

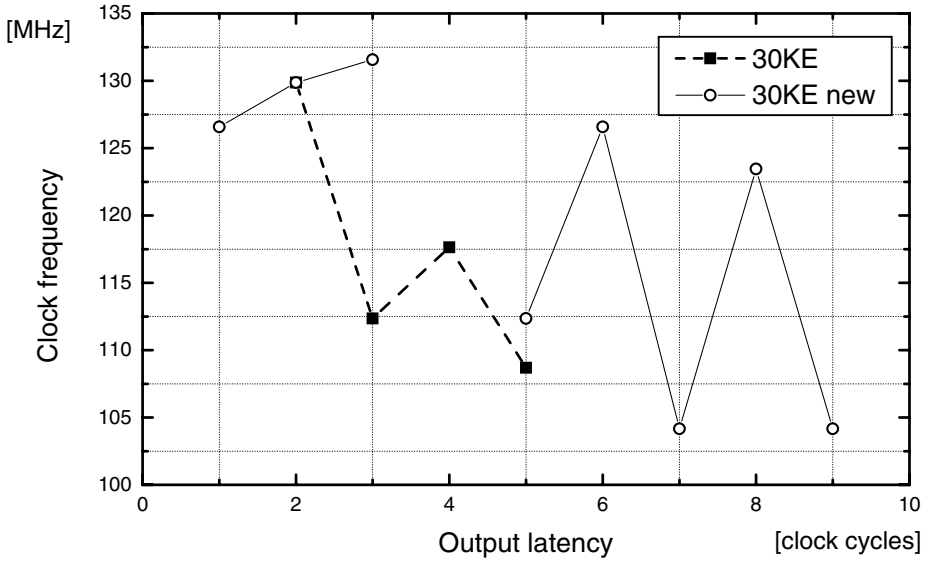

Figure 5.7: The simulation results for digital part of the TFS implemented in the 30KE. The "30KE new" version was simulated with flip-flops at each digital input and output.

Clock distribution

A clock with low jitter is required for an appropriate system. For high speed signal processing, the clock signal has to be distributed to avoid the signal asynchronism [4]. The clock cannot be running through some digital parts of the system but it should be distributed directly to the chips (all ADC, memory and other). Special care should be taken of a layout for the PCB (printed circuit board) [3]. The chip for distribution clock signal with clock generation is shown in figure C.6. Using the ECL technology (in this case, namely PECL) a low jitter of the clock signal can ensure the required stability. This is shown in figure C.4.

5.1.3 Control card

The main task of the control card is data processing from the main control room (revolution time, multiplication coefficients and amplification factor). For this purpose a fixed point DSP clocked at 100 MHz (10 ns instruction cycle) is used. The VLIW (Very Long Instruction Word) architecture allows to execute up to eight instructions every cycle [112, 115]. The main DSP software is running in endless loop and is waiting for external interrupt. The data flow diagram is shown in figure B.4.

Generating the interrupting signal means that new data (revolution time, multiplication coefficients and amplification factor) are ready and DSP can read and process them. For this purpose, four independent interrupts are used. Since the interrupt signal is generated at most every 1 μs (given by function generator), DSP has approximately 100 cycles for processing four interrupts. In this time DSP has to read data, process and

calculate new data, correct the value for revolution time and distribute the processed data to the main card.

To enhance the data rate one can employ both data and address bus for data transfer. Due to only unidirectional address bus available, it should be used for output data. Bi-directional data bus is used for reading the digital words [112]. With this method, the processor "read" and "write" cycle can be done at once. The data rate can be improved two times in this alignment.

For communication between both main and control boards, the state automate for generating short impulses (generated only for one clock period) is used. The input signal acts on the rise edge or on the fall edge.

Software environment

In order to develop, commission and operate the TFS system efficiently, an integrated development environment running on PC is used. This software development system is a PC based JTAG emulator [116]. The code composer is a system development tool that supports an integrated development environment for TMS320C6x [118].

Software for all three chips was written and put into operation. For both integrated chips, the JTAG interface is used for testing purposes. The software for DSP was written in C [114], and for time critical routines, an optimized linear assembler was applied [113, 115]. The XILINX chip was programmed in VHDL language and was simulated in real time by means of XPLA software [135]. The ALTERA chip was designed using MAX+plus II software [2].

Practical realisation

One of the technological challenges is to implement a high speed digital signal processing system at a peak data processing rate of 800 Mbytes/s (600 Mbytes/s input, 175 Mbytes/s output + 25 Mbytes/s controlling). To keep the data signals synchronous with each other, the propagation delay has to be carefully controlled during the circuit card layout [75].

The work of PCB layout is complicated by the mixed signals running at high speed, which requires impedance control, skew control and to avoid cross talks between signals [3]. Multilayered design of the printed circuit boards was used with 10 layers so that the interface between layers can be avoided. The connection diagrams for both main and control cards are shown in Appendix C and D.

5.1.4 Measurement results in the time domain

To check the correct operation of the system some measurements should be done to demonstrate a correct and properly function of the system and its components without beam. In the following we will define some measures to characterise circuits for generating delays.

Resolution and Accuracy

The measured delay t for a programmed delay value is given by

$$t_n = n_{\text{big}} \cdot \Delta t_{\text{D}} + n_{\text{small}} \cdot \Delta t_{\text{D}} + n_{\text{fineb}} \cdot \Delta t_{\text{A}} + n_{\text{fines}} \cdot \Delta t_{\text{A}} + t_0 + \delta_n \tag{5.1}$$

where t_0 is the intrinsic delay, Δt_{D} is the delay step value for digital delay, Δt_{A} is the delay step value for analogue delay, δ_n is the deviation from the ideal value. The n_{big} and n_{small} values are calculated by control card for counters of the main card and are set up only at the beginning of the acceleration process. The n_{fineb} and n_{fines} values are changed always when the value of the variable delay is changed.

The Δt_{D} depends only on the system clock frequency. If this frequency is chosen to be of 100 MHz, the $\Delta t_{\text{D}} = 10$ ns. The Δt_{A} is equal to the LSB what corresponds to 25 ps. Since the revolution time is coded by means of the 16 bits, Δt_{A} depends only on the maximum long delay value and not on the number of waiting revolutions. That means if TFS works in the first turn, Δt_{A} is 146 ps and the same time resolution value corresponds for feedback working in the second turn. By means of external switches, which are positioned at the control card, it is possible to set up the number of waiting revolutions.

The intrinsic delay t_0 is the sum of the digital and the analogue parts. The intrinsic digital delay is 250 ns and the one for two analogue parts is 3 ns. This intrinsic value should be subtracted from the minimum value of the delay.

The accuracy of a circuit is commonly measured by **differential non-linearity** [128]

$$dnl_n = \delta_{n+1} - \delta_n \tag{5.2}$$

and **integral non-linearity**

$$inl_n = \delta_n \tag{5.3}$$

Both differential and integral non-linearity are a function of the tap number n or *programmed delay value*. To summarise the overall quality of a circuit it is convenient to calculate their standard deviation and peak-to-peak range over all N delay taps.

Monotonicity

A delay characteristic is said to be monotonic, if for all n the following condition is satisfied [128]:

$$\tau_{n+1} > \tau_n \ . \tag{5.4}$$

Hence, increasing the delay step value n must also result in an increase of the measured delay. Monotonicity is an important property of a programmable delay because by using dual port memory it is possible to change the value of the delay without interrupting of signal processed.

Figures 5.8, 5.9, and 5.10 contain results of the variable delay. The curve displayed in figure 5.8, shows the measured delay vs. programmed delay and demonstrates correct operation of the circuit.

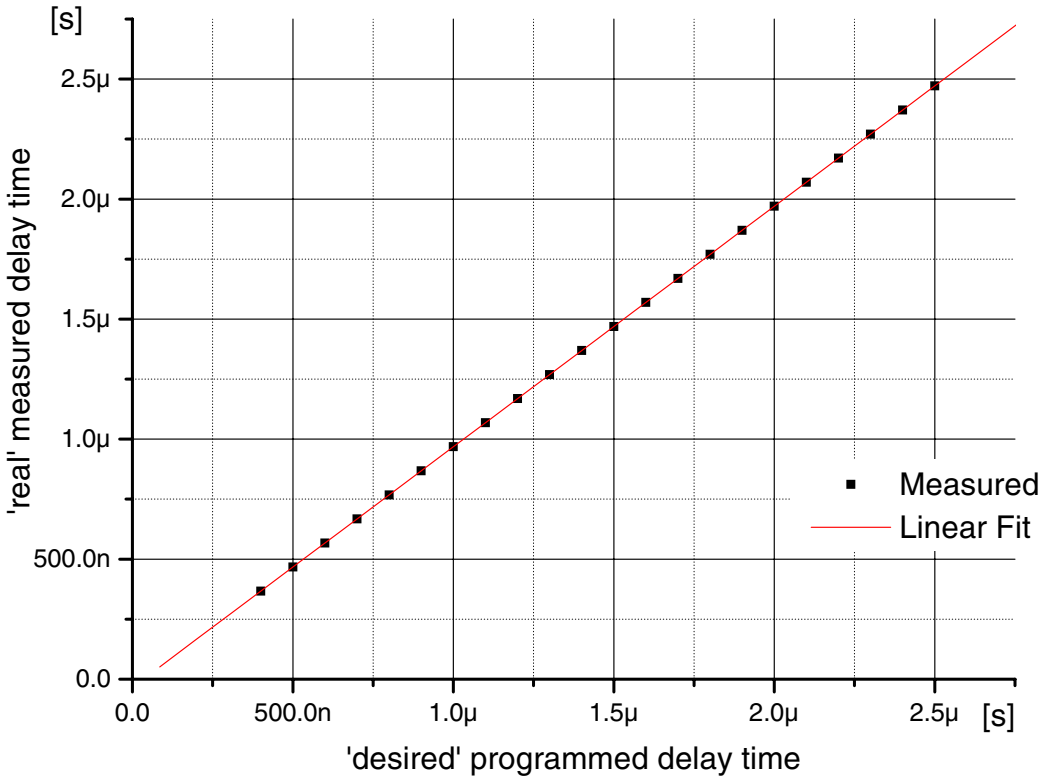

Figure 5.8: Measured delay vs. programmed delay.

To quantify the differential non-linearity, the distribution of delay steps is calculated as shown in figure 5.9. The RMS value of the deviation from the nominal value was found to be 201.4 ps. It is important to say that while measuring the delay step value was n = 100 ns. It represents an error of 0.2%. From this point of view the more important parameter is a standard deviation. For measured delay the standard deviation is 13.5 ps.

The integral non-linearity of the circuit is shown in figure 5.10. It can be seen that the delay is confined to a maximum deviation of less than 4 ns.

An improvement of integral non-linearity is to be carried out by the control card. For better a accuracy, the control processor modifies the value by a correction factor. With fitting curve (see figure 5.8), the control processor is recalculating the programmed value in such a way that the output value is corrected with respect to the programmed value. The following fitting function is used:

$$t = 1.00201 \cdot t_{\text{programmed value}} - 33.875 \text{ ns} \, . \tag{5.5}$$

The error calculated for the slope is about $4.53604 \cdot 10^{-6}$. The minus sign of the -33.875 ns term indicates that the control processor tries to compensate the intrinsic delay caused by the rest of the TFS system.

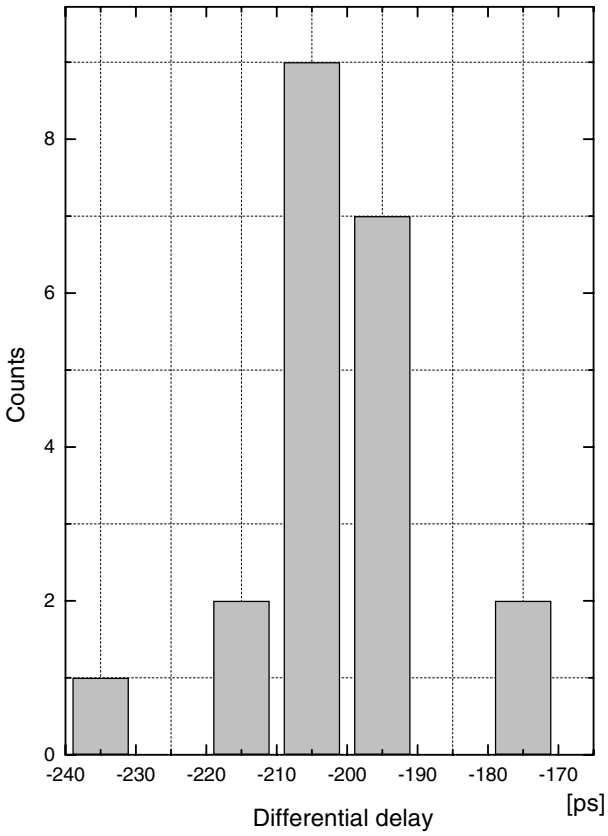

Figure 5.9: Distribution of differential delay steps. The RMS value of the differential non-linearity amounts to 201.4 ps.

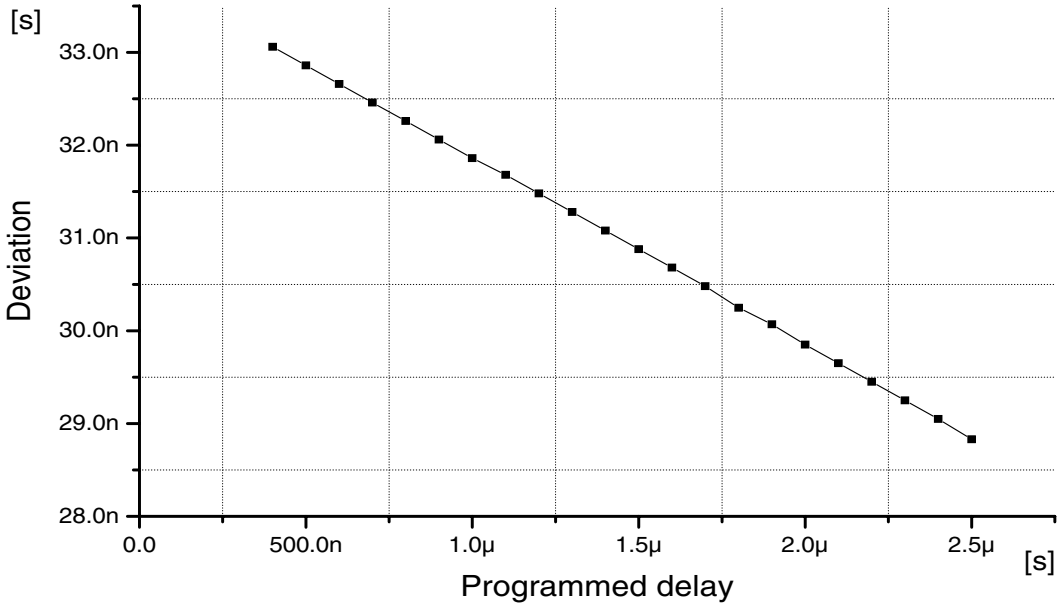

Figure 5.10: Integral deviation of the delay value from its nominal value.

5.1.5 Measurement results in the frequency domain

The network analyser HP4396A [67] has been used to measure and to check parameters of the system in the frequency domain.

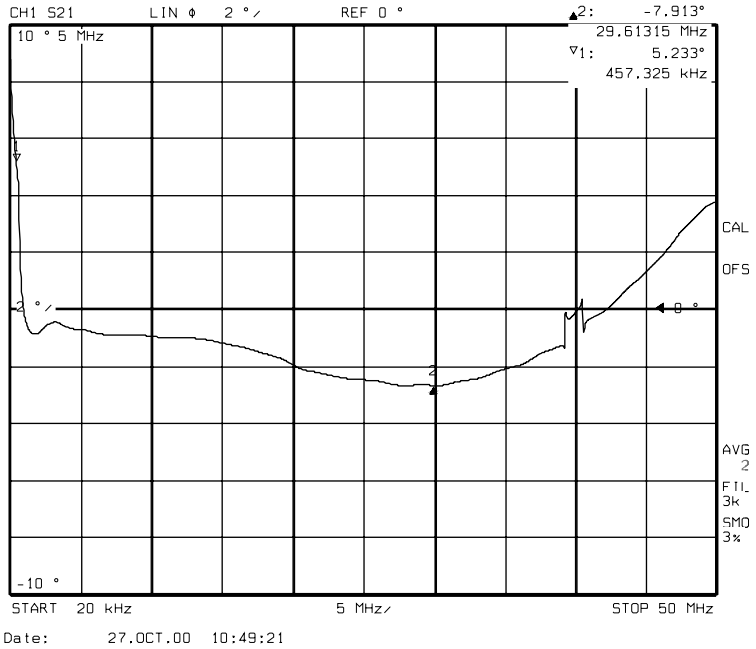

Figure 5.11: The measured phase characteristic of the digital system for the time delay $T_{\text{delay}} = 0.5$ μs in the frequency range from 20 kHz to 50 MHz. The phase error is only $\pm 2°$. (2 degree/division)

Because for the first measurement it was planned to use the digital delay together with the fine analogue delay two different phase characteristics are shown in figure 5.11 and 5.12 for comparison. The method for measuring of the phase error (dispersion) is following. After calibration of the measuring equipment the phase and by means of calibration the actual delay time value was measured. This technique allows to evaluate the dispersion in the entire measured frequency range.

Programmable variable time delay

At first only *the digital signal processing part* was tested without analogue fine delay. The measured range is the theoretically calculated range where transverse coherent instabilities are expected. To compare the influence of the variable delay two different times are shown. Figure 5.11 contains results with delay time value equals to 500 ns and in figure 5.12 the delay time value was 2.5 μs. In the frequency range from 20 kHz to 40 MHz the phase error is only $\pm 2°$. The main advantage of the system is that the change of the parameter has a minimal effect on the transfer characteristic of system. The "peak" at 40 MHz represents the frequency limit of the digital device.

To compare the effect of both analogue and digital part on the phase error, measurements on both systems were done. Measured phase characteristics of both digital signal processing part as well as of analogue fine delay are shown in figure 5.13 for time 1.3 μs. In figure 5.14 the amplitude characteristic for the same condition is shown. In the frequency range from 20 kHz to 40 MHz the measured phase error is $\pm 4°$ in this case. It represents

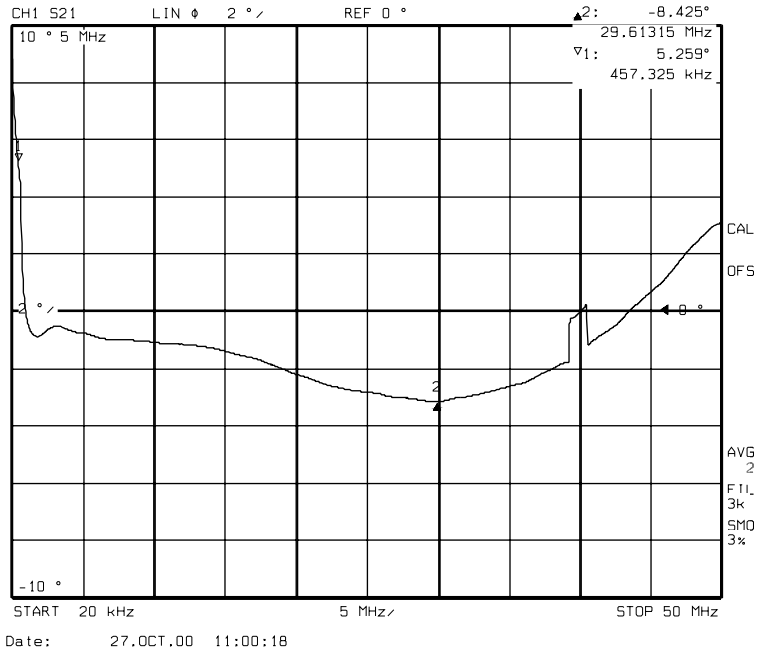

Figure 5.12: The measured phase characteristic of the digital system for the time delay $T_{\text{delay}} = 2.5$ μs in the frequency range from 20 kHz to 50 MHz. The phase error is only $\pm 2°$. (2 degree/division)

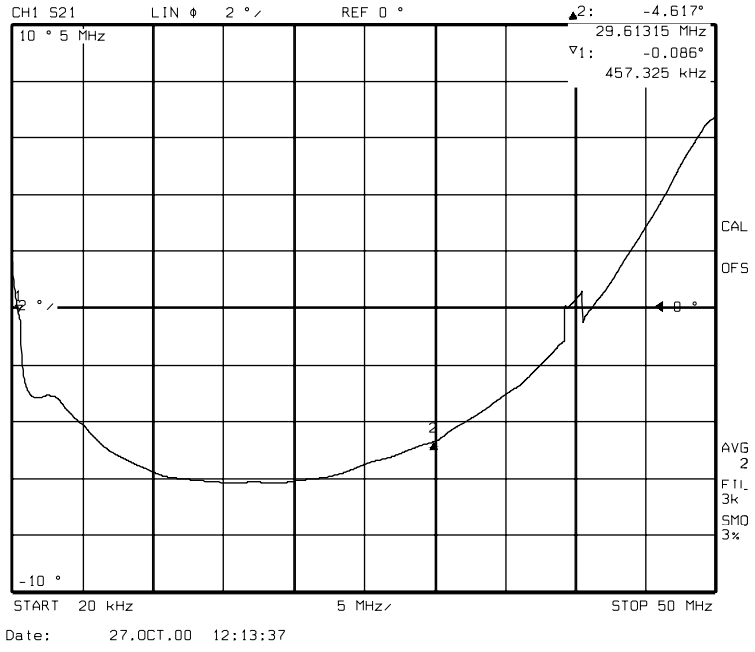

Figure 5.13: The measured phase characteristic of the combined digital and analogue systems for the time delay $T_{\text{delay}} = 1.3$ μs in the frequency range from 20 kHz to 50 MHz. The phase error is only $\pm 4°$. (2 degree/division)

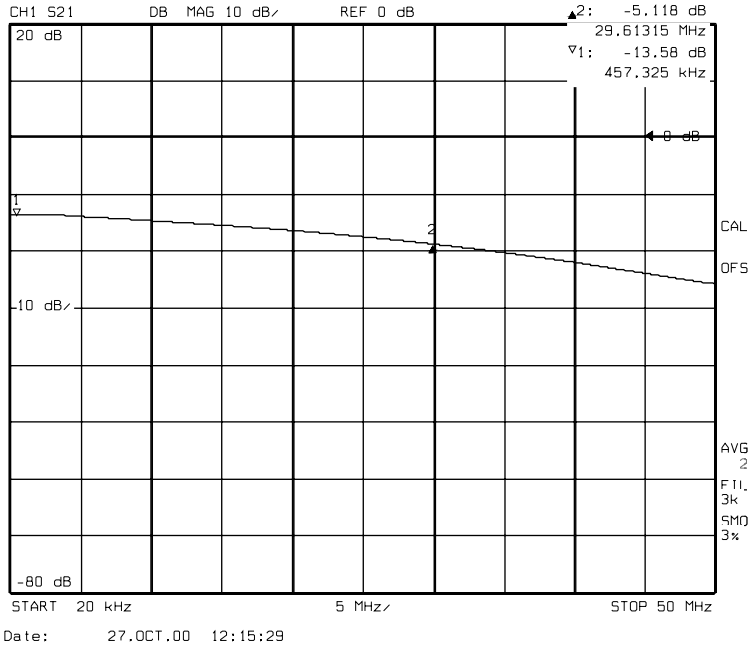

Figure 5.14: The measured amplitude characteristic of the combined digital and analogue systems for the time delay $T_{\text{delay}} = 1.3$ μs in the frequency range from 20 kHz to 50 MHz.

phase degradation which is acceptable and no important influence of analogue part on TFS efficiency was measured.

5.2 Time dependent notch filter

Because the transverse feedback system is supposed to be used for both coasting and bunched beam mode the suppression of the longitudinal signals at all revolution harmonics in the bunched beam mode is required. Before using the pickup signal for the feedback system, this signal should contain neither DC components nor closed orbit parts. The consequence of including this common mode signal in a feedback signal sent to the exciter results in a feedback system trying to correct the closed orbit offset. The exciter efficiency in damping the instabilities is severely diminished by allowing the unwanted signal to excite the beam. A Beam Offset Signal Suppressor (BOSS) [42, 107] or a notch filter [34, 105] can remove the closed orbit offset signal at all revolution harmonics before the feedback system excites the beam.

A Notch filter requires information about the revolution time in the synchrotron. The cancellation depends on how accurately known is the value of revolution time. The notch filter has only one input and one output. By introducing a feedback a notch depth can be up to -40 dB [34, 105, 107].

Closed orbit suppressor compares the two signals from both plates in one direction. In this case, the notch depth depends on the electrical phase error between both pickup plates on the way from the pickup to the processing unit [42, 107].

5.2.1 Theoretical analysis

Because the function of the notch filter is required during the acceleration mode, a variable notch filter was realised. Such kind of the dependent notch filter was realised on the basis of aforementioned variable delay.

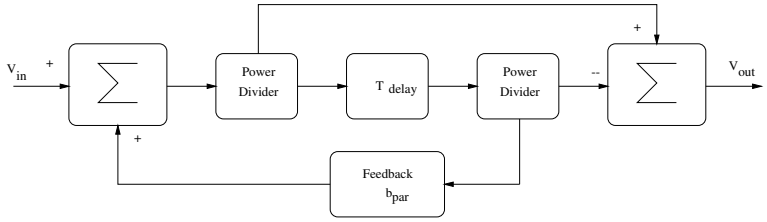

Figure 5.15: Delay line for generation of a periodic notch filter structure with feedback factor $0.0 \leq b_{par} \leq 1.0$.

A simple implementation that accurately generates such a large number of contiguous notches is referred to as a delay line canceller. The canceller consists of delayed and not delayed feedforward paths as shown in figure 5.15. Then signals from both paths are combined in a combiner $(0 - 180°)$. The delay is precisely equal to the revolution time in the ring. The required time response for the variable notch filter is the same as for the variable delay. The variable delay is to be changed every 44 μs with a delay step of 1 ns. The output signal y(t) can be written as a difference of two input signals with attenuations α_{att} and β_{att} as

$$y(t) = \alpha_{att} x_0(t) - \beta_{att} x_0(t - T_{\text{delay}}) \tag{5.6}$$

The cancellation quality depends on the attenuation of the two waves in two cables that should be equalised over the whole useful bandwidth. Since the notch depth is sensitive to the mismatch of delays and attenuation of two delay lines, they are precisely adjusted by a variable delay line and a variable attenuator to obtain the best notch depths. The transfer function of the notch filter with feedback is [90, 91]

$$H(e^{\mathrm{j}\omega t}) = b_{par} \cdot \frac{1 - e^{-\mathrm{j}\omega t}}{1 - b_{par} \cdot e^{-\mathrm{j}\omega t}} \; . \tag{5.7}$$

The feedback helps to flatten the passband and to narrow the notch. Figure 5.16 plots the passband shape for $b_{par} \approx < 0.0, 0.9 >$. The curve for $b_{par} = 0$ corresponds to no-feedback case, which gives the most rounded response. For better understanding, only three notches are shown in the frequency range from 5 MHz to 10 MHz.

5.2.2 Measurement results

For correct operation of the transverse feedback system with a bunched beam a notch filter has to be used. The second reason why the variable notch filter should be used is to decrease the power requirements. In figure 5.17 the amplitude characteristic is shown. In this case the setting parameters are following:

$$T_{\text{revolutiontime}} = 2.0 \; \mu \text{ s} \quad \Longrightarrow \quad f_{\text{notch}} = 500 \text{ kHz} \; .$$

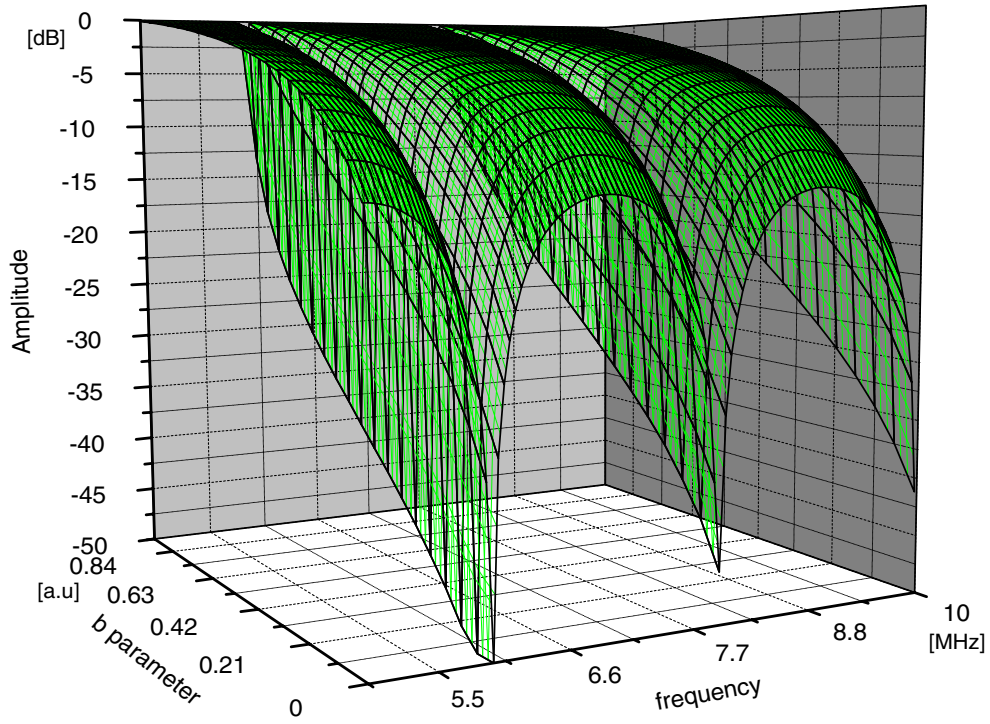

Figure 5.16: Amplitude of a periodic notch filter structure with feedback factor $0.0 \leq b_{par} \leq 1.0$ in the frequency range from 5 MHz to 10 MHz.

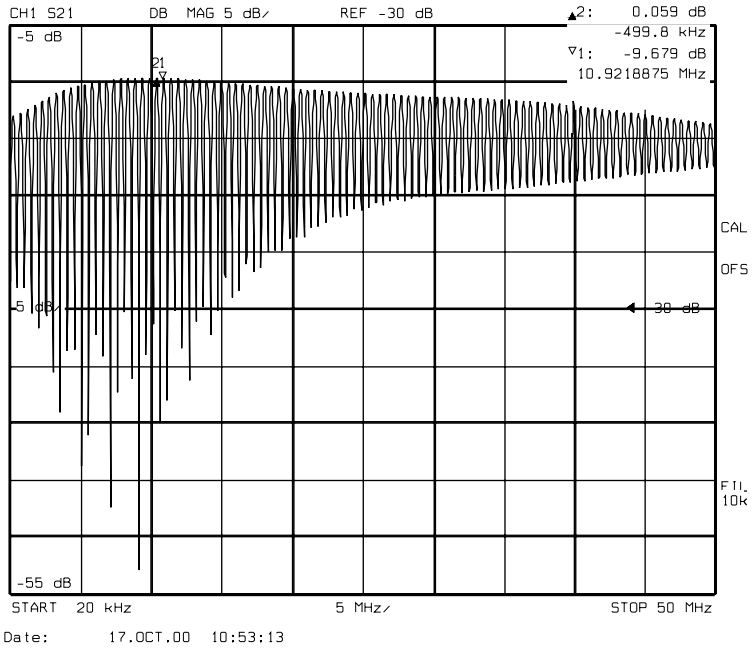

Figure 5.17: Amplitude characteristic (5 dB/division) for the time dependent notch filter in the frequency range from 20 kHz to 50 MHz. The set value $f_{\text{notch}} = 500$ kHz. The frequency range from 2 MHz to 15 MHz is characterised by a notch depth of up to 35 dB.

The frequency range from ≈ 2 MHz to ≈ 15 MHz is characterised by a notch depth of up to ≈ 35 dB. The phase characteristic shown in figure 5.18 is changed drastically. The effect of this phase error on efficiency and operation of the TFS is subjected to further investigation. Due to analogue components such as analogue splitters and combiners the variable notch filter is less effective above ≈ 20 MHz. The transfer characteristics of the analogue splitters and combiners are dominating at higher frequency.

The goal of the measurements described above were the calibration and first tests before putting the system into operation with beam.

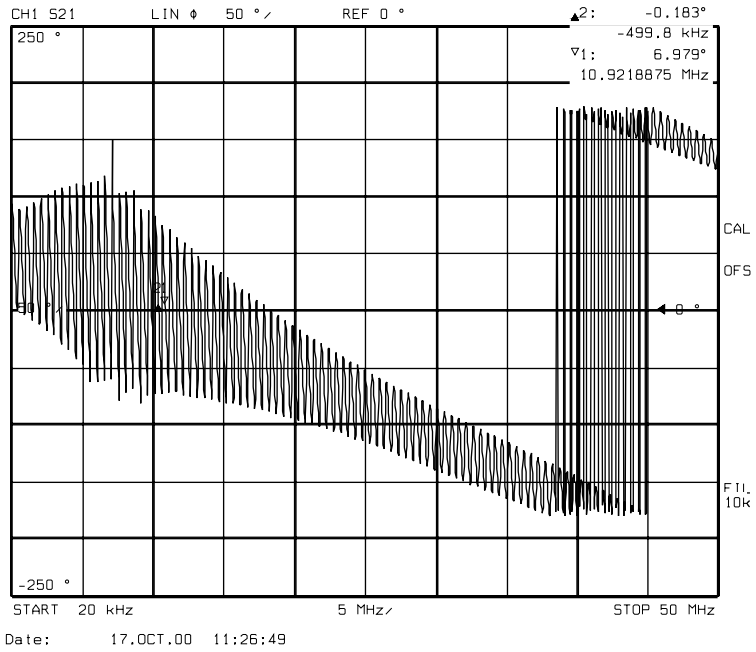

Figure 5.18: Phase characteristic for a variable notch filter in the frequency range from 20 kHz to 50 MHz. The set value $f_{\text{notch}} = 500$ kHz.

5.3 TFS electronic realisation

The design of the entire TFS system for one plane is shown in figure 5.19. The TFS location in the SIS is shown in figure 2.1.

At first, the signal will be detected by position pickups S05DX5H (S05DX5V) and S04DX5H (S04DX5V) with preamplifiers for each pickup plate. The input amplifier impedance is 1MΩ ‖24 pF. The preamplifier gain can be adjusted in 30 dB steps (+20, -10, -40 dB gain). In order to match impedance (75Ω/50Ω) and to monitor the signals from the pickups, the power splitters are used. The cable length from both S04DX5H and S05DX5H should be the same because of the minimal value of the variable delay (63 ns). In our case, the delay between S04DX5H and S05DX5H has to be changed from 63 ns to 402 ns.

Due to high requirements of the BOSS (Beam Offset Signal Suppressor) on the phase matching a cable delay has to be used. This cable delay is important to adjust

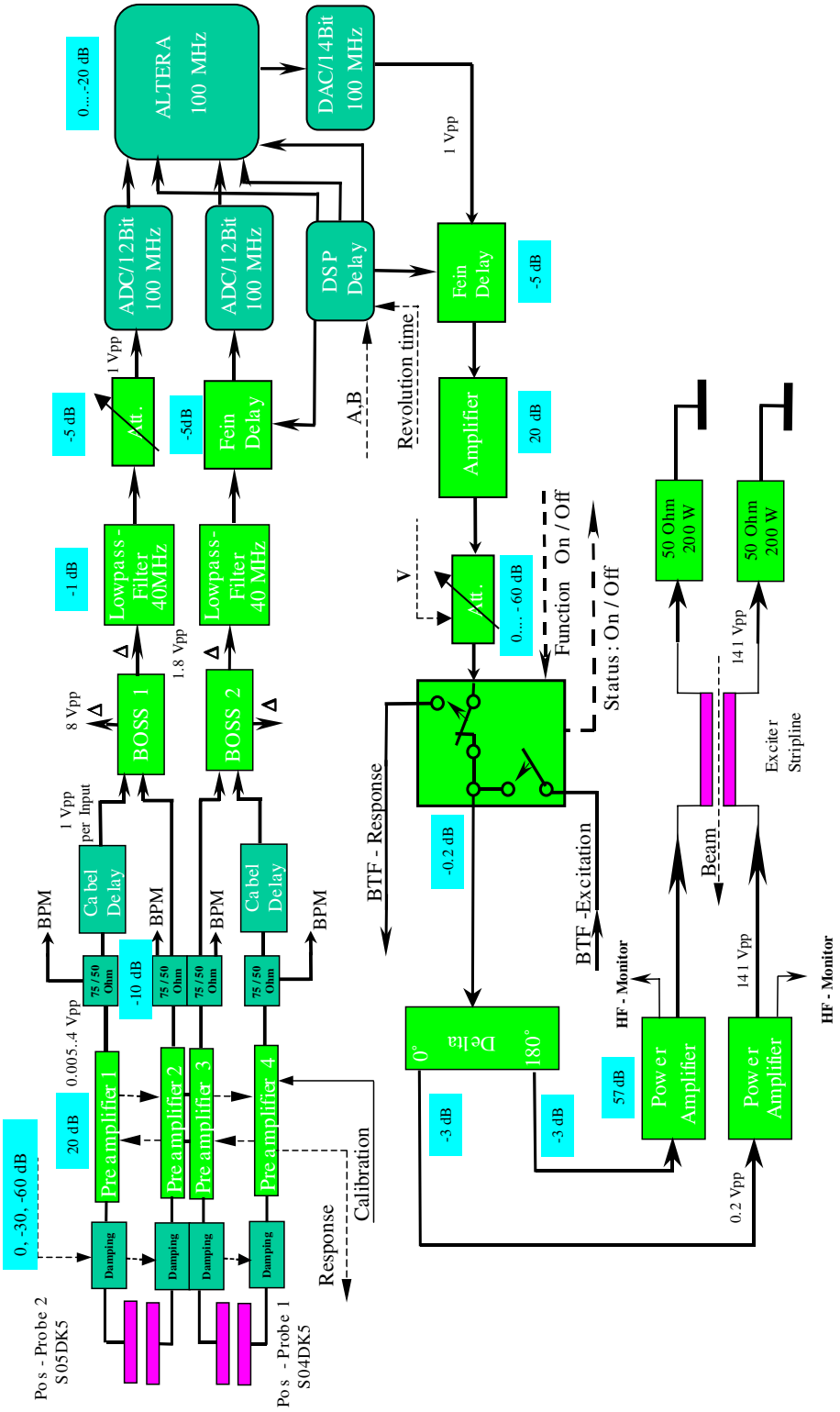

Figure 5.19: Design of the transverse feedback system - vertical or horizontal plane. (Because the transverse feedback system is needed in two transverse planes, only one is considered.)

delay between both plates with precision down to approximately 10 ps. In the bunched beam case, the BOSS is used. In this case, its task is to damp the longitudinal signals as well as to create the difference signal from both plates for each pickup. Damping up to 45 dB can be achieved. Two output signals from the BOSS are available. The first output is without amplifier and is used for the processing in the TFS. The second one is amplified (+20 dB) and is used for signal monitoring in the TFS. This is important when putting the TFS into operation.

Since the analog signal from the pickups is processed digitally, a lowpass filter is used. According to the sampling theorem, any signal can be accurately reconstructed from values sampled at uniform intervals as long as it is sampled at a rate of at least twice as high as the maximum signal frequency. A failure to satisfy this requirement will result in aliasing the higher-frequency components, meaning that these components will appear to have frequencies lower than their true values. One way of avoiding this problem is to apply a low-pass filter to the signal prior to the sampling stage in order to remove any frequency components above the "folding" or Nyquist frequency (half the sampling frequency). In this case, such an anti-aliasing filter is implemented using conventional analog circuitry of the 7.order with a frequency limit of 40 MHz.

The main function of fine and of short delays, where the latter is realised in the dual port memory in the ALTERA chip, is to adjust the variable delay between both pickups. This is important for creating the vector summation and calculation of the correct signal for the exciter. The fine delay value is calculated by the control card and it can be adjusted each 1μs. Because the delay has 9 bits for controlling and a precision of 25 ps, the maximum adjusted value of the fine delay is 12.5 ns. In the whole range, the fine delay inserted in one path has an attenuation of -5 dB. In order to ensure the signal matching for both pickups the variable attenuator is inserted in the second path.

The analogue signal with amplitude $\pm$1V is converted by means of the 12bits/100 MHz ADC and both converted signals are processed in the ALTERA chip. Such a processed digital signal is going to the 14bits/100 MHz DAC and is converted back to an analogue signal with amplitude $\pm$1V. Since the input and output amplitudes are the same in the whole range of the variable delay no damping is introduced to the analogue signal. The DSP processor controls the whole operation and automatically adjusts the all important parameters for the coasting and bunch beam. Both coefficients for vector summation as well as the revolution time and corresponding values for short, long, and both fine variable delays are calculated by the control processor. All delays cover the whole range of energy in the SIS. The inherent delay is introduced not only by the digital signal processing part and by the TFS components but also by the cables from the pickups to our TFS electronic and by the cables from the TFS electronics to the exciter for very high energy. Thus, it is possible to correct in the second turn. The disadvantage of this method is that after such a long time, the signals from pickups can have changed and do not correspond to the real ones.

After digital signal processing, the analogue signal is going through the second variable delay. A resolution better than 10 ns is achieved for the variable delay. This fine delay is working together with the long delay implemented in the ALTERA chip and it should ensure such a synchronisation between the "not-delayed" pickup and exciter.

The following two parts of the system, phase correction and attenuator are important for testing purposes and for better TFS operation. To correct some phase errors introduced by some analogue parts a phase correction is used. If needed, an attenuation of the entire TFS can be achieved in range from 0 to -60 dB by means of a variable attenuator. This

variable attenuator is controlled manually directly from the control room or automatically during the acceleration process if required.

For the BTF (Beam Transfer Function) measurements, closed loop measurements or open loop measurements are allowed by a relay switching matrix. These measurements are important for commissioning of the whole system as well as for calibration purposes.

Two signals are needed due to the two plates of the exciter. For this purpose, a power splitter ($0 - 180°$) working in the frequency range from 20 kHz to 50 MHz is used. Both the inverted and the non-inverted signal is going to the power amplifier in which the total gain of the whole system is controlled. The system gain is 57 dB.

5.4 Computer process control

The device network shown in figure 5.20 is used for controlling the TFS as well as for monitoring the entire transverse feedback system. The devices in the *Main control room* and the *Electronic room* were already installed and only the new devices in the *Kicker room in SIS* were new installed.

To put the TFS into operation one needs a control signals from the *main control room*. For correct working conditions, it is very important to have accurate and exact timing from the *control system*. Ramps for the revolution time, both coefficients A and B for vector summation and coefficient V used for controlling the power amplifier gain are generated from the control system.

The TFS has two modes of operation:

Automatic - that means 'free running'. The TFS system is running automatically without human intervention during the acceleration cycle.

Manual - that means one should adjust the TFS system for the specific energy. This is done by means of the *NODAL* program. This mode is very useful for the first tests and TFS commissioning.

A *VAX-Cluster* with running program *NODAL* is connected to an equipment unit in the electronic room through an *Ethernet*. The equipment unit has its own μP - *grouped microprocessor*. Communication of the μP with the *control system* is provided by a *ETH - Ethernet interface card*, on one side, and communication with the devices in the ring is provided by a *SE - control unit*, on the other side. The *SE* storage holds magnet and RF data (the points) of the appropriate ramp.

By means of the *IK - interface card* the necessary information from the *SE - control unit* are received. Then, this data are processed in the TFS electronics in the *Kicker room of the SIS*.

The transverse feedback processing electronics consists of two VME chassis: one for the horizontal and one for the vertical plane. Each of them will host one main card, one control card, two fine delays (between two pickups and pickup and exciter), four function generators (revolution time, A, B, and V coefficients), and some I/O cards. The VME bus will be used to initialise, control, and monitor the system.

A proper TFS function is monitored in the *main control room* by means of the spectrum analyser, FFT, network analyser, and digital oscilloscope. These devices are connected to a GP-IB-bus system. With such a set-up, it is then possible to use the

measured data for data processing on a PC or a workstation. A very important feature of monitoring and measuring devices is the input for external triggering. With this external triggering, it is possible to measure exactly within an actual accelerator cycle. It is also possible to trigger a desired measurement exactly in the time. For this purpose the appropriate *Event* is generated from the *central pulse unit* through the *timing bus*. Monitoring and measuring devices with GP-IB-bus system are connected to the SIS control system through the *SCSI 488/D bus controller*.

For every μP exists one *TIF - Timing Interface* which is dedicated to process the *Event* generated from the *central pulse unit*, which allows to work in the event triggered mode or so called *Event-mode*.

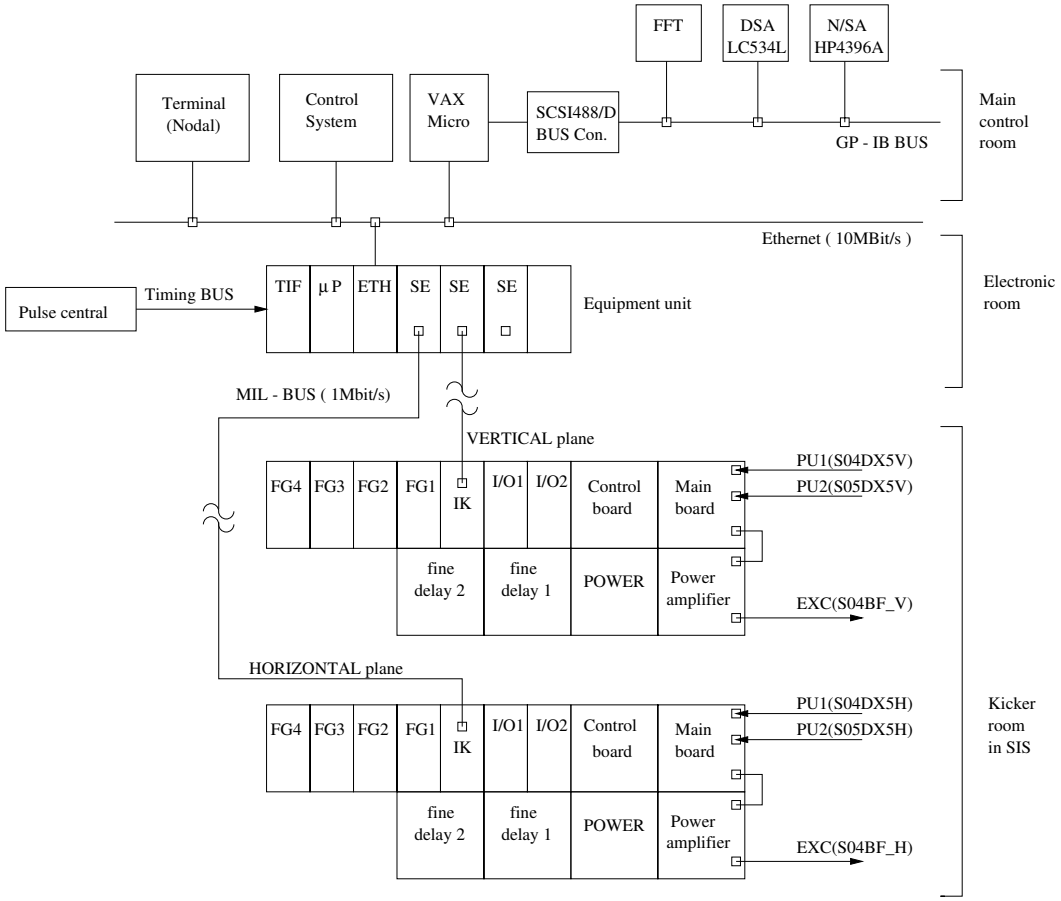

Figure 5.20: Structure of the control system for controlling the TFS in the SIS.

5.5 Conclusions

The 12 bits/100 MHz automatic digital transverse feedback system was analysed, designed, simulated and constructed. Both PLD and DSP digital processing technologies were applied together - ALTERA PLD is used as DSP co-processor due to the fact that the PLD can handle repetitive functions with extremely high performance and a DSP processor performs remaining control functions.

The time critical mathematical operations such a multiplication were simulated. System-clock frequency dependence on output latency has shown that the clock frequency of 100 MHz cannot be achieved without pipelining. The best results were achieved with 4 or 5 clock cycles output latency (40 or 50 ns). With *speed optimization method*, it is possible to achieve a maximum system clock frequency about 15% higher than for *area optimization* method. Maximum achievable frequency for 5 clock cycles output latency of 164 MHz was simulated. The novel methods for the variable delay were presented and successfully realised. This was done in the dual port memory with automatically running counters.

From the analyse given in section 4 a time resolution for the variable time delay better than 1 ns is required. The possibilities with digital and analogue techniques were discussed. The practical realisation of delays (dual port memory, digital) in combination with an analogue *fine delay* was demonstrated. For higher stability the ALTERA chip 30KE with flip-flops at each digital input and output was realised. The maximum simulated system clock frequency was 131.5 MHz. A high speed digital signal processing system at a peak data processing rate of 800 Mbytes/s was constructed. This is in good accordance with the theoretical requirements.

A series of the measurements in the time domain as well as in the frequency domain were presented. The RMS value (the delay step value was $n = 100$ ns) of the deviation from the nominal value (*the differential non-linearity*) was found to be 201.4 ps. This value corresponds to the theoretical time resolution of the variable delay (146 ps). For the *integral non-linearity* of the circuit a maximum deviation of less than 4 ns was measured. Improvement of integral non-linearity is done by a control card. The measured phase error in the useable frequency range from 20 kHz to 40 MHz is only $\pm 2^\circ$. The main advantage of the digital system is that the change of the delay time value has minimum effect on the transfer characteristic of system. The realized time dependent notch filter is characterised by the notch depth of up to ≈ 35 dB in the frequency range from 2 MHz to 15 MHz. These measurement results match the theoretical calculated parameters in the section 4.2.

A design of an entire TFS system for one plane was described in detail. The device network used for controlling the TFS as well as for monitoring of the entire transverse feedback system was designed and constructed.